PROCESSING OF PREMIXED AND PREALLOYED BRONZE THROUGH TRANSIENT AND SUPERSOLIDUS LIQUID PHASE SINTERING

By

SUKANTA GHOSH

DEPARTMENT OF MATERIALS AND METALLURGICAL ENGINEERING

Indian Institute of Technology Kanpur

NOVEMBER, 2001

PROCESSING OF PREMIXED AND PREALLOYED BRONZE THROUGH TRANSIENT AND SUPERSOLIDUS LIQUID PHASE SINTERING

A Thesis Submitted

In Partial Fulfilment of the Requirements

For the degree of

Master of Technology

by

Sukanta Ghosh
(Roll No. Y010648)

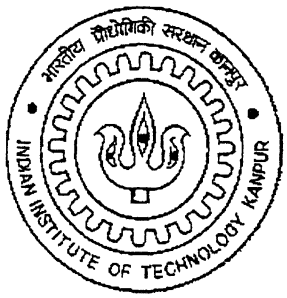

to the

DEPARTMENT OF MATERIALS AND METALLURGICAL ENGINEERING

INDIAN INSTITUTE OF TECHNOLOGY KANPUR

NOVEMBER, 2001

CERTIFICATE

19-11-2001

It is certified that the work contained in the thesis entitled **"Processing of Premixed and Prealloyed Bronze Through Transient and Supersolidus Liquid Phase Sintering"** by **Sukanta Ghosh (Roll No. Y010648),** has been carried out under our supervision and to the best of our knowledge this work has not been submitted elsewhere for a degree.

13 Nov '01

Dr. A. Upadhyaya
Assistant Professor
Department of Materials and
Metallurgical Engineering.
Indian Institute of Technology,
Kanpur.
November, 2001

Dr. R.K. Ray
Professor
Department of Materials and
Metallurgical Engineering.
Indian Institute of Technology,
Kanpur
November, 2001

ABSTRACT

The current work investigates the processing of premixed and prealloyed bronze through transient and supersolidus liquid phase sintering. The research closely looks at the microstructural evolution in these alloys sintered in different conditions. So far, the use of bronze is limited in the fabrication of porous or self-lubricating bearing. Because of porosity in sintered alloys, use of P/M bronze has not been extended for fabrication of structural applications. This work has been carried out to shift the use of bronze from the bearing to the structural applications. In this study Cu-12wt.% Sn composition was chosen for both prealloyed and premixed state. This particular composition gives three different sintering conditions i.e. solid-state, transient liquid phase and supersolidus liquid phase sintering depending on the variation in the sintering temperature from 220°C to 880°C. Two different pressure conditions were chosen for compaction. This study determines the effect of pressure on the properties of the sintered component. In solid-state sintering three different temperatures were selected. Supersolidus liquid phase sintering were done under two different temperatures depending upon the liquid formation, which could be determined from the phase diagram. DSC and dilatometric studies measured insitu changes of the samples during sintering. The change of phases and dimensional change could be found from the curve easily. Post-sintering characterizations for both macro and microstructures were done. SEM and optical micrographs were taken to characterise the microstructure of the compacts before and after melt formations. Other characterization techniques include porosity determination by xylene impregnation, hardness, x-ray diffraction etc. The results show that premixed and prealloyed powder behave differently in same processing condition. Final properties are very much dependent on the initial powder characteristics. Prealloyed samples showed shrinkage whereas premixed samples showed expansion with the increase in the sintering temperature. Too much liquid formation for premixed samples caused compact distortion.

Table of Contents

List of Figures

List of Tables

Acknowledgments

I would like to express my deep gratitude to Dr. A. Upadhyaya and Dr. R.K. Ray for their expert guidance, support and encouragement throughout my graduate studies at Kanpur. Their leaderships were immeasurable help to my early identification of an industrially significant area of research.

I gratefully acknowledge Dr. Mungole, Mr. Soni and Mr. Umashankar for providing me with guidance and letting me benefit from their experience during the experimental work.

My time at the P/M lab was enriched by the interaction with my fellow students. I am thankful to Shankar, Maya, Sanjib, Kausik, and Chiru. Many of the above are close friends I hope to keep for life.

I must acknowledge the support provided by my loving parents and my sister. I could not have come this far without their unconditional love and support. This thesis is dedicated to them.

At last but not the least, I extend my special thanks to all the staff of Materials and Metallurgical Department and Advanced Centre for Materials Science, for their unconditional help.

Sukanta Ghosh
IIT, Kanpur
November, 2001.

Chapter 1

INTRODUCTION

The name 'bronze' was originally used to denote the copper-tin alloys, and is still used, though they are also called as tin-bronzes. This term 'bronze' is now broadly used for any copper alloy with the exception copper-zinc alloys [1]. Alloys such as copper-aluminium are called aluminium bronzes; copper-beryllium are called beryllium bronzes, and so on. In this study we will stick to copper-tin bronze only.

Historically, the use of tin as an alloying element with copper started in the *Bronze Age* with the making of artefacts and implements. Bronze was the first alloy intentionally manufactured and used by man. Early bronze was an alloy of copper and arsenic that occur together naturally, and was used from about 4,000 BC until about 3,500 BC. About 3,500 BC, true bronze started to appear, which is an alloy of copper and tin. This bronze was harder and less brittle than copper-arsenic bronzes.

Bronze was widely used for utilitarian and artistic purposes until iron became cheaper and more plentiful. Bronze continued to have wide utilitarian uses until it became cost prohibitive. Now other than applications such as a bearing metal in the engineering and automobile industries, bronze is also used in structural parts. Artistically, bronze is still widely used in casting sculptures of all sizes, plaques, and bells.

Bronze still constitutes a significant tonnage use for tin and is likely to remain so in the foreseeable future. Many different copper alloys exist, some of which constitute alternative materials to tin bronze, but for many specific applications (self-lubricating bearing, filters etc.) tin bronzes are still indispensable. Gunmetals are bronzes which contain additionally some zinc and these are widely used as casting alloys in place of binary bronzes.

Bronzes are utilized in three forms – as castings, as wrought material and as sintered powder components for special applications.

- *Wrought bronzes:* These contain tin upto 8%.
- *Cast bronzes:* These bronzes have Sn from 8 to 20%.

- *Sintered bronze:* Powder metallurgy bronzes typically originates as premixes consisting of elemental copper plus 0.5 to 0.75% dry organic lubricants such as stearic acid or zinc stearate. These bronzes have tin from 5 to 15%.

Industrial alloys have a maximum of 20% tin. Nowadays, bronze is indispensable in many specific applications as stated earlier and powder metallurgy is the most convenient route in manufacturing those products. The main advantages of powder metallurgy (P/M) are its near net shape, cost reduction, equivalent mechanical properties to cast products, etc. Moreover, as these components are small, the implementation of P/M technology from laboratory to industries is very effective.

A wide range of bronzes and leaded bronzes is manufactured by the powder metallurgy route, usually by atomization of prealloyed metal but sometimes by sintering together elemental powders. In this study we will deal with both premixed and prealloyed approaches.

In this work we will consider only the copper-tin bronze for our purpose. Chapter 2 gives the background for our studies. This includes phase diagrams of bronze and the development of powder metallurgy (P/M) bronze, different aspects of sintering technology, solid-state vs. the liquid phase sintering, brief description of textures in P/M materials and the influence of textures on P/M bronze.

In Chapter 3 scope of our present work is discussed. This includes the reason for system selection, identification of phases in microstructure, effect of pressures on properties of bronze. A special emphasis on the dilatometric study of bronze is also given.

Chapter 4 describes in detail the experimental procedure. It includes the methodology for powder characterization, premixed powder preparation and compaction press. In addition, the sintering procedure is also discussed in detail. This is followed by a brief description about the dimensional changes, xylene impregnation, dilatometric studies, XRD studies and metallographic procedures. Chapter 5 deals with the experimental results. Chapter 6 and 7 consist of discussion and conclusion, respectively.

Chapter 2

BACKGROUND

2.1 Bronze

Typically all copper-tin alloys with more than 78% copper are called bronzes. The use of tin bronze has remained economically viable in part due to the recycling of scrap. About 50% of all bronzes are cast in a foundry. They are likely to come from secondary material. Alloying with tin not only gives increased strength to copper but also imparts improved bearing performance and good corrosion resistance in certain environments. They are chemically very stable. In dry air, bronze does not degrade at all, however in moist air bronze produce a beautiful, green, pore-free, surface film (patina) which protects it from corrosion.

The tin content makes the alloy hard, bronzes with 6% tin can still be rolled, or hammered, while bronzes with 10-20% tin are usually require casting. Bronzes with more than 20% tin are used for bell casting, these alloys are hard and rather brittle, but when struck they emit a clear note. Even higher tin content (up to 40%) produces radiantly white alloys; like the bell alloys these are brittle and hard, but accept a beautiful polish. They were used for bronze mirrors even in antiquity, and today are called speculum (mirror) alloys.

There are few bronzes which are pure copper-tin alloys as the addition of certain elements improves the characteristics of bronzes. The elements usually added are Zn, Fe, P, Ni, Pb etc. Zinc improves the foundry properties as well as the fluidity with improvements in hardness, strength and antifriction properties. Nickel improves mechanical properties and corrosion resistance with reduction in segregation. Lead, as rounded particles due to its insolubility on copper improves antifriction properties.

Bronzes are utilized in three forms – as castings, as wrought material and as sintered powder components for special applications. In general, the cast alloys may contain up to about 12% tin but there is a demand for higher tin levels (for example 15%) and for applications, such as bells and musical cymbals, 20 to 25% tin is needed to produce the required tonal qualities. Gunmetals are a cheaper substitute for certain

castings, while lead to the extent of as much as 20% may be present where superior bearings properties are necessary.

Industrial alloys have a maximum of 20% tin. As stated earlier the bronzes can be classified into three major groups:

1. *Wrought bronzes:* These contain upto 8% tin. These are single-phase α solid solution-bronzes having good ductility and malleability, and, thus, can be easily cold worked by rolling to sheets, bars, or by drawing to wires (for springs), and mint coins.
2. *Cast bronzes:* These bronzes have Sn varying from 8 to 20%, and can be produced only in the cast-form as these have two phase structures, $\alpha + (\alpha + \delta)$, and thus cannot be easily cold worked. These bronzes may have larger content of zinc and phosphorous. These have high corrosion resistance, low shrinkage and high antifriction properties. These bronzes can be divided into three classes:
   I. Cast bronzes having 8 to 12% tin: These are used for casting pumps, gears, machine parts, heavily loaded bearings, and marine parts to resist sea-water corrosion.
   II. Cast bronzes having 12 to 20% tin: These are mainly used for bearings.
   III. Bronzes having 20 to 25% tin: Bell metals are used for making bells. They are very hard and relatively brittle. They can only be cast.
3. *Sintered bronze:* Powder metallurgy bronzes typically originates as premixes consisting of elemental copper plus 0.5 to 0.75% dry organic lubricants such as stearic acid or zinc stearate. These bronzes have tin from 5 to 15%. Some of structural parts, however, are fabricated from prealloyed powder.

A wide range of bronzes and leaded bronzes is manufactured by the powder metallurgy route, usually by atomization of prealloyed metal but sometimes by sintering together elemental powders. In this study we will deal with both premixed and prealloyed approaches.

Copper-Tin Equilibrium Diagram

The binary copper-tin equilibrium diagram is given in Figure 2.1 [1]. This figure shows the truncated version of equilibrium diagram contains upto 35 wt.% Sn. This much amount of Sn is mainly used for industrial purpose. However, the full version of copper-

tin equilibrium is shown in Figure 2.2 [2]. Copper-tin phase diagram consists of several peritectic reactions, and two eutectoid reactions. The solid solubility of tin in copper decreases from 11% at 350°C to around 1% at room temperature. At 520°C, γ-phase undergoes eutectoid reaction to form a mixture of (α + δ)-phases. Then, δ decompose to produce a mixture of (α + ε)-phases by eutectoid reaction at 350°C. The reactions occurring at lower temperatures are very low in nature and, equilibrium is not easily attained even at 600°C. in commercial bronzes, the phase ε phase is normally non-existent, and cast alloys have a structure of α + (α + δ) eutectoid. The δ-phase, based on electron compound $Cu_{31}Sn_8$, is pale-blue in colour, hard and brittle [1]. This decreases the strength and elongation. However, alloys upto 8% tin usually show single phase, α solid solution at room temperature. But, bronzes with higher than 8% tin are neither rolled nor forged as δ makes them brittle, and are used only for castings.

From a practical view-point, the α and δ phases are the only ones likely to be present at room temperature in most commercial bronzes. It will be better if the hard δ phase is distributed uniformly in the soft α matrix.

The body centred cubic structures β and γ are metastable phases which transform on slow cooling; they can be retained to some extent by quenching, more especially if the tin content of the alloy exceeds about 20%. These phases are ductile which is of practical importance in connection with the hot working of bronzes. The ζ and η phases have hexagonal structures, corresponding to $Cu_{20}Sn_6$ and Cu_6Sn_5 respectively, the latter being regarded as a superlattice based on nickel arsenide structure. These phases are unlikely to be found in commercially produced bronzes although sometimes η may be formed by diffusion reaction. The ε phase has an orthorhombic structure and corresponds to the composition Cu_3Sn [2].

Changes in the solid solubility of tin in copper below 500°C proceed so sluggishly that as far as the normal production, heat treatment and fabrication of bronze are concerned it is permissible to modify the equilibrium diagram to show the δ phase existing down to the room temperature and the α phase boundary as a vertical line at 16% tin exceeding from just below 600°C to room temperature. Annealing at or above 500°C

followed by slow cooling retains 13% to 16% of tin in solid solution, the exact amount retained being dependent on the time and temperature.

The addition of tin to about 8% significantly increases the strength as well as ductility of copper but results in a steep drop in ductility.The strength falls drastically at 25% Sn, when the structure contains too much brittle δ phase. Thus, tin content above 25% is less important for industrial applications, rather they are only for academic interest. The presence of hard eutectoid in the cast structure ensures a high resistance to wear and abrasion. 10% Sn alloy is best antifriction material, and is widely used as a ball-bearing alloy [2].

Cast tin-bronzes invariably show pronounced coring as there is a wide separation of the liquidus and solidus curves, and the diffusion takes place very slowly. By powder metallurgy route we can avoid the coring by proper selection of sintering temperature and time.

2.2 P/M Processing

Powder metallurgy (P/M) is the study of the processing of metal powders, including the fabrication, characterization, and conversion of metal powders into useful engineering components. P/M has the distinction of being at the same time one of the oldest and one of the most modern methods known for the fabrication of metal articles. In prehistoric times, P/M techniques were used to process metals with melting points above those attainable (or, in some instances, practical) by means of the technology which then existed. But, with the advancement of the civilisation P/M also developed rapidly, especially in the last few decades. Nowadays, P/M is the most promising and emerging field to produce materials with novel properties which cannot be produced by any other technique.

The P/M processing sequence involves the application of basic laws of heat, work, and deformation to the powder. It is the processing which changes the shape, properties and structure of a powder into a final product. The P/M manufacturing process can be looked at as consisting of three basic steps:

(a) Powder mixing

(b) Powder compaction

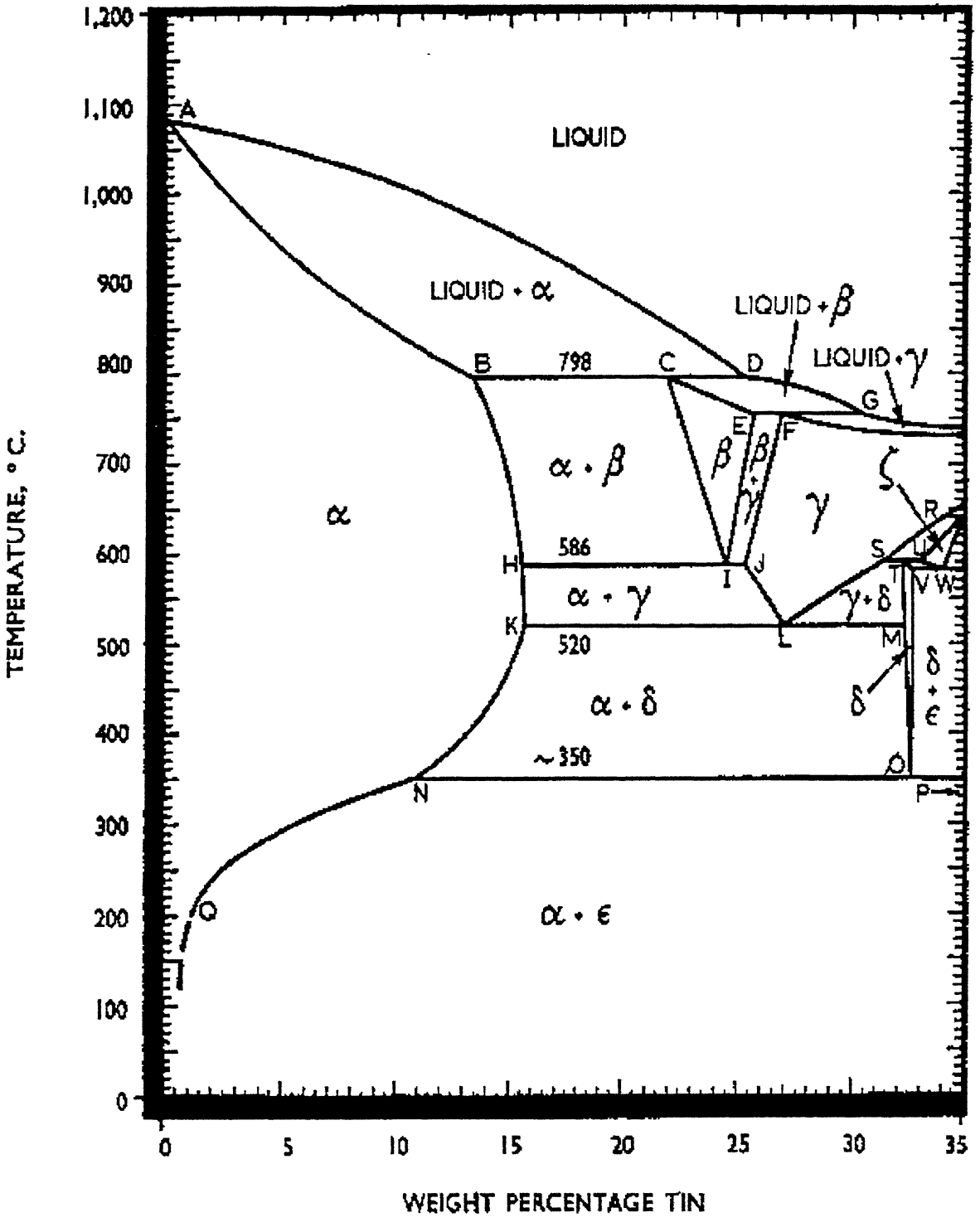

Figure 2.1. Copper-Tin Equilibrium Diagram [1].

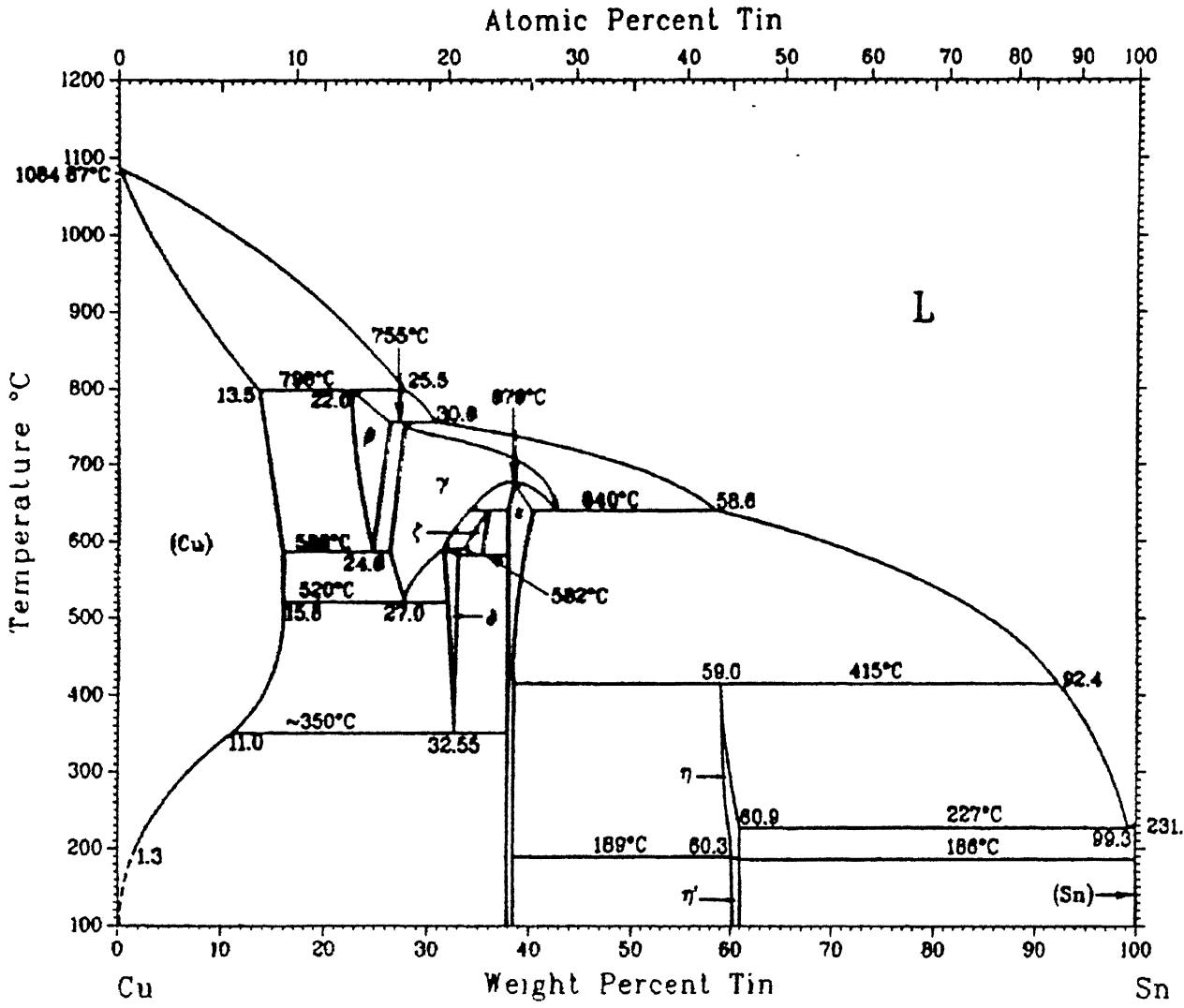

Figure 2.2. Copper-Tin Equilibrium Diagram [2].

(c) Consolidation or sintering

Metal powders can be produced by physical, chemical and mechanical methods. Both elemental and alloy powders are produced in substantial quantities by the process designated 'atomization'. In this process a stream of molten metal is broken up into droplets which are rapidly quenched to powder by high velocity jets of either water or gas. Powders of high purity are produced electrolytically. The behaviour of powder during the subsequent consolidation process is determined by both particle and bulk properties. A powder is characterized, therefore, not only by chemical composition but also particle shape, size and surface chemistry and in bulk by compressibility. Powders are blended to meet the required specifications and mixed with a lubricant – usually a metal stearate – which aids compaction. The compression of the powder in the closed die reduces the voids between the particles.

The pressed compact is given a thermal treatment designated "sintering" under a protective atmosphere or in vacuum, during which the lubricant is evaporated and porosity is reduced by metal transport involving surface and volume diffusion. This leads to chemical bonding of the particulate. The driving force for sintering is the reduction in total system energy. This occurs by the formation of interparticle bonding and removal of solid-vapour (pore) interfaces. As sintering proceeds, the original inter-connected porosity is reduced, closed pores are formed, and the overall shrinkage is controlled to ensure the final dimensions of the compact come within the required engineering tolerances. Variations on the foregoing process are made to meet particular product requirements.

Advantages of P/M

The development of P/M is due to its great advantages over other methods. The P/M process is many times competitive than other fabrication methods like casting, stamping or machining and avoids the casting defects such as blow holes, shrinkage and inclusions [3]. Through powder metallurgy processing, it is possible to produce those alloys which aren't possible by other techniques. P/M is the choice when requirements for strength, wear resistance or high operating temperatures exceed the capabilities of die

casting alloys. Processing of refractory metal and alloys fall in this group. P/M alone can produce alloys made from metal insoluble in each other, which is not possible by ordinary methods [4].

Through P/M, non-metallic components can be incorporated into a metal base (e.g. Al_2O_3 in the matrix of Cu), which can't be accomplished by other means. A special advantage is the possibility of obtaining porous materials with a controlled porosity, which is impossible to achieve by melting and casting. This property is fully exploited in preparing bronze based bearing. In the subsequent sections this will be discussed in details. P/M enables products to be made from both the heavy metals (tungsten, uranium) and the light metals (beryllium, porous aluminium).

P/M also makes it possible to obtain metals and alloys of high purity (uncontaminated by material from the furnace lining or by deoxidation), unlike the metal produced by conventional processes.

An essential advantage of P/M is its ability to provide finished parts without machining. This makes P/M a competitive technique for mass production scale, as it not only saves time but also results in higher material utilization (>95%). So, the basic advantages of P/M process can be summarised as follows:

- Metal powders are high purity materials
- Close dimensional tolerances can be maintained
- High volume process with excellent reproducibility
- Quality control is inherent in the process
- Low labour input
- Machining is eliminated or reduced
- Scrap losses are eliminated or reduced
- Segregation is avoided
- Controllable porosity and density can be precisely controlled
- Complex immiscible metals
- Complex shapes can be produced
- High material utilisation (~ 98%)

Drawbacks of P/M

The drawbacks of P/M, which render its use difficult and restricted, ought to be mentioned alongside its advantages. The first drawback of P/M is the cost of high purity metal powders. In the manufacture of products from metal powders, the impurities contained in them go over into the end product, and therefore it is necessary to use powders of the highest purity. The lack of simple methods of obtaining alloy powders – of steels, bronzes, brasses, etc. also impose some restriction in the use of P/M. Articles made out of metal powder, as a result of their porosity, an increased tendency to oxidation, moreover oxidation may occur not only on the surface but also throughout the whole body of the article. P/M products processes comparatively poor mechanical properties such as, impact strength, elongation etc because of the presence of porosity. The presence of porosities also decrease the thermal and magnetic properties of the products. If blend of two materials with large difference in density are used for P/M processing then problem of segregation may occur. In many case depending on the system used, shrinkage or expansion occur after sintering. To get dimensions conforming to the required specifications in the end products, special care should be taken in manufacturing the pressing die. It is unprofitable to manufacture articles in small quantities on account of the high cost of dies. But inspite of all the limitations the role played by P/M in technology is extending more and more [5]. Table 2.1 provides a brief summarization of the key points of contrast between powder metallurgy and other production routes.

Applications of P/M

Because of its inherent advantages, nowadays P/M products are used in a wide array of applications ranging from washing machines, refrigerators, airconditionar, compressors, bicycles, lawn mowers, farm machinery, industrial hydraulic equipment's, data processing equipment, office copiers, postage meters, microelectronics, thermal management, computers etc. This list is increasing day by day. Table 2.2 summarizes the applications of P/M in several fields.

Table 2.1. Comparison of P/M and Competitive Production Techniques.

Technique	Advantages versus P/M	Disadvantages versus P/M
Cold forming	Faster production Higher strength Good surface finish	Lower precision Shorter tool life Limited materials
Extrusion	Long parts Smooth surface Rapid production	Constant cross section Lower precision High energy consumption
Stamping	Flat, high precision High production rates Large area parts Precise feature location	Single level, thin parts only Limited materials Waste, rough edges Small features are difficult
Casting	Widely employed technique Small to large size range Low set-up cost	Not useful for refractories Flashing, parting line Heterogeneous, pores, defect
Hot forging	High mechanical properties Complex shapes and large sizes Fast production	Flash and material waste Poor dimensional control Inclusions and blemishes
Machining	Most all materials and shapes Used for wide size range High precision Short lead time, no tooling	Waste Low productivity Nonuniform properties Costly, labour intensive

Table 2.2. Applications of P/M.

Applications	Materials	Requirements
Automotive	Fe-C-Cu, Fe-C, Fe-C-Ni, Fe-C-Ni-Mo	Light weight, precise dimension, shape complexity
Electrical: *(i) Electrodes* *(ii) Electrical contacts* (iii) *Superconductor*	 Cu-Al_2O_3, Cu-Cr, W-Cu, WC-Cu Ag-W, Ag-Mo, Ag-Ni, Ag-Ni-C, Ag-WC, Ag-CdO Nb_3Sn, Nb_3Al, Nb-Ti, Nb_3Ge	 Tailored thermal properties, good conductivity
Magnetic	Fe-Si, Fe-P, Fe-Ni, Ni-Fe-Mo, $SmCo_5$	Magnetic performance, environmental resistance
Aerospace	*Superalloy:* IN-100, Rene 95, MA 754, MA 6000, MA 956 *Aluminium:* Al-Cu-C, Al-Mg-C, Al-Li-Cu, Al-Fe-Cr, Al-Ni-Co *Titanium:* Ti, Ti-6Al-4V, Ti-6Al-6V-2Sn, Ti_3Al	High specific modulus, fatigue and fracture strength, light weight, shape complexity, creep resistance, dimensional precision

Medical	Co-Cr-Mo, Ti-6Al-4V, 316L	Uniform alloying, corrosion resistance, light weight
Dental	Ag-Sn-Cu, Co-Cr-Mo	Aesthetics, shape complexity
Nuclear	Zr-Sn-O-Fe-Cr-Ni, Zr-O-Sn-Fe-C, B_4C, Eu_2O_3	Low absorption coefficient
Cutting tools	WC-Co, Wc-TiC-Co, HSS, Si_3N_4	High wear resistance, high abrasion resistance
Porous Parts: *(i) Filters* *(ii) Bearings*	 Cu-Sn, 316L, Monel Cu-Sn, Cu-Sn-P	Small pore size, uniform pore distribution, corrosion resistance
Ordnance: *(i) Missile nose cones* *(ii) Kinetic Energy Penetrator* (iii) *Military vehicles*	 Ti, Ti-6Al-4V W-Ni-Fe, W-Ni-Cu-Fe AISI 1340, AISI 4600	Full density, net shaping

2.3 P/M Bronze

Powder metallurgy bronzes typically originate as premixes consisting of elemental copper and tin powders plus 0.5 to 0.75% dry lubricants such as stearic acid or zinc stearate. These lubricants can be mixed with the powders before pressing (i.e. admixed) or can be used as the die wall lubricant during pressing. This is necessary to reduce friction between the powder and the tooling surfaces (die cavity, punches, core rods), permitting higher effective pressures to be transmitted to the powder mass and thus yielding a higher compacted (green) density for a given applied pressure. Some structural parts, however, requiring densities greater than 7.0 g/cm^3 are fabricated from prealloyed powders, where as the theoretical density for Cu-10Sn is around 8.77 g/cm^3. Premixed and the prealloyed powders have been in use depending on the applications of P/M bronze. Due to solid solution strengthening, prealloyed powders have higher yield strengths and work hardening rates than premixed powders. Generally atomisation technique is preferred for the production of copper, tin or the prealloyed powders. Spherical powders are preferred for producing porous bronze. Gas atomisation technique is the popular technique in this respect. Water atomized powders are irregular in shape because of the comparatively high cooling rate than the gas atomization technique. For spherical samples the contact area between the particles are less, so the chance of bonding and therefore green strength is also low. But as these bronze products are generally used as porous body where the strength is not the main criteria, spherical powders suffice. For structural application strength is important and therefore irregular water atomized powder is to be preferred. Pressing load required to achieve given green densities in prealloyed powders are higher than the pressures required for elemental powder mixes. In the later sections it will be shown that by proper selection of sintering technique and by adopting a suitable sintering window, the effect of the pressure on the sintered densities for prealloyed powders can be minimised. Also the difference between the densities of premixed and prealloyed powder compacts could be minimised by increasing the sintering temperature.

Depending on applications, sintering furnace temperatures for bronze range from 350 to 870°C; total sintering time within the hot zone may range from 15 to 30 min, depending on the furnace temperature selected [6]. It also depends upon the required

dimensional change and most importantly, the presence of an optimal α-bronze in the matrix. Sintering atmospheres should be protective, preferably reducing to aid densification during sintering. Generally, reducing atmosphere is used during sintering, such as, nitrogen, hydrogen or cracked ammonia to reduce the chance of oxidation of powders. The reduction of the surface oxides of copper and tin leads to an increased diffusion rates.

It is found that the copper-tin blends of coarser powder have shown the higher growth values than a blend composed of finer powders The final dimensional change during sintering depends a lot on the powder characteristics such as shape, size, and morphology. So the proper choice of the powders plays a very important roles in terms for obtaining the desired product. Sintering is favoured by the decrease in the interfacial energy and typically leads to shrinkage due to the elimination of pores. Sintering. At elevated temperatures, the rate of mass transport is increased and this enhances diffusion. Consequently, the point contacts between the contacting particles form interparticle necks, which causes dimensional changes. However in case of bronze tin melts and goes into the copper matrix due to its high solubility in copper. This leads to the expansion of the lattice and tin sites leaves behind the pores in the microstructure. This phenomenon is called bronze compact growth.

Engineering/Production/Economic Advantages of P/M Bronze

Bronze P/M parts can be pressed and sintered to their final shape and size, usually with the desired surface finish and with no draft angles. They can also be sized to close tolerances by coining or repressing, thus eliminating much of the machining required when other metal forming procedures are used. They can be machined, plated and joined by brazing. Using commercial automatic presses, bronze P/M parts can be produced rapidly and accurately at an average rate of 1000 parts per hour [3,5,6]. Sizes can range from miniature parts smaller than the ball of a ball-point pen to bearings weighing over 100 pounds. The physical and mechanical properties of bronze P/M parts are comparable with those of cast and wrought bronze of similar composition. However, the P/M process permits a flexibility that the other processes do not possess. Parts can be produced that vary in density from the low-density required for self-lubricating bearings or filters to

almost theoretical density for structural parts. P/M parts are produced with a minimum of raw material loss and greatly reduced processing wastes improves the production economy by lowering overall cost. As a further advantage, there is no pollution of the environment in the production of P/M parts.

Applications of P/M bronze

As discussed before P/M bronze has been in use for a long time. Conventional use of bronze is as a porous body with controlled porosity. Self lubricating bearing and filters fall in this group. But with the advancement of the technology, sintered bronze is used nowadays in structural applications also. Other recent trends of bronze applications are in the area of automotive and industrial equipment. Table 2.3 gives the generalised view of P/M bronze applications. Figures 2.3 and 2.4 show different bronze bearings and filters used industrially. Figure 2.5 gives us the general idea about the different P/M bronze parts which are in use nowadays.

Properties of P/M Bronze

P/M bronze has got good mechanical strength and hardness which are quite comparable with the cast product. Comparison of different mechanical properties of cast, wrought and P/M bronze are given in the Table 2.4. Typically, P/M bronze inherently has some porosities. This leads to decrease in the electrical conductivity. Bronze produced by P/M shows reasonable working properties. The main attractive feature of P/M bronze is its excellent corrosion resistance properties. It shows neutral behaviour in almost all kind of environment. P/M bronze is featured by the presence of well distributed porosities throughout the matrix. These pores are subsequently infiltrated by oil, which excellent bearing characteristics. Bronze can be easily soldered to other alloys also.

Table 2.3. Applications of P/M bronze [8].

Applications	Equipment
Self-lubricating bearing:	
(a) Home appliance	Dishwashers, cloth dryers, washing machines, vacuum cleaners, refrigerators
(b) Farm and lawn	Tractors, combines, cotton pickers, lawn mowers, chain saws
(c) Consumer electronics	Phonographs, record changers, tape recorders
(d) Business machines	Typewriters, computers, copiers
Automotive	Starters, light generators, oil and water pump, heaters, air conditioner, window raisers, power seat adjusters
Structural parts	Paint-spraying equipment, outboard motors, automobile clutches
Industrial	Textile machines, packaging machines, electric fans, drills, saws

Table 2.4. Typical properties of 90Cu-10Sn bronze processed by different routes [8].

Property	Wrought	Sand cast	P/M
Tensile strength, MPa	420-455	300-325	130-150
Yield strength, MPa	180-195	150-160	80-90
Elongation, %	30-60	15-20	10-20
Hardness, HRB	97-100	80-85	-

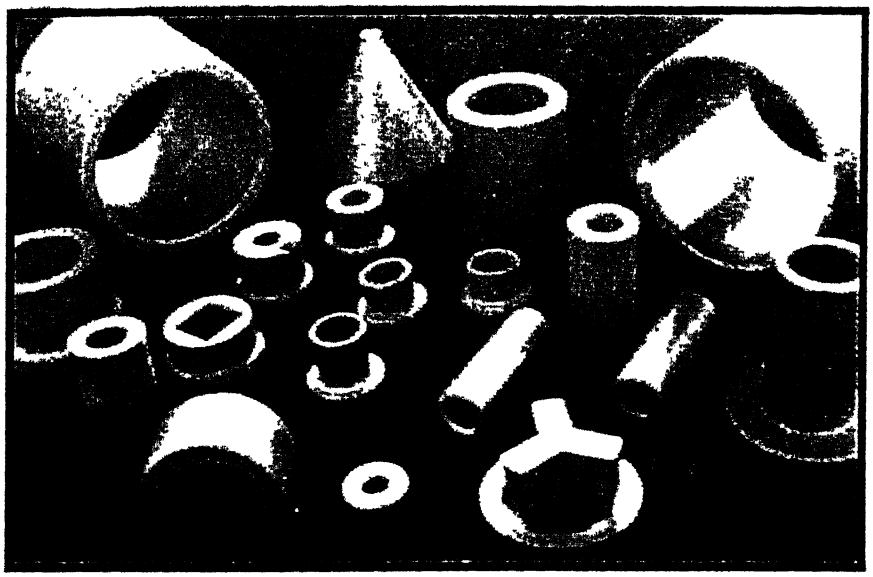

Figure 2.3. Assorted P/M bronze bearings [5].

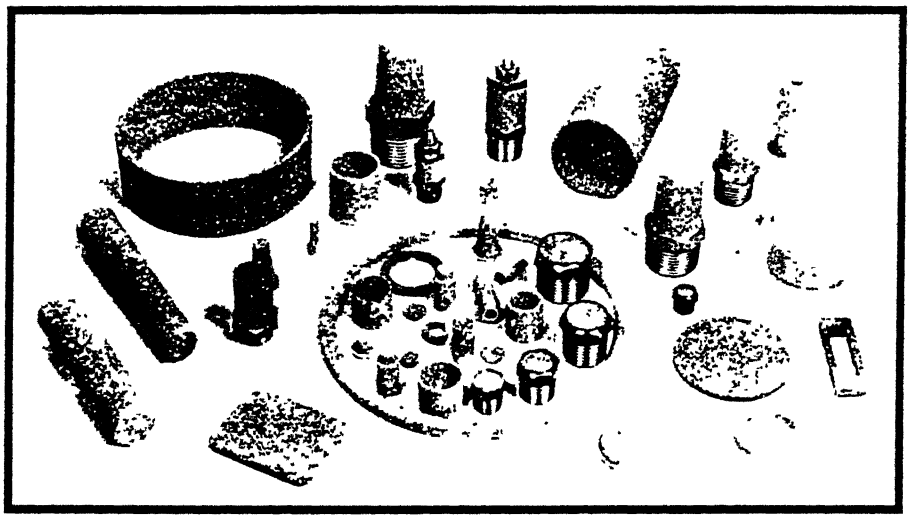

Figure 2.4. Assorted filters made from P/M bronze [6].

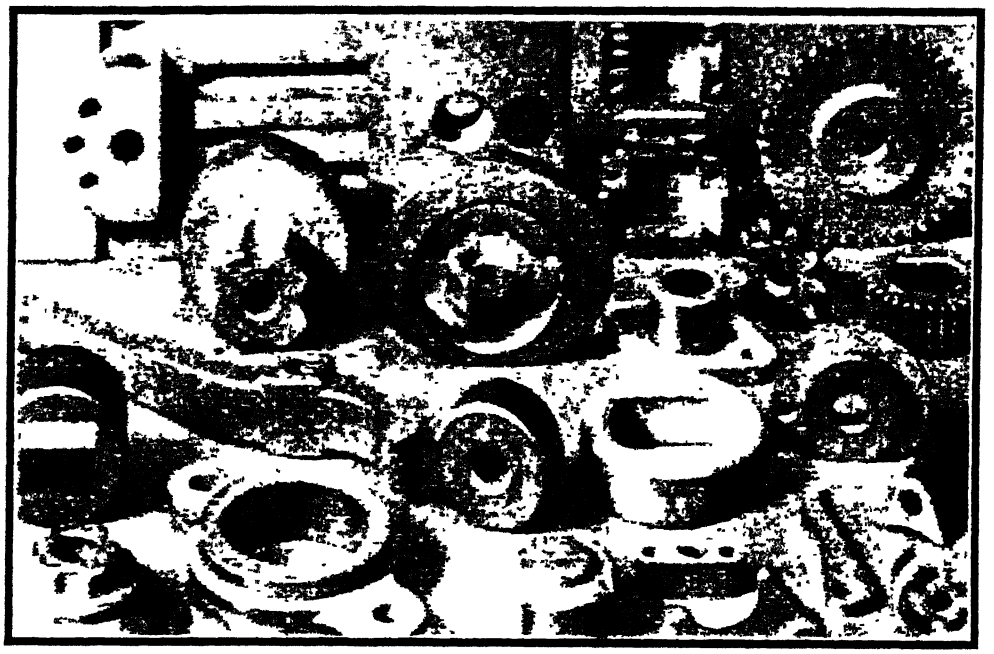

Figure 2.5. Assorted P/M bronze parts [5].

Structural parts

By any reckoning, this is by far the largest group. Nowadays, the trend is shifting towards the use of inexpensive bronze in structural applications nowadays. Excellent corrosion resistance and ease of fabrication makes the P/M bronze attractive in the structural applications. In general such parts do not have mechanical properties superior to those of equivalent parts made by forging or machined from wrought bar, often the reverse, but they are entirely suitable for the required duty. They often have advantage over forgings in dimensional accuracy (± 0.1%), but in a large number of cases, the main justification for their use is economic - i.e. P/M is a cheaper production process. Recently, however, developments have taken place that will contribute towards the cost-effectiveness [7]. It is now possible to produce sintered parts with properties equal to and even superior to those of parts made by more traditional routes. Application of P/M bronze in structural parts is new area of development. Actually modern research has been carried out to replace the conventional structural materials by bronze. P/M bronze are selected for these applications because of its excellent corrosion and wear resistance properties. They are generally produced by methods similar to those used for self-lubricating bearings. These parts are generally used in automobile clutches, copiers, outboard motors, and paint-spraying equipment [6].

Porous Materials

Most of the metal products are porous to some extent, sintered metals more so than most, but here we are concerned with the production of parts having a significant carefully controlled porosity designed to serve a useful purpose. The chief products in the group are filters and oil-retaining bearings often referred to as self-lubricating bearings. Again the above products cannot readily or satisfactorily be produced by alternative processes.

Self-Lubricating Porous Bronze Bearings

Porous bearings are usually made of bronze by the sintering together of copper and tin powders, with or without the addition of graphite or other dry lubricants. The

advantage of porous bearing is that the pores can be filled with lubricating oil, so that the bearing requires no further lubrication during the whole life of the machine in which it is used. A self lubricating bearing must combine together several characteristics [9]:

(i) The porosity must be so arranged as to contain, and retain in use, the maximum possible amount of oil.

(ii) The porosity should be interconnected as much as possible, and it should be substantially isotropic in distribution. Not only is permeability required for the purpose of bringing the oil to the bearing surface, but it must also be possible for the oil to move axially and circumferentially within the bearing.

(iii) The bearing must exhibit some minimum strength values.

(iv) It must be manufactured to very close dimensional tolerance.

Starting materials for the fabrication of porous bearing may be mixed elemental powders of copper and tin as stated earlier, fully pre-alloyed bronze powder, or mixtures of the three. If pre-alloyed bronze is used shrinkage on sintering normally results, while with elemental powder a significant compact growth can be obtained. One of the objective of this study is to investigate the densification behaviour and porosity level as a function of the proper novel sintering technique and sintering temperature. The control over the porosity could be enhanced which is not possible by normal sintering technique. Clearly it is possible by using the appropriate proportion of pre-alloyed bronze to achieve a situation in which the dimensions of the finished part are approximately the same as those of the die. In addition to the normal lubricants, graphite is often added to the mixes used for porous bronze bearings. For the present study, no graphite was added with the powders. It is essential that the pores form an interconnected system of controlled size and volume, so that oil is supplied to the entire bearing surface. The rate of oil supply automatically increases with temperature and, therefore, with increasing speeds of rotation, to achieve optimum working conditions. For most applications, the porosity should lie between 20% and 35% by volume, the upper limit being imposed by strength considerations which varies inversely with its porosity [7].

Additionally, porous bearings made of iron, iron copper, or iron mixed with bronze may be used in non-critical applications, but 90Cu/10Sn bronze is the most widely used, having a low coefficient of friction, high wear resistance, and also resistance to

seizure with the steel shaft. The processing steps include compacting at between 150 and 600 MPa, sintering between 750 to 870°C for about 5 to 30 min, followed by sizing and oil-impregnation. Typical atmosphere for sintering is reducing atmosphere, such as dissociated ammonia or hydrogen gas. Very high production rates are possible because of the short sintering times required. Typical applications of self-lubricating bearing includes- automotive components, home appliance, farm and lawn equipment, consumer electronics, business machines, industrial equipment's etc.

There are some advantages as well as some disadvantages of the porous bronze bearings. The advantages are: (a) self-lubricating, (b) minimum oil drip, (c) use in inaccessible position, and (d) inexpensive. The limitations are: (a) impact and fatigue loading, (b) frictional losses, (c) size of bearing, (d) shape, and (e) composition [5].

Filters

Filters constitutes one of the major applications for porous P/M parts. The ability to achieve close control of porosity and pore size is the main reason filters are fabricated from metal powders. Controlled porosity is employed in the manufacture of metal filters and diaphragms which have the advantage over their ceramic counterparts of higher strength and resistance to mechanical and thermal shock. Powders used in the fabrication have got a narrow range of particle size. Perhaps the most commonly used filter elements are made of bronze (89/11 Cu/Sn), and spherical powder are used. There are two kinds of pores present in the filters, open and interconnected. For filters, these interconnected pores should be as high as possible (25-40%). The major advantage of P/M bronze materials over other porous metals is cost.

P/M bronze could be obtained with the tensile strength from 20 to 140 MPa and appreciable ductility, upto 20% elongation. P/M bronze also has the same corrosion resistance as cast bronze of the same composition and thus can be used in a wide range of environments.

For making the P/M filters prealloyed spherical bronze particles are used and they are generally produced by gas atomisation technique. To produce filters with the highest permeability for a given maximum pore size, powder particles of a uniform particle size must be used. The filter profile is formed by a loose packing of the powder in the mould

and the inherently poor compressibility of spheres is no disadvantage. Where products are required to have limited or localised porosity, conventional pressing is necessary and irregularly shaped particles are more suitable [7]. During sintering the filters shrink slightly. To avoid excessive shrinkage, filters from powders with the fine particle size require low sintering temperatures in the neighbourhood of 815°C.

Metal filters are widely used for the filtration of fuel oils, chemical solutions and emulsions. They are also efficient in separating liquids of varying surface tension, and have been successfully applied to jet engine fuels, where water is removed at the same time as the fuel is filtered. Similar devices are widely used for sound damping on air compressors and the like. Bronze filter materials can be used as flame arrestors on electrical equipment operating in flammable atmospheres, where the high thermal conductivity of the bronze prevents ignition. They can also be used as vent pipes on tanks containing flammable liquids. In these applications, heat is conducted away rapidly so that the ignition temperature is not reached [6].

2.4 Sintering

Sintering may be considered the process by which an assembly of particles, compacted under pressure or simply confined in a container, chemically bond themselves into a coherent body under the influence of an elevated temperature. The temperature is usually below the melting point of the major constituent [3].

It was very difficult to put the theory of sintering or to give the exact model of it because many changes take place simultaneously during the sintering itself. Some of these changes may be unique to the heating of a porous material, while others are typical of the effects of elevated temperatures on any polycrystalline material [10]. The subject of sintering is best approached from the viewpoint that any green compact or mass of loose powder is at the very least a two phase material – porosity and solid material. Each has its own morphology; that is, size, shape, distribution and amount. Densification or shrinkage of the sintered part is very often associated with all types of sintering. Sintering can also take place without any shrinkage; expansion or no dimensional change is also possible. Having a slight shrinkage to compensate for the elastic expansion of the green compact upon ejection from the die, leading to no net dimensional change with respect to

the die dimensions, is an extremely advantageous approach. Figure 2.6 lists various sintering processes and the subdivisions in terms of the key processing parameters [11].

2.4.1 Solid-State Sintering

The driving force for solid state sintering is excess surface free energy. Sintering is a complex process and for any given metal and set of sintering conditions there are likely to be different stages, driving forces and material transport mechanisms associated with the process.

2.4.1.1 Different Stages of Solid-State Sintering

One of the basic aspect of sintering is that it usually takes place at a constant temperature (or at least a major part of it) and the time is varied to achieve certain result. Consequently, it becomes useful to attempt to describe the stages of sintering in terms of their relative order with respect to time. In Hrischhorn's [10] discussion of this subject, sintering is divided into six stages:

(i) Interparticle bonding among particles
(ii) Neck growth
(iii) Closure of pore channels
(iv) Rounding of pores
(v) Pore shrinkage (densification)
(vi) Pore coarsening

However, the problem in describing the different stages is that, the sequence and extent of the stages depends on the green compact. Green compact may contain high amount of porosities where the pores are interconnected or they may be near to theoretical density. In the second case the pores are isolated. As a result of that the stage two and three would be minimised or entirely absent. We will now describe the six stages individually in some details.

Interparticle Bonding

Bonding takes place very early in the sintering process as the material heats up. Transport of atoms at particle contact points leads to the establishment of physical

Sintering Pathways

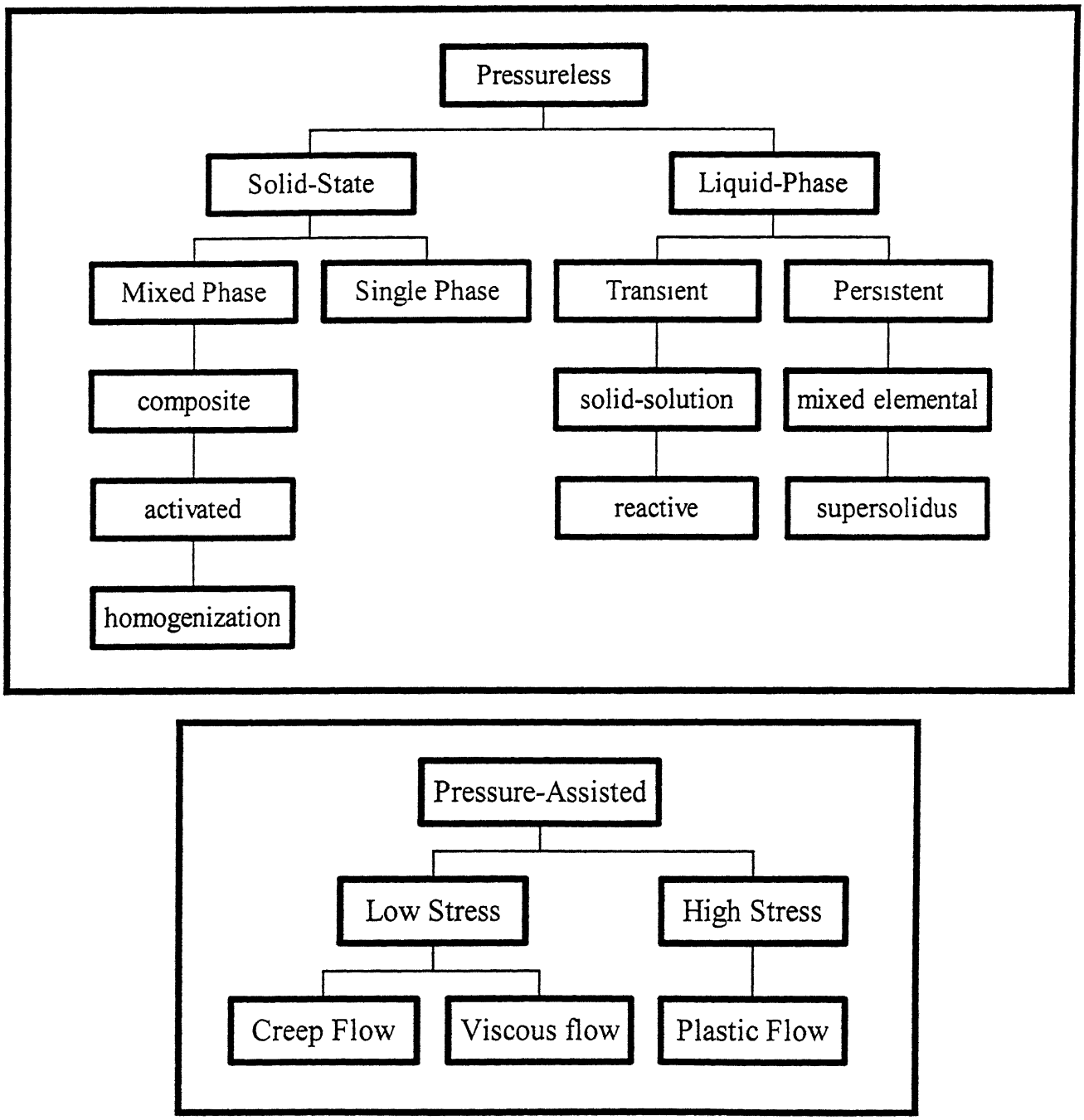

Figure 2.6. Map to sintering process and the subdivisions in terms of the key processing Parameters [11].

bonding and grain boundaries at these points. The essential condition for this bonding is the intimate contact between the particles. However, there are, of course, many such place in a pressure formed compact, but even in a mass of loose powder there is contact between particles sufficient in magnitude to allow bonding. These initial bonds are developed very rapidly – even as the compact is being heated to temperature. This stage of sintering does not lead to any dimensional change of the material. But bonding in this stage imparts a high degree of coherency and integrity to the material, which is extremely important. This can be proved by the achievement of high strength and hardness even after relatively short exposures to an elevated temperature. It is quite obvious that, greater the original density of the material, the greater the amount of contact area and potential grain boundary area. Moreover, this stage plays an important role in the production of high porosity material. It should be remembered that in such case, the sintering process may only lead to this one stage of sintering only.

Neck Growth

It is the second stage of sintering and is related to the first stage of initial bonding. Continuing mass transport leads to the development of distinct "necks" between particles, growing from the initial bonds. The newly formed bond areas are termed necks. In the second stage, the neck grows in size. This stage greatly increases the strength of the compact but does not involve any densification. The interconnected porosities, which are present as somewhat irregular channels are turned into smooth channels after this stage. Although neck growth is generally accepted to take place rather rapidly and early in the sintering process, in fact its continuation may lead to its overlap in some later stages. This is generally seen in stage three and five. Though spherical particle model is assumed for simplification, it is to be remembered that, the original powder systems are much more complex. Neck growth is also illustrated in terms of a three sphere model in Figure 2.7.

Pore Channel Closure

This stage represents the major change in the nature of the porosity in the sinter mass. Continued neck growth can cause pore channels within the compact to be closed, leading to isolated porosity. It is very important to control this event in sintering powder

metallurgy products which utilized interconnected porosity – for example, filters, self-lubricating bearing, etc. However, pore shrinkage in stage five can also lead to channel closure by causing new contacts to be formed among pore surfaces. As a result, this stage may proceed for some time and overlap stage four and five.

Pore Rounding

Pore rounding may be considered a natural consequence of neck growth. As neck growth reaches an advanced stage, the material transported from the general particle surfaces to the neck regions results in a smoothing of the pore walls (reduction of surface area). No pore shrinkage is necessary for pore rounding, although it too may be taking place during the same time. Though the rounding process pertains both to isolated and interconnected porosity; however it is usually considered with respect to the former. It is possible to achieve almost perfectly spherical pores by allowing sufficient time at suitable temperature. This can be an important structural change with respect to improving the ductility and toughness of the sintered compact. This stage of sintering is illustrated by the idealised three-sphere models in Figure 2.7. But, it should be noted that, it is possible to carry out sintering for a given material without this stage taking place to any significant degree.

Pore Shrinkage

As sintering progresses, the pores in the compact may begin to shrink in size and decrease in number, resulting in densification. this stage must involve extensive diffusion and annihilation of vacancies. Not all porosity can be eliminated during this stage of sintering; some residual pores will be left (particularly inside of grains) even after very long sintering times. For single component systems densification may be equivalent to pore shrinkage, but in more complex materials other processes can lead to both shrinkage and expansion. Densification in this process involve the movement of solid into the porosity and movement of any gas in the porosity to the external surfaces. Pore shrinkage becomes less important as a stage of sintering with increasing density of the green compact. An example of a sintered structure in which significant pore shrinkage has occurred is shown in Figure 2.8.

This material is Mo whose green density after isostatic compaction was 70% theoretical. After sintering at 1850°C for 9h, the density increased to 98% of its theoretical density. Note that most of the residual porosity is in the interior of grains and that the grain size is about 30 μm, which is an order of magnitude larger than the average particle size (3 μm) of the starting powder.

Pore Coarsening

This stage is not considered to be very important in most commercial sintering operations. When it occurs, it involves an increase in the size of some of the larger pores and concurrent elimination of some smaller pores. No net change in the pore volume fraction is involved, so the average distance between the pores is increased. Hence, no densification of the material is associated with this stage In many respects, this microstructural change is analogous to the precipitate coarsening which occurs during severe overaging of conventional age-hardening alloys [5].

We have discussed the sintering stages based on the three sphere model so far. But in many case, for simplification, different sintering stages are shown based on the two sphere sintering model. We have to remember that, a two-sphere geometry is a starting point for many sintering models [11]. Figure 2.9 illustrates the neck profiles for two spheres initially in point contact at various levels of densification. Volume conversion and surface energy minimization dictate a final geometry of one sphere with a diameter 1.26 times the initial diameter. The bonds between contacting particles enlarge and merge as sintering progresses. At each contact, a grain boundary grows to replace the solid-vapour interface as shown in Figure 2.9.

2.4.1.2 Sintering Mechanisms

The various structural changes that take place during sintering obviously depend on mass transport to and from various regions within the powder compact. A net decrease in free energy must be associated with sintering if these structural changes are to occur spontaneously. In a simple material, this decrease in free energy is associated with a decrease in the total surface area (and therefore surface energy) of the compact. All of the basic structural changes, such as neck growth, pore rounding, etc., lead to reduced total

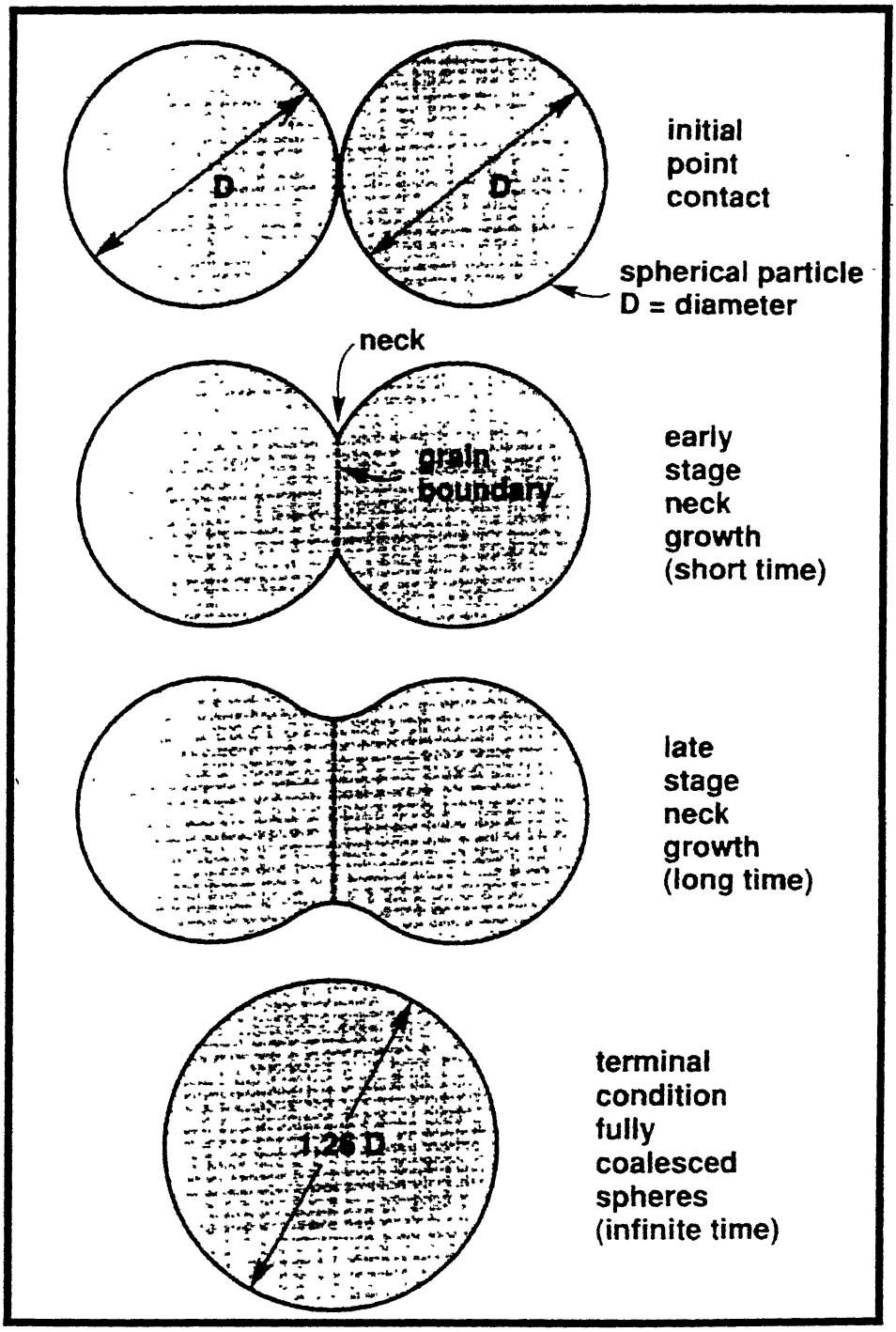

Figure 2.9. The two sphere sintering model with the development of the interparticle bond during sintering, starting with a point contact. Neck growth creates a new grain boundaries and, if time is sufficient, the two particles will eventually coalesce into a single large particle [12].

surface area within the compact. Thus it is not surprising to find that the greater the original surface area the larger the driving force for sintering – i.e. compacts of fine powders sinter faster than compacts of coarse powders [5].

Transport mechanisms determine how mass flows in response to the driving force provided by the driving force for sintering. Total mass transport can be the summation of many stages. They are generally classified as evaporation and condensation, surface diffusion, grain boundary diffusion, volume diffusion etc. Nabarro–Herring mechanism and creep mechanism are also very helpful in explaining various consequences during sintering. We will discuss those mechanisms in brief in the following sections. Probably the most dominant mass transport mechanism involved in normal sintering is solid-state diffusion through the crystalline lattice and via short-circuit paths such as particle surface and grain boundaries. In metals with very high vapour pressure, evaporation of material from the convex particle surfaces and subsequent condensation of these materials at the concave necks between particles is a probable transport mechanism. However, this mechanism is not considered to be particularly active in the sintering of most of P/M materials, because their vapour pressure are quite low at normal sintering temperatures. It is also possible, due to effects of surface tension at the particular necks, to promote some mass transport by self-induced plastic deformation early in the sintering cycle, when the radii of curvature of the necks are very small [13].

As sketched on the two sphere model in Figure 2.10, two classes of mechanisms, surface transport seems to be dominant. Each class is composed of several actual atomistic mechanisms contributing to the mass flow. Pore is nothing but the accumulation of the vacancies. As a result, sintering mechanisms examine the motion of vacancies as a basis for understanding pore elimination. The vacancies and atoms move along particle surfaces (surface diffusion), across pore spaces (evaporation-condensation), along grain boundaries (grain boundary diffusion), and through the lattice interior (viscous flow or volume diffusion) [11].

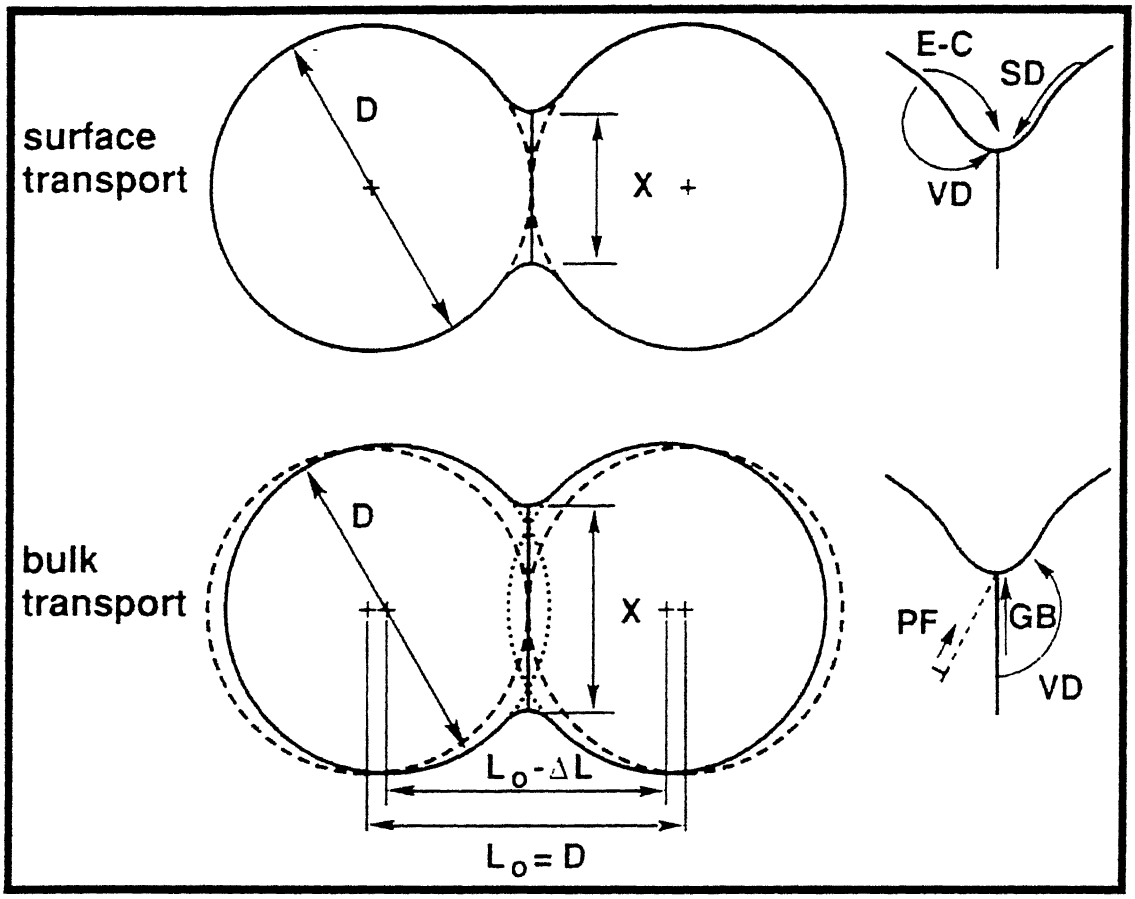

Figure 2.10. Two classes of sintering mechanisms as applied to the two-sphere sintering model. Surface transport mechanisms provide for neck growth by moving mass from surface sources (E-C, evaporation-condensation; SD, surface diffusion; VD, volume diffusion). Bulk transport processes provide for neck growth using internal mass sources (PF, plastic flow: GB, grain boundary diffusion; VD, volume diffusion). Only bulk transport mechanisms give shrinkage with the approach of the two particles [12].

Evaporation and Condensation

Vapour transport during sintering leads to the repositioning of atoms located on the particle surface, without densification. Across the surface evaporation occurs and transport occurs across pore space, leading to condensation on a nearby surface. The vapour pressure is high in a convex surface compared to neck regions or concave regions. As a result it is possible in some systems for material to be transported as vapour to neck region. Neck growth, pore rounding and pore channel closure can be accomplished by this mechanism. No reduction in pore volume occurs here. The distance between two particles also remains same. The process operates till the difference in curvature remains. Kuczynski [14] and Kingery and Berg [15] were the first to treat this as a sintering process. The equilibrium vapour pressure P depends on absolute temperature T with an Arrhenius dependence (thermally activated),

$$P = P_0 \exp\left(-\frac{Q}{kT}\right) \qquad \textbf{(2.1)}$$

where P_0 is a pre-exponential constant, Q is the activation energy for evaporation, and k is the Boltzmann's constant. Higher temperatures give a higher vapour pressure and more vapour phase transport, since the flux depends on the evaporation rate.

This mechanism would only be important for a material whose vapour pressure is relatively high so that significant amount of materials are transported. Except Zn and Cd, most of the common metals have low vapour pressure. A quantitative description of the kinetics of the neck growth for spherical particles resulting from evaporation and condensation of the vapour in the neck region is given by:

$$x^3/a = (9\pi/2MRT)^{1/2} V_0 p_0 t \qquad \textbf{(2.2)}$$

where, M = molecular weight of the material

t = time of sintering

The equilibrium vapour pressure p_0 increases exponentially with increasing temperature. Hence, it is seen that neck growth by this mechanism would increase with increasing temperature, increasing intrinsic vapour pressure of the solid and increasing surface tension [10]. Materials that have been reported to exhibit a large sintering

contribution from evaporation-condensation are NaCl, PbO, TiO_2, H_2O, Si_3N_4, BN, and ZrO_2.

Volume Diffusion

Three kinds of diffusion mechanisms is believed to be operative in case of sintering. They are surface diffusion, grain boundary diffusion and volume or lattice diffusion. Volume diffusion, or lattice diffusion, involves the motion of vacancies through a crystalline structure as sketched on the two-particle geometry in Figure 2.11 [11].

Three factors are dominant with respect to the volume diffusion rate: temperature, composition, and curvature (or pressure). However, there are number of precise mechanisms invoking volume diffusion. In "vacancy exchange" mechanism, the atoms moves into vacant lattice sites, i.e. vacancies. The magnitude of this mass transport is described by the diffusivity D of the particular atomic species within a given crystalline solid; and this is given by:

$$D = D_0 \exp(-Q/RT) \tag{2.3}$$

where, D_0 = pre-exponential material constant

Q = activation energy for diffusion

R = gas constant

T = absolute temperature

The activation energy is associated with the energy needed to create and move a vacancy in the lattice. The diffusivity D may refer to the diffusion of atoms in a pure metal, referred to as self-diffusivity, or the movement of an impurity or alloying element in a particular solid [10].

One way in which material transport by volume diffusion takes place consists of the existence of vacancy concentration potentials in the solid, and the movement of vacancies from regions of high concentrations to regions of lower ones. The atoms then move in the opposite directions. For a particular diffusional mechanism explaining one or

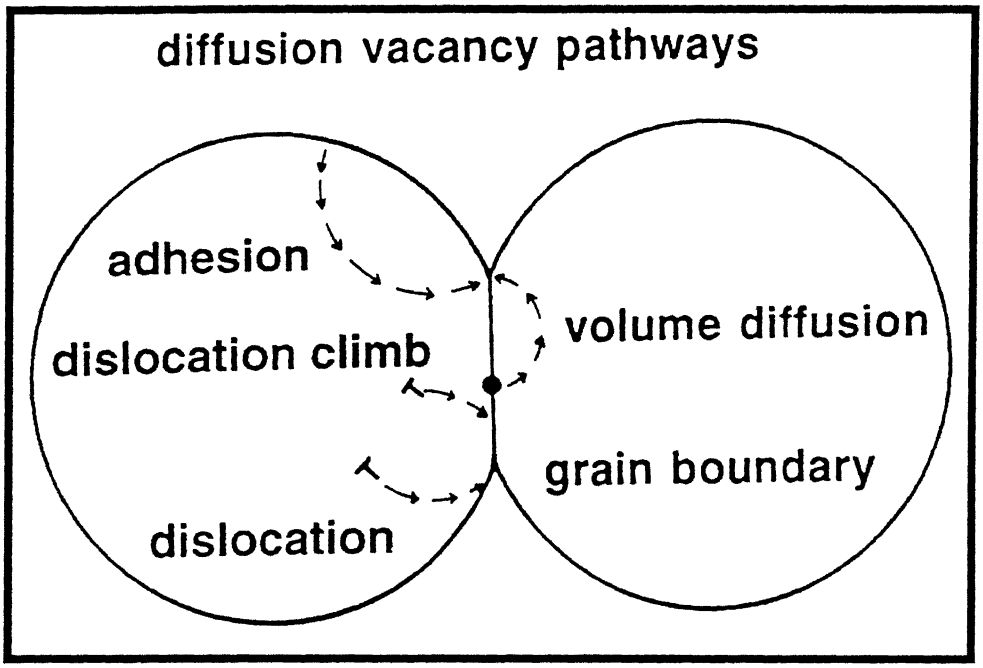

Figure 2.11. Several possible volume diffusion processes are illustrated on this two-particle sintering model. The candidate paths involve vacancy flow (and atomic flow in the opposite direction) from dislocations, free surfaces, and grain boundaries [11].

more stages of sintering, the main interest is focused in the regions of excessive vacancy concentrations (sources) and those where vacancies are deposited or absorbed (sinks). The major variations of the volume diffusion mechanism are summarized in Table 2.5 [10].

Dislocations plays an important role in controlling the volume diffusion. Dislocations might provide vacancies that travel through the lattice to particle surfaces. Finally, the vacancies can be emitted or annihilated by dislocations via a process termed dislocation climb. It involves co-operative action by both dislocations and vacancies [16]. But a point to be noted here that, the grain boundaries may act as either source or sinks for vacancies because of the stress acting on them. The Nabarro-Herring viscous creep theory of deformation is based on this effect and may be applied to sintering [10]. Deformation is a consequence of the higher vacancy concentration at boundaries under a tensile stress as compared to ones under a compressive stress, and the diffusion of atoms through the lattice in the opposite direction. For a sinter mass with high amount of grain boundaries, this mechanism might lead to neck growth and pore shrinkage. This is not necessary that, the load should always come by external application, but they may come from gravitational force acting on them. Residual stress resulting from compaction or stress fields associated with the pore surfaces have also a contribution on this mechanism. It has been found that this mechanism of plastic deformation tends to be operative at very low stresses and high temperatures. Volume diffusion is a controlling process in the sintering of many narrow stoichiometric compounds, including the oxides of beryllium (BeO), calcium (CaO), chromium (Cr_2O_3), copper (CuO), titanium (TiO_2), uranium (UO_2), and yttria (Y_2O_3).

Surface Diffusion

Surfaces of crystalline solids are usually not smooth but consist of defects that include ledges, kinks, vacancies etc. Surface diffusion involves the motion of atoms between these sites. Surface diffusion is an initial contributor to the sintering of almost all materials. Its importance was first recognised in the work of Kuczynzki [14] and has subsequently been the subject of considerable theoretical analysis.

Table2.5. Volume diffusion paths and their sintering effects [10].

Case	Vacancies from this source	Moving to this sink	Lead to these stages
I	Concave neck surfaces	Convex particle surfaces	Neck growth Pore rounding
II	Concave neck surfaces	Grain boundaries	Neck growth Pore rounding Pore shrinkage
III	Concave neck surfaces	Dislocations	Neck growth Pore rounding Pore shrinkage
IV	Small rounded pores	Larger pores	Pore coarsening
V	Small rounded pores	Grain boundaries	Pore shrinkage Pore coarsening
VI	Small rounded pores	Dislocations	Pore shrinkage Pore coarsening
VII	Dislocations	Grain boundaries	Pore shrinkage Pore coarsening
VIII	Dislocations	Particle surfaces	Neck growth Pore rounding
IX	Grain boundaries	Grain boundaries	Neck growth Pore shrinkage

Surface diffusion is characterized by several atomic movements. Generally in this step the migration of atoms occur over the external surfaces. Exchange takes place between the surface atoms and the surface vacancies. As we know that the atoms of the surfaces are loosely bonded. As a result the diffusivity through the surface is higher than the grain boundary diffusivity. It should be noted that the surface diffusion rate is affected by the presence of dopants in atmosphere. This step does not contribute to the shrinkage phenomenon. Neck growth is the natural consequence of this stage.

Surface diffusion becomes an active process during heating to the sintering temperature. A typical surface diffusion event involves three steps; any one can be rate controlling. In the first step, an atom breaks away form the existing mechanical bond. The population of the kinks depends on the surface orientation and temperature. After the bond breaks, the atom moves faster across the surface. Finally, the atom reattach at an available surface site, possibly again at a kink. There is an activation energy associated with the slowest step that is known as the surface diffusion activation energy, which often changes with the temperature. Usually, the activation energy for surface diffusion is less than that for other mass transport process. Consequently, it initiates at lower temperature in comparison with other sintering mechanisms. As the sintering progresses, the importance of surface diffusion declines, although it may play a role in affecting pore mobility during grain growth. The major role of surface diffusion in sintering is quite important because of the potential use of manipulation of the sintering atmosphere to promote sintering. boron and several covalent ceramics such as SiC exhibit surface diffusion dominance. Other example include very fine alumina powders at low temperatures, and low temperature sintering of MgO, FeO, TiO_2, Ag, Fe, Au, Cu, and Pd, especially when the particle size is small.

Grain Boundary Diffusion

This mechanism is important to the sintering densification for most metals and many compounds. It has been suggested that vacancies may move directly on to grain boundaries in contact with the neck surface and other pore surfaces. The activation energy for the grain boundary diffusion is usually intermediate between that for surface diffusion and volume diffusion. Though the grain boundary is rather narrow, but it is still

an active transport path. However, the net effect on sintering depends on the number of grain boundaries per unit volume.

A theoretical description of grain boundary diffusion-controlled sintering was first presented by Coble [17]. The grain boundaries usually formed between adjacent particle of the sinter mass. The mass flows along the grain boundary, to be deposited at the bond between particles [18]. The vacancies might move along the grain boundaries to external surfaces or perhaps in some way accommodated at locations along the boundaries within the solid. This will result neck growth, pore rounding or pore shrinkage.

Naturally, in most sinter masses both volume and grain boundary diffusion paths are possible. An analysis of diffusion data indicates, however, that grain boundary diffusion would become more important or effective with decreasing sintering temperature [10]. This is a consequence of two factors: (a) at all times there is much more lattice than grain boundary volume available for diffusion; (b) because the activation energy for grain boundary diffusion is usually considerable less than that for volume diffusion, as stated above. Grain boundary diffusion-controlled sintering is evident in many materials as they undergo densification. example systems where this is true include Ni, W, Mo, Fe, Cu, and various ferrous alloys. Examples of compounds include ZrO_2 with Er_2O_3 additives, Ni_3Al with small quantities of B, and Al_2O_3 with TiO_2 additives.

2.4.1.3 Limitations of Solid-State Sintering

As the whole solid-state sintering process occur in solid-state, the diffusion rate is slow compared to the other sintering process. So, this process takes more time than others. When we are considering the theory of solid-state sintering, many assumptions have been made to simplify the situation. But in actual process, these assumptions may not be valid, which results into a serious problem in predicting the process. Generally the sintering concepts deals with the powders of spherical shapes that sinter under isothermal conditions. But in reality, most of the powders are nonspherical in nature with wide particle size distributions. Compaction repacks the particles, collapses large pores, and enlarge the particle contact but may introduce new defects. It should be noted that, though we are providing the holding time at maximum temperature, most of the bonding between particles occurs prior to that. Again the assumption of isothermal conditions may

not be valid for most of the models. Actually, the compacts faces a very dynamic situations, with gradients introduced by thermal stresses and atmospheric interaction. In many cases the gradients have a significant effect on the sintering process.

Because of these problems, the available diffusion data does not always reflect the actual sintering processes [19]. In industry the heating rate is very slow and sintering time is short also. This will lead to the errors in actual calculation. However, these problems have been reconciled by the use of new computer simulation techniques that attempt to embrace all of the complexities of real sintering situations.

2.4.2 Liquid Phase Sintering

Liquid phase sintering is characterized by the presence of one or more than one liquid phase throughout or in a part of sintering cycle. The formation of a liquid phase sintering usually increases the sintering rate. Various forms of liquid phase sintering have been practiced since as early as 4000 B.C., largely in the fabrication of pottery and glass bonded ceramics, such as porcelain [11]. Modern liquid-phase sintering is traced to the development of cemented carbides, bronze bearings, and magnetic alloys during the 1920s. The tungsten heavy alloys (W-Ni-Fe, or W-Ni-Cu) in the 1930s provided an important theoretical basis of the process. Today, liquid-phase sintering, including dental porcelains, cemented carbide cutting tools, automotive connecting rods, and refractory ceramics. Some are sintered using a low-viscosity glassy phase at the sintering temperature, leading to a variant designated as viscous-phase sintering. Modern development of liquid phase sintering is traced to the origin of bronze alloys (Cu-Sn) for self lubricating bearings and cemented carbides (WC-Co) for cutting tool applications in the 1920s [20-22]. These systems provided an important basis for understanding liquid phase sintering. After that the researches with the copper-based steels (Fe-Cu or Fe-Cu-C alloys) provides further insights on the phenomenology of the process [23]. Liquid phase sintering offers many advantages compared to the conventional solid state sintering. Higher sintering rate is one of them. Other advantages are a high material utilization (>95%), near-net-shape fabrication, high productivity and superior control over the microstructures, which results into better properties. The whole process can be automated and as a result higher production rate can be achieved compared to other conventional

foundry techniques. Because of these advantages nowadays around 70% of the sintered product are made from the liquid phase sintering [24]. It is quite obvious that the mass transport rate through the liquid is much higher than the solid. The capillary attraction due wetting liquids gives rapid compact densification without the need for an external pressure. The liquid also aiding to the rapid rearrangement of particles by reducing the friction. Liquid phase facilitates efficient packing and high compact density.

Figure 2.12 provides a conceptual summarization of the key solubility factors encountered in liquid-phase sintering. From the figure it is clear that there are four possible combinations. The higher densification is achieved when the solubility of the solid in liquid is high but the solubility of the liquid in solid is low. In contrast, the opposite solubility situation gives swelling and a transient liquid, such as in Fe-Al system. But the combination of low liquid and solid solubilities correspond to a system such as W-Cu, which requires high temperatures to induce significant liquid-phase sintering. For such systems, solid state sintering is more significant than liquid phase sintering. The combination of high inter-solubilities is the least predictable stage. This will lead to swelling and densification and is sensitive to many processing variables. Figure 2.13 schematically shows the effect of the liquid content on densification [25]. This figure indicates the contribution of the solid-state densification prior to melt formation, which is not considered in the classical conceptualization of liquid phase sintering. The relative importance of each process depends on the quantity of the liquid and solubility.

On melt formation there is a burst of rearrangement densification, followed by solution-reprecipitation with concomitant grain growth and grain shape accommodation. If there is a high liquid level, full density can be achieved via rearrangement upon liquid formation. On the other hand, at low liquid contents the solid skeleton inhibits densification, requiring the participation of solution-reprecipitation events. Residual final porosity is eliminated by solid state sintering of the rigid solid skeleton. A limiting case is no liquid phase and total densification by solid-state sintering. The classic example of LPS is attributed to Price *et al.* [26] in their work on tungsten heavy alloys. In this case the liquid persists throughout the high temperature portion of the sintering cycle, giving

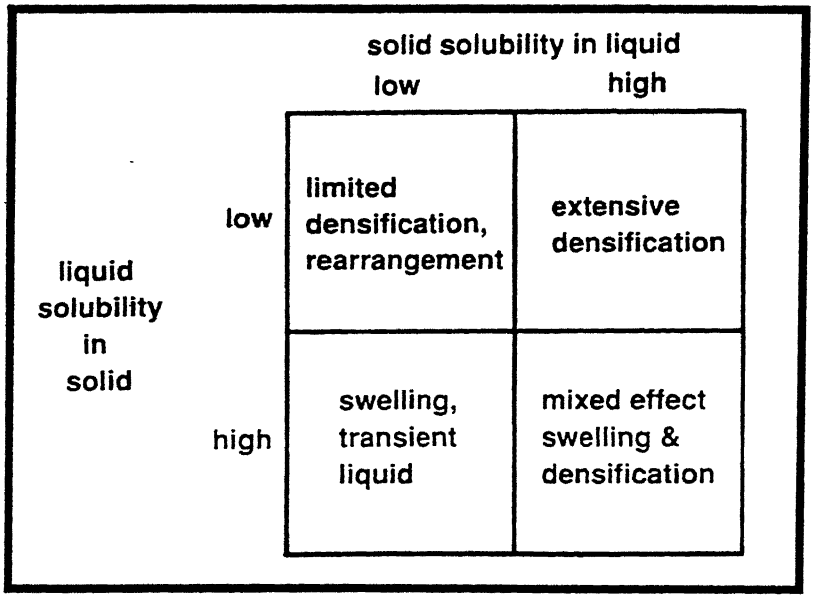

Figure 2.12. Conceptual summarization of the interactions and sintering behaviour as dictated by solubility interactions during liquid-phase sintering [11].

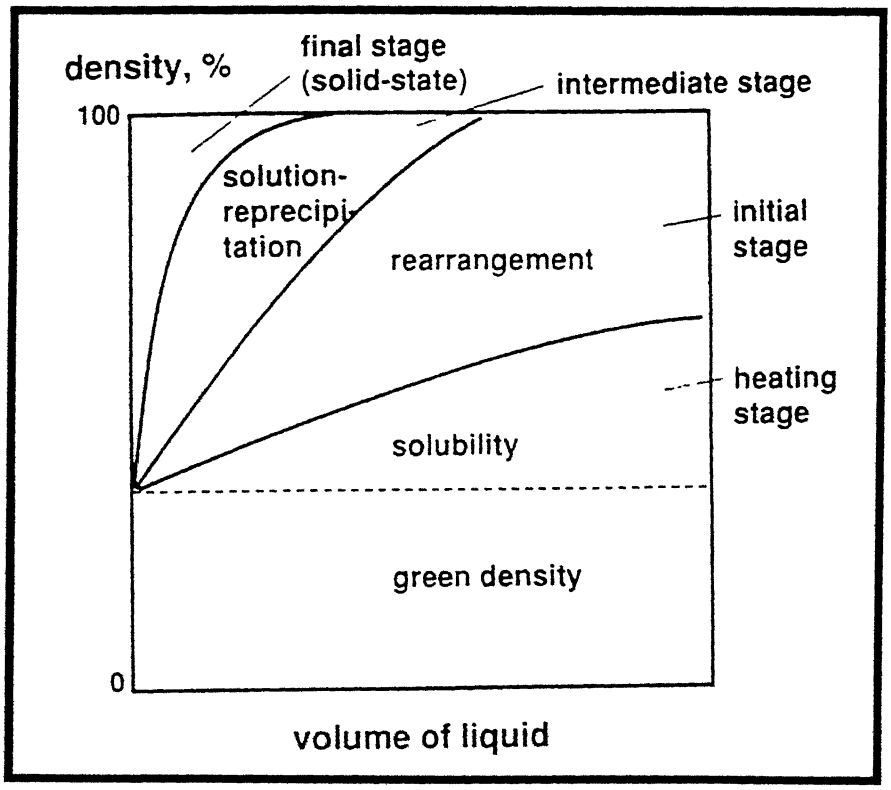

Figure 2.13. A map of density versus liquid content with indications of the dominant regions [11].

rapid densification and grain growth. The classic liquid phase sintering system densifies in three overlapping stages [23,27]. The schematic representation of the microstructural evolution is shown in Figure 2.14.

Initially, the powders are heated to a temperature where a liquid forms. With liquid formations there is a rapid initial densification due to the capillary force exerted by the wetting liquid on the solid particles. The elimination of pores reduce the surface energy of the system. In many systems, solid-state diffusion yields considerable densification prior to formation of the first liquid. Subsequent densification depends on the amount of liquid phase. Kingery and Narasimhan [28] conducted a series of experiments on iron-copper and cemented carbide systems and found that the densification in those alloys occur in three distinct stages, as discussed by Cannon and Lenel [29]. These three stages of densification are: rearrangement, solution-reprecipitation, and final-stage sintering. These three stages of classic (persistent) liquid phase sintering are summarized in Figure 2.15. The following sections describe the various stages of liquid phase sintering briefly.

2.4.2.1 Particle Rearrangement

In liquid phase sintering, once the liquid forms, it will flow to wet the particles. With the condition of good wetting (wetting angle $\theta < 90°$), the liquid phase is pulled by capillary forces into particle necks and small pores [11]. The liquid phase acts as the lubricant and prevents interlocking of particles. Rearrangement is often composed of two phases. Primary rearrangement involves the individual particles. The liquid forms at the additive particles sites. They form liquid which spreads and wets the particles to form cluster. The cluster then continue to compress as the liquid spreads.

Secondary rearrangement involves particle disintegration into fragments and subsequent repacking of those fragments. The low melting liquid forms and penetrate into the grainboundaries thereby causing particle fragmentation.

Huppmann and Riegger [30] experimentally confirmed that a low wetting angle and uniform powder homogeneity enhance the contribution of rearrangement of densification. It was shown that a very large contact angle promotes swelling rather than shrinkage. The other important variables to control the process are, particle size, shape

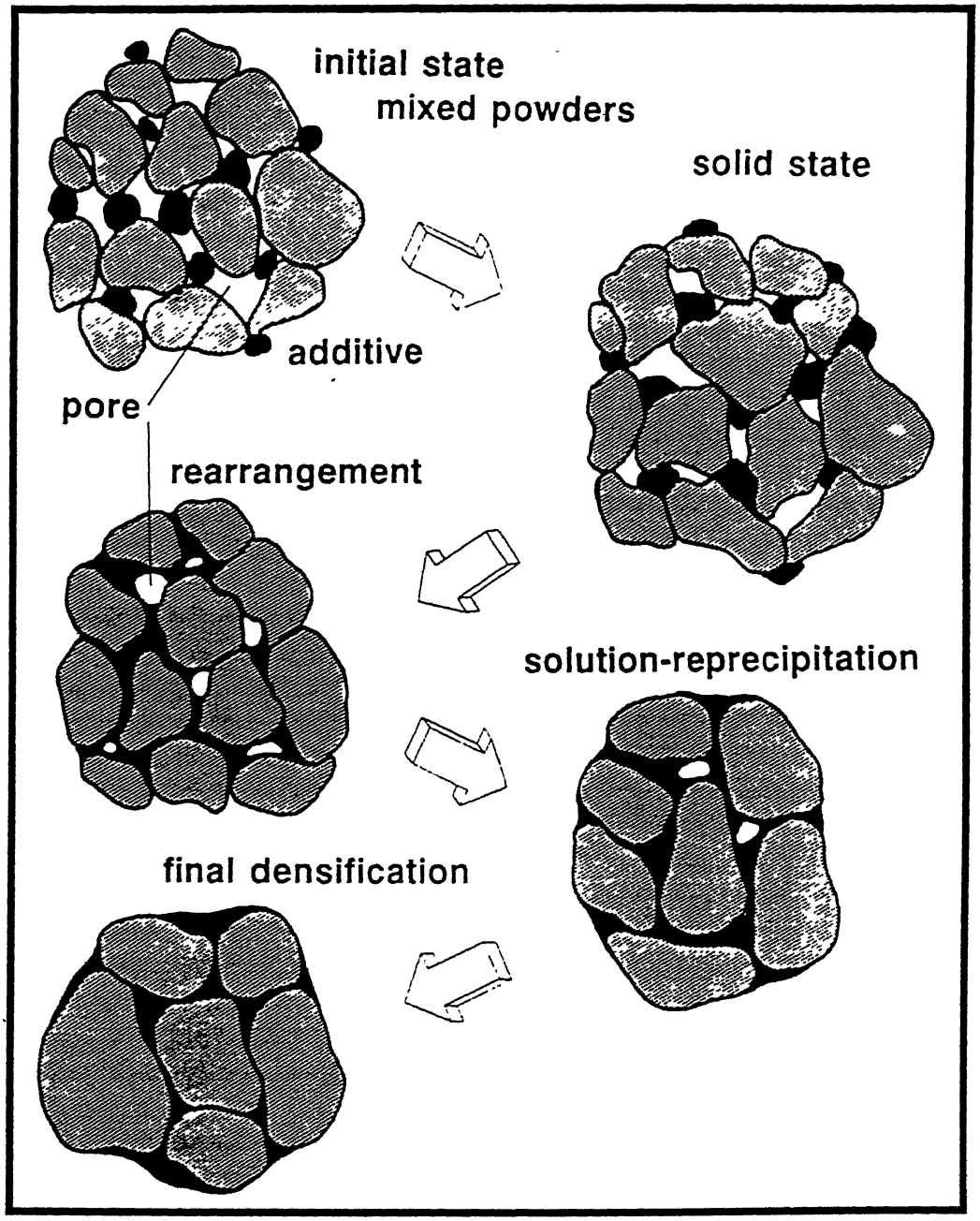

Figure 2.14. The classic stages of liquid phase sintering involving mixed powders which form a liquid on heating [24].

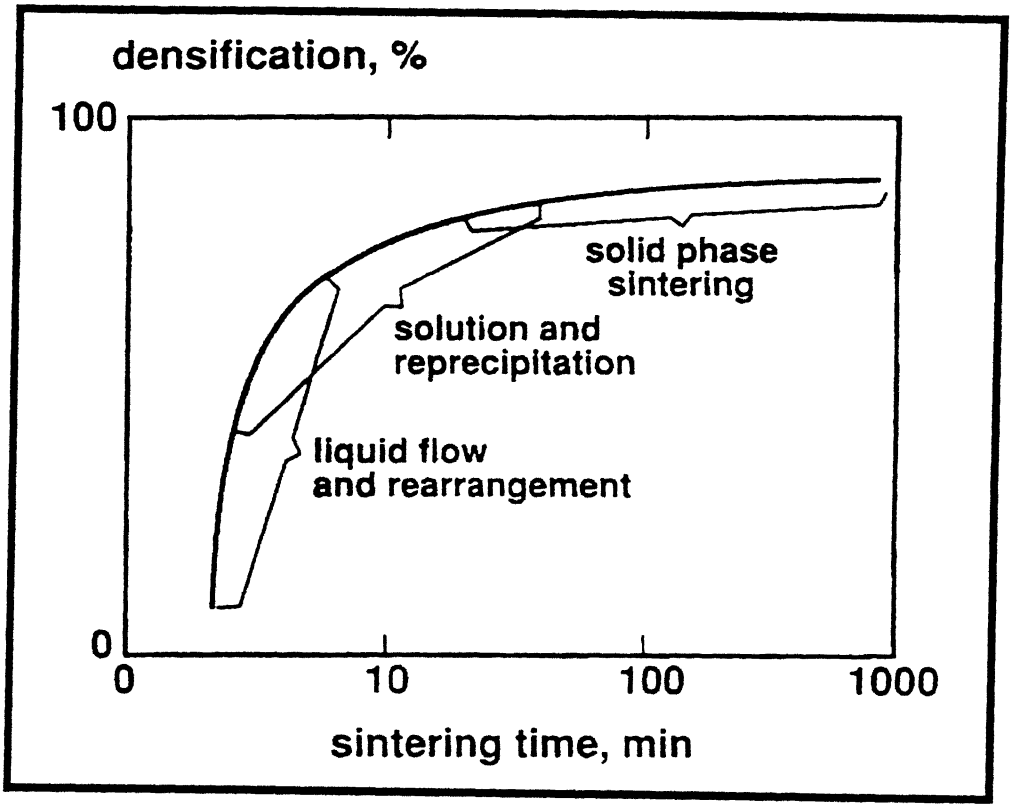

Figure 2.15. The process stages associated with classic liquid phase sintering, giving the main microstructural changes [24].

and volume fraction of the liquid. Smaller particles have got more surface area, so the surface energy will be higher. This results into the higher densification compared to the coarse particles. Lower green densities also improves the densification rate. In general, the densification rate is reduced by a high green density; because as the green density increases, there is more mechanical interlocking and less vapour phase. As a result capillary force responsible for rearrangement is reduced. However, the final density improves because of the lower initial porosity. At a high volume fraction of liquid, complete densification is possible by rearrangement and pore filling on liquid formation. As the volume fraction of liquid decreases, other processes like solution-precipitation must be active for full densification. it is estimated that 35 volume percent liquid is needed to obtain full density by rearrangement alone [31]. In actual case, rearrangement occurs over few seconds. Belhadjhamdia [32] showed that heat transfer was the rate controlling factor which dictates shrinkage time during the rearrangement stage of liquid phase sintering.

2.4.2.2 Solution-Reprecipitation

In most liquid phase sintering systems, the quantity of liquid is insufficient to fill all the pores space on melt formation. Hence, there will be some remaining porosities after the first stage. Thus, the grain must change their shape and size distribution to achieve a higher packing density for further densification [33]. Thus, further densification occurs from solution reprecipitation wherein the smaller particles preferentially dissolves in the melt and reprecipitated from the saturated melt on to a larger grain. As a result the large grains become larger and small grains become smaller. This phenomenon is also known as Ostwald ripening. This stage involves particle fragmentation, contact flattening, and grain shape accommodation [34].

Two different sets of theories have been proposed to describe the densification mechanism during this stage. Price *et al.* [26] proposed that the difference in the chemical potential results in the dissolution of the smaller grains into the liquid phase and their subsequent precipitation on to the larger grains. But according to Kingery [27] the densification occurs from the hydrostatic pressure applied at the interparticle contact because of the capillary action of the pores present at the particle junctions.

A general attribute of solution-reprecipitation processes is microstructural coarsening [35]. The coarsening is due to a distribution of grain sizes. The solubility of a grain inversely varies of its size. The difference in the solubilities establishes concentration gradient in the liquid. Material transportation occurs from the small grains to large grains as stated earlier. It should be remembered that this stage not only gives rise to the grain coarsening, but contributes to densification also.

2.4.2.3 Microstructural Coarsening and Coalescence

As the grain contacts, neck growth occurs by solid-state diffusion along the grain boundary that focus at the contact to give densification [36]. This is the third and last stage of liquid phase sintering. In this stage is controlled by densification of the solid structure. Rigid skeleton of contacting solid grains, decreases the densification rate in this step. The residual pores will enlarge if they contain entrapped gas. During the pore growth, pressure in the pores decreases, giving compact swelling. Prolonged sintering time will lead to the increase in the grain size and as a result the properties of the sintered material will degrade. Hence the stage is avoided by use of short sintering time.

This stage is not so important in liquid phase sintering. However, in the systems like W-Cu, W-Ag, WC-Cu etc., which have got limited solid solubility in the liquid, this process plays an important role. There the densification generally occurs by rearrangement and solid-state sintering.

2.4.3 Supersolidus Liquid Phase Sintering

Supersolidus liquid phase sintering (SLPS) is an attractive approach for processing prealloyed powders. This process should be used with precise control because the conditions for prealloyed approach is very closed to the compact distortion. It is known that the presence of liquid phase in the sintering system will increase the sintering rate and densification. Traditional liquid phase sintering relies on a mixture of two or more powders to form a liquid between the particles at the sintering temperature. Super solidus sintering is the variant of this. Here we take the advantage of prealloyed powders to create a situation where liquid forms inside the particle [24]. When the prealloyed powders are heated to the partially molten condition they exhibit rapid densification. The

liquid forms within the particles, causing each particle to fragment into individual grains. The wetting of the grains by the liquid will provide some kind of capillary force which will further cause repacking of the fragmented grains. This process is most fruitful when applied to highly alloyed materials [37]. Figure 2.16 illustrates the mechanism of densification during SLPS. The liquid cause disintegration of the rigid solid skeleton by forming along the grain boundaries and interparticle contacts as stated earlier. Further, the liquid also acts diffusional transport medium for the solid allowing densification similar to classical LPS.

The main advantage of SLPS is that, even the coarse powders show rapid densification since they fragment to individual grains. Thus, this technique is best suited for relatively coarse (20 to 50 μm) prealloyed powders produced by atomization.

The term supersolidus sintering was introduced by Cambal and Lund [38]. Lund and Bala [39] performed the first studies on the densification mechanisms during SLPS. They suggested that mechanisms responsible for densification included,

(i) redistribution of liquid formed due to melting at particle contacts

(ii) flattening of the wetted particle contacts by a solution-precipitation mechanism

(iii) grain growth due to solution-precipitation leading to release of intergranular liquid

(iv) pore elimination due to the escape of the entrapped gas by diffusion

Compared to solid-state sintering, the densification process shows an extreme temperature sensitivity. Densification takes place in the first few minutes after passing a critical temperature. Prolonged high temperature holds give relatively minor densification gain and often cause property or density decrements. The characteristics of SLPS is that, here the prealloyed powder exhibits rapid densification when heated slightly above the solidus temperature. Liquid is nucleated at heterogeneous sites, typically grain boundaries or interdendritic spaces, where the last solidification took place in powder fabrication. Even if the nucleation is not homogeneous also, as temperature increases the liquid spreads to form a continuous film. This will decompose the solid-state sinter bonds. Densification rate is roughly proportional to the volume fraction of liquid. Sufficient liquid formation should take place for the proper densification. On the other hand, excess amount of liquid results in compact slumping,

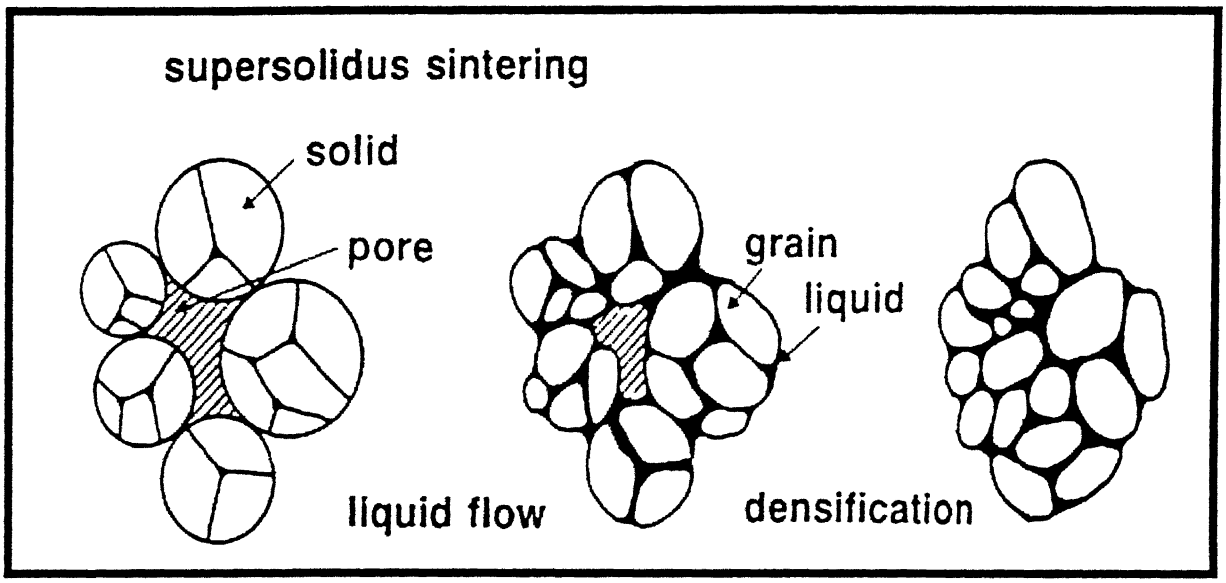

Figure 2.16. A sketch illustrating the basic densification process during SLPS [11].

especially when the liquid quantity exceeds 40 vol.% [11]. Jeandin *et al.* [40] performed quench studies to identify the densification mechanisms and quantify liquid distribution in powders which formed considerable interdendritic liquid. Murley and German [41] used quenching techniques to demonstrate that grain fragmentation was a key event for SLPS. It was found later that at the sintering temperature, SLPS microstructure were similar to those obtained in traditional LPS where liquid was present at the grain boundaries [42]. German [43] presented a theory assuming densification by viscous flow involving formation of liquid along the interfaces in polycrystalline prealloyed powder. Liu *et al.* [44] presented a model to calculate the capillary force under a variety of processing conditions during SLPS. Based on this model, they analyzed shrinkage due to viscous flow [45]. Tandon and German [46] performed model experiments to demonstrates particle fragmentation and grain sliding during SLPS.

2.4.3.1 Parameters Affecting Supersolidus LPS

SLPS is dependent on both materials and processing parameters. Those parameters are liquid fraction, sintering temperature, holding time, additives and alloy modification, initial powder microstructure, powder characteristics, heating rate, sintering atmosphere etc. [42]. Among them the most important contribution comes from the sintering temperature. Temperature will directly influence the amount of liquid formation during SLPS. It should be remembered that SLPS is extremely rapid and the whole process occurs within a narrow temperature range above the alloy solidus temperature. The excess liquid formation should be avoided. Because that will form deleterious brittle phases, exaggerated grain growth, swelling, slumping of the compact etc.

Phase diagram will be useful to predict the dependence of liquid fraction on temperature for binary alloys. A schematic section of a binary phase diagram is shown in Figure 2.17. The figure identifies the alloy composition X_A, solidus and liquidus temperatures T_S and T_L, and the compositions of the solid and liquid X_S and X_L at the sintering temperature T. In general a large separation between the liquidus and the solidus temperature is desirable for a low sensitivity to temperature [37].

In eutectic system, the liquid forms suddenly above the eutectic temperature. The amount of liquid depends on the temperature above eutectic point. If the quantity of

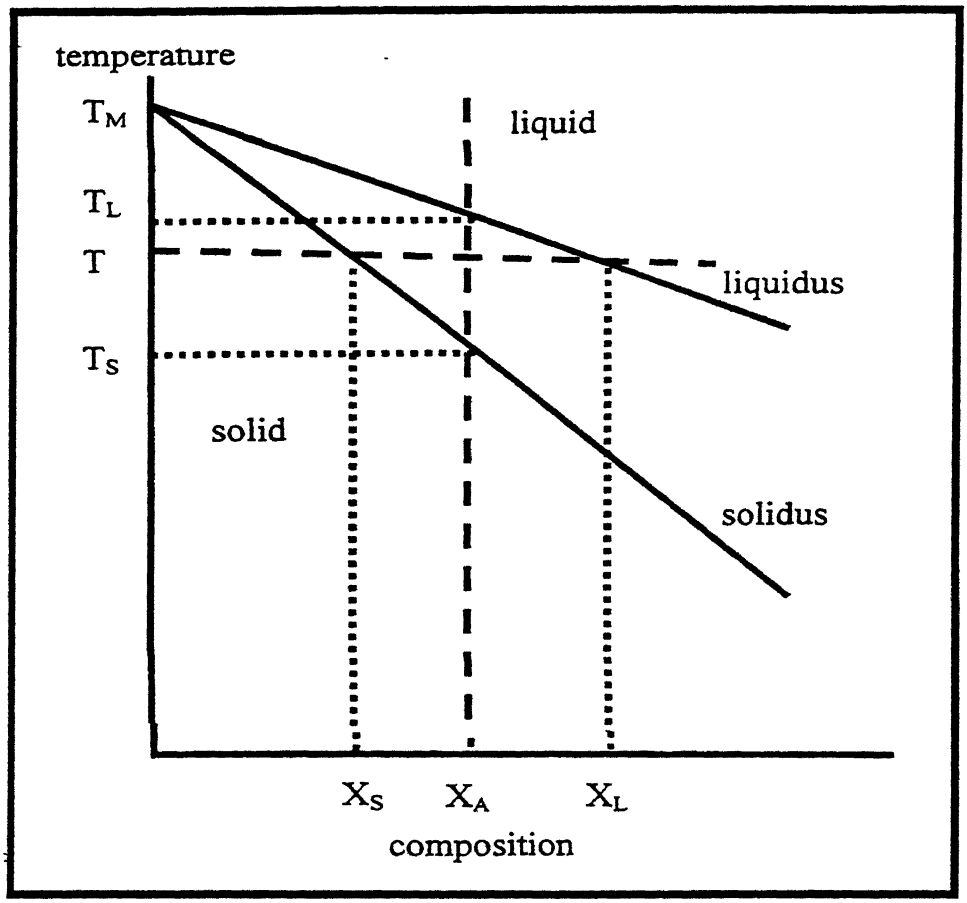

Figure 2.17. A schematic of a binary phase diagram [42].

liquid is large, then the sintering of the system will be very temperature sensitive leading problems with process controls. For complex alloy compositions, detailed experimental phase diagram data are not usually available. Differential thermal analysis (DTA) is useful in this regard as it gives information on the melting range and the dependence of the liquid volume fraction on temperature [42].

The non-equilibrium character of prealloyed leads to initial melt formation below the melt formation below the melt temperature. This occurs because of the solidification of the particles in a non-equilibrium during atomization.

Holding time is also important for SLPS. Most of the densification took place in the first 10 to 30 min when sufficient liquid exists (upto 30 vol.%). Under such conditions rearrangement is sufficient to cause complete densification. Longer holding will generally lead to coarser grain which will decrements the density. The determination of optimal temperature-time is more an art than the technology. That will depend ultimately on the furnace capabilities, mechanical properties etc. Refined microstructures were obtained by minimising the time at the higher sintering temperature [47].

The another parameter affecting the SLPS is the alloy modifications and additives. The additives will segregate in the grain boundaries and alter the liquid formation temperature and liquid quantity. They may be utilized to improve the sinterability of alloys. The addition often broadens the sintering temperature window and thereby helping in controlling the sintering.

Initial powder microstructure have also an important contribution to SLPS. Liquid may form in the grain boundaries or in the inter-dendritic region. A cellular structure is preferred over a dendritic structure since liquid at the grain boundaries leads to grain refinement and sliding. The isolated interdendritic liquid pools do not directly contribute to densification. SLPS is generally done with the prealloyed powders which are usually fabricated by gas atomization. The gas may be entrapped during the process as spherical pores which are very difficult to remove during sintering.

SLPS works with relatively coarse powders. However it is advantageous to use smaller particles since they usually give more densification similar to classic LPS [37]. Particle size also controls the solidification rates and undercooling for atomised powders.

Large particles form less liquid at the grain boundaries during melting. Particle size also affects the segregation of the liquid forming alloying elements within particles.

Larger particle size in SLPS generally lead to negligible heating rate dependent solid state sintering prior to liquid formation. However, faster heating rates give faster densification [42]. Slow heating rates or annealing steps reduce the compositional gradients. In Table 2.6 comparison between LPS and SLPS has been made.

The use of gas during sintering is also important because the gas may be entrapped in pores and inhibits densification during the final stages. Often the limiting density is higher for sintering in hydrogen, which dissolves in many metals, than in inert gases like argon. By vacuum sintering we can avoid the gas entrapment and subsequent pore swelling. Ultimately the choice of sintering atmosphere is dependent on the alloy used.

2.4.4 Transient Liquid Phase Sintering

An interesting variant to traditional liquid phase sintering involves a transient liquid which solidifies by diffusional homogenization during sintering [24]. In this processes liquid exists for a certain length of time during the sintering cycle. In many material systems, starting a sintering cycle with a mixture of powders will allow a transient liquid phase to form during sintering. A common example is mixed copper and tin powders, where in tin melts at 232°C [48]. The molten tin dissolves into the copper to leave behind a pore. Because tin is soluble in solid copper, the molten state persists for a short time before homogenization forms solid bronze. Figure 2.18 gives the example phase diagrams of systems that could be processed using a transient liquid from mixed A and B powders. In first case, a low melting temperature additive, A is used to generate the liquid, yet the overall composition is in a single-phase region at the sintering temperature. The sintering temperature is between the melting temperatures of the two components. Most importantly the solid does not change the crystal structure due to alloying with the liquid. Liquid can form during this process by eutectic formation. This eutectic reaction provides the liquid from interdiffusion of the components during sintering. The sintering temperature is greater than the eutectic temperature and the final

Table 2.6. Comparison of LPS and SLPS [42].

Feature	LPS	SLPS
Powder type	Elemental powder mixture	Prealloyed powder
Melting	One elemental powder melts or melting by reaction between constituents	Partial melting of alloy particles
Liquid location	Between particles	Mainly within polycrystalline particles (results in particle fragmentation)
Dihedral angle	Variable, system dependent	Low
Liquid volume fraction	Mainly determined by composition not temperature	Depends on both temperature and composition according to lever rule
Solid-liquid segregation	Solid grains settle in tungsten heavy alloys	Negligible settling

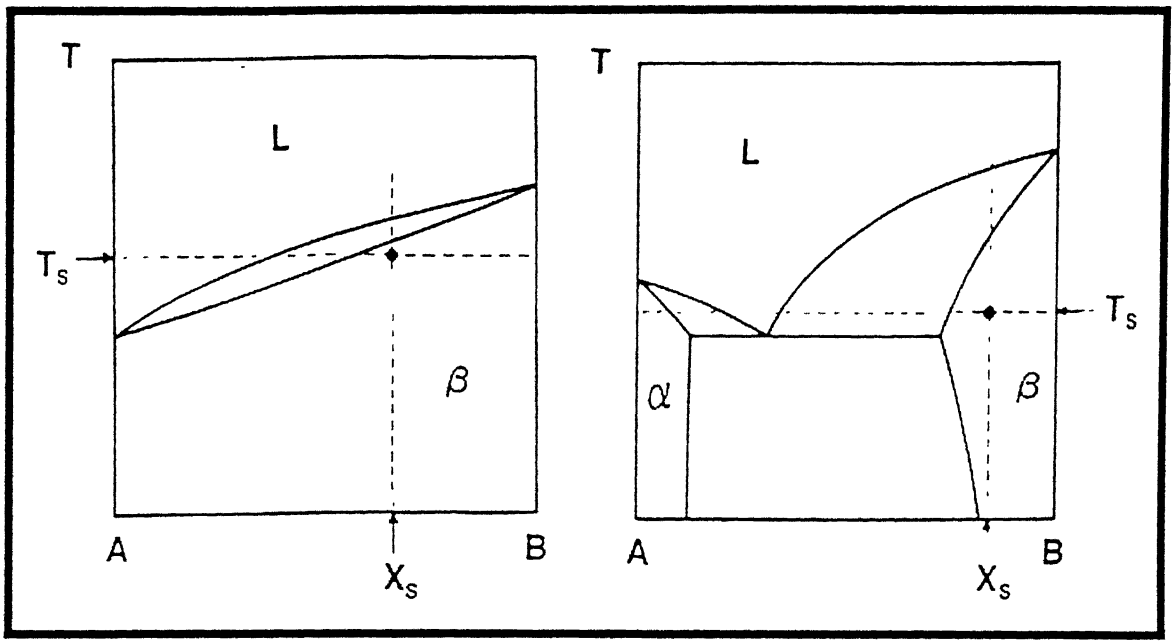

Figure 2.18. Two binary-phase diagrams showing possible conditions where transient liquid phase sintering occurs [11].

composition is in the single phase field. As the amount of liquid varies continuously, the process becomes very temperature sensitive.

The requirements for transient liquid phase sintering include solubility between the components, with the final composition existing within a single phase region at the peak sintering temperature. Finally, we can summerize the sequences of steps as follows [49, 50]:

1. Swelling by interdiffusion prior to melt formation
2. Melt formation
3. Spreading of the melt and generation of pores at prior additive particle sites
4. Melt penetration along solid-solid contacts
5. Rearrangement of the solid grains
6. Solution reprecipitation induced densification
7. Diffusional homogenization
8. Loss of melt
9. Formation of a rigid solid structure
10. Densification by solid state sintering

It is to be remembered that the actual steps depend on several process variables, including particle sizes, amount of additive, heating rate, and maximum temperature.
A detailed investigation of the dependence of transient liquid phase sintering on phase diagram is discussed by German [51]. The benefits of transient liquid phase sintering are easy compaction of elemental powders (as opposed to prealloyed powders) and excellent sintering without coarsening difficulties associated with a persistent liquid. Transient liquid phase sintering can be applied in processing of dental amalgams based on silver and mercury, porous bronze bearings, structural ferrous alloys, copper alloys, magnetic materials and alumina-based ceramics. Problems can arise in TLPS if an intermediate compound forms between the additive and the base. A system with an intermediate compound would be expected to give swelling. However, for applications such as porous bronze bearings this swelling is beneficial. Modelling of transient liquid phase bonding in the real system has been tried by researchers [52].

The possible advantages of this are clear. Primarily TLPS offers increased flexbilities in design and processing [53]. The other advantages of TLPS include a

reduction in the processing temperature, enhanced densification, reduced microstructural coarsening and reduced cost by avoiding the use of expensive prealloyed powders [54].

2.4.5 Limitations

In spite of all the advantages, liquid phase sintering suffers from certain disadvantages as well. The major problem is the compact distortion. It may occur due to the formation of too much liquid during sintering. the large dimensional changes which occurs during sintering puts limits on dimensional tolerance [55]. The microstructure controlling parameters are also responsible to control the final properties. Separation of these effects is sometimes difficult. In initial compact, at least three phases are present- vapour, solid, and liquid [24]. There are several interfaces and energies associated with such a structure. The associated solubility, viscosity, and diffusivity of multiple phases have hindered a full analytical treatment of liquid phase sintering. The maximum content of liquid during liquid phase sintering is limited by the loss of shape during sintering which can be tolerated in the desired end product [25].

2.5 An Overall Summary

Two main routes of sintering are, (i) solid-state sintering, (ii) liquid phase sintering. Among them liquid phase sintering is the most important one. Nowadays, around 70% of the sintering is done at liquid phase. Solid state sintering also plays in important role in the fabrication of many important materials. There are six stages in solid state sintering. These stages do not occur in a sequential manner rather overlap. However, several theories have been put to describe the densification mechanism during the solid state sintering. Surface and volume diffusion mechanism are the two most important mechanism regarding that. Role of Nabarro-Harring creep is also discussed briefly. But the main problem associated with solid state sintering is its slow rate. In this respect, liquid phase sintering has an edge over the solid state sintering. In addition to provide faster diffusion pathway, the liquid phase also induces capillary stress. There are several variant of liquid phase sintering. We have discussed only supersolidus liquid phase sintering and transient liquid phase sintering. These sintering variants are applied successfully depending on the systems and powder characteristics. The phenomena of

reduction in the processing temperature, enhanced densification, reduced microstructural coarsening and reduced cost by avoiding the use of expensive prealloyed powders [54].

2.4.5 Limitations

In spite of all the advantages, liquid phase sintering suffers from certain disadvantages as well. The major problem is the compact distortion. It may occur due to the formation of too much liquid during sintering. the large dimensional changes which occurs during sintering puts limits on dimensional tolerance [55]. The microstructure controlling parameters are also responsible to control the final properties. Separation of these effects is sometimes difficult. In initial compact, at least three phases are present- vapour, solid, and liquid [24]. There are several interfaces and energies associated with such a structure. The associated solubility, viscosity, and diffusivity of multiple phases have hindered a full analytical treatment of liquid phase sintering. The maximum content of liquid during liquid phase sintering is limited by the loss of shape during sintering which can be tolerated in the desired end product [25].

2.5 An Overall Summary

Two main routes of sintering are, (i) solid-state sintering, (ii) liquid phase sintering. Among them liquid phase sintering is the most important one. Nowadays, around 70% of the sintering is done at liquid phase. Solid state sintering also plays in important role in the fabrication of many important materials. There are six stages in solid state sintering. These stages do not occur in a sequential manner rather overlap. However, several theories have been put to describe the densification mechanism during the solid state sintering. Surface and volume diffusion mechanism are the two most important mechanism regarding that. Role of Nabarro-Harring creep is also discussed briefly. But the main problem associated with solid state sintering is its slow rate. In this respect, liquid phase sintering has an edge over the solid state sintering. In addition to provide faster diffusion pathway, the liquid phase also induces capillary stress. There are several variant of liquid phase sintering. We have discussed only supersolidus liquid phase sintering and transient liquid phase sintering. These sintering variants are applied successfully depending on the systems and powder characteristics. The phenomena of

Chapter 3

SCOPE OF THE PRESENT WORK

From the previous chapter, it is evident that bronze plays an important in the fabrication of many industrial parts ranging from porous bearing to full density structural parts. One of the most important routes of making those products is through powder metallurgy technique. Both solid and liquid phase sintering are applicable towards the production of near-net shape product from bronze. Currently about 70% of the total sintered product are being produced by liquid phase sintering. Various novel sintering techniques have also been attempted for the processing of P/M bronze. However, bronze has primarily been processed by solid state sintering alone. This is partly attributed to the requirement of the end applications, i.e. bearing wherein a controlled porosity is required. Hence solid state sintering was the only resource. Recently, there has been a considerable attempt to use P/M bronze and bronze-based composites for structural applications, wherein achieving high density is a primary requirement. To achieve this full density liquid phase sintering would be the only way. This present work relates the response of prealloyed and premixed copper-tin powders as a function of sintering temperature. Unfortunately, the potential of the use of Cu-Sn bronze as a structural material have not been fully explored. This study aims to get an optimization of the prealloyed and premixed route of Cu-Sn bronze fabrication. The sintering response of the different powders are compared with respect to the phase diagram prediction. It is important to know the deviation of the powder behaviour form the equilibrium as the powder characteristics changes. This chapter briefly reviews the existing body of work relating these attributes. Until now, not much effort has gone into systematically identifying the difference between prealloyed and premixed approach. In the literature not much work related to dilatometry of premixed and prealloyed powder was found. Proof of the existence of different phases in the final microstructure have not been supported by the XRD studies. In the following sections, the existing work in these field are briefly discussed. Subsequently, these ideas were modified and extended to derive a new

optimization technique for the use of premixed and prealloyed powders. We will also describe the reason for the alloy system chosen in this study.

3.1 System Selection

There are several reasons for selecting the particular Cu-Sn system. They are as follows:

- Copper and tin powders are easily available in almost pure form.
- Good enough difference in the melting point (1083°C of Cu to that of 232°C of Sn).
- It provides both eutectic and peritectic reactions.
- Tin has fairly high solubility in copper.
- Copper and tin both have got mutual solid solubility in each other.
- High solubility of tin in copper provides rapid densification during liquid phase sintering.
- Low melting point of tin (232°C) provides a scope for transient liquid phase condition.
- As bronze system can be sintered within 900°C, handling with the furnace would be more easier.
- Although this system is known for several years for bearing applications, virtually no research has been there in the open literature about its potential in the field of structural applications.
- Gas atomized prealloyed powders of Cu-Sn are easily available.
- Powders of all size and shapes can be economically fabricated and available commercially.
- Powders compressibility is good as compared to refractory and other ferrous metals.
- Not that much high sensitive to the requirement of reducing gases, and therefore sintering can be done in forming gas well which is much cheaper.
- In one system we can get two types of liquid phase sintering (supersolidus and transient) and solid state sintering.
- All the microstructural evolution depending on sintering process can be shown.

3.2 Sintering Study of Cu-Sn System

Cu-Sn system is relatively well known and investigated over the years. It is also known that this particular system can be used as the porous bronze bearing. Production of self-lubricating Cu-10Sn bronze bearings is underway since the 1920's and still constitutes a major use for copper and tin metal powders. It was observed that the P/M route for processing bronze bearing offers many advantages compared to the other processes and are described in the previous chapter. So, the attention is then focused on the P/M processing of the same. Actually people used to manufacture the bearings by solid state sintering only. If we briefly review the historical background of bronze bearings, it appears that the ground work was initiated at Chrysler-Amplex and Delco-Moraine in the 1920's. In order to satisfy their powder needs, Everett Hall established the pioneer company – Metals Disintegration [56]. A good review of sintering work copper and tin was reported by Hall [57]. But the basic mechanisms of liquid phase sintering was unknown at that time. It was the late '70s, when the people focused attention to the logical aspects of liquid phase sintering of bronze. Nowadays both prealloyed and premixed powders are used in the industries. Moreover the advantages offered by LPS supplied the driving force to the researchers for investigating the liquid phase sintering mechanisms of this system.

Dowson [58] discussed the sintering aspect of bronze in a concise fashion. Phase diagram attribute on the sintering is also mentioned. Dowson's work clear that in equilibrium condition tin is soluble in copper lattice at least 15 wt.% in the temperature range of 500°C to 600°C. At those temperature Cu-10/12 Sn would consist of single α phase. But at lower temperature solubility of tin decreases and below 340°C second phase should begin to appear. Decomposition of α phase requires extremely slow cooling rate. But industrially it is not possible all time. So, in final microstructure we can get the phases which may not be supported by phase diagram. When we are heating elemental Cu and Sn powder under the fairly rapid heating and short sintering cycle, it is possible to get, at various stages in the heating process, significant amounts of δ, γ, and β phases. Theoretically, at room temperature α and little ε should be present but it is seen that the second phase was δ, not ε. But proper sintering practice should only led to homogeneous α phase in the microstructure.

The sintering operation is believed to be affected by powder characteristics, sintering atmosphere, compact density, rate of heating etc. [56,58]. Lower apparent density and smaller particle would lower the growth. Lower the density of green compact, lower the growth. Greater reducing potential of the gas also lowers the rate of growth. To minimise the growth, lower heating rate is adopted.

Pore content in the sintered product varies from 20 to 40% by volume. Larger the pore content, oil impregnation is more and that is helpful in case of self lubricating bearing. But strength factors also should be considered. Optimization between the strength and porosity is done depending on application. However, if prealloyed powder is used, sintering and dimensional control are relatively easy, but the problem is, the temperature needed for sintering will lead to shrinkage which is not desirable for bearing. Furthermore, prealloyed bronze particles are harder than pure copper, greater pressure is needed.

Krishnakant *et al.* [56] also reported that prealloyed powders in premix formulations helps to produce bearings with less distortion. The surface of fully sintered bearings is often less smooth and may contain high spots. Some of these may still be present after sizing, which add to the noise and inferior performance of a bearing. In such instances, higher prealloyed powders were found to help retain the surface smoothness. Berry [59] had studied the role of prealloyed powders in various mixtures along with other factor influencing the dimensional changes.

Premixed powders are seen to provide linear growth as high as 4%. Other complication is that growth is not the same in radial direction as in the axial direction.
So, the problems and undesirable effects that can occur with elemental powders are identified as:

(i) Increased distortion

(ii) The presence of significant quantities of δ phase as a result of inadequate sintering.

(iii) Areas of gross porosity consequent on the presence of large tin particles.

The control of the powder mix and of the sintering regime need to be much more precise if unacceptable variations is to be avoided.

In light of this, our present work is to determine the relevance of premixed powders to be used for bearing and a comparative study between premixed and prealloyed powders in terms of better dimensional control.

Deegan and Sarkar [60] discussed the effect of compacting pressure and sintering temperature on the properties of copper-tin compact upto 10% tin. The sintering time was kept to maximum 15 min. Within this temperature range, progressive volume growth was observed. More the tin content, more the growth. At higher compacting pressure, the trend was for a greater force with increasing tin content. It is possible that, at high compacting pressure, the tin will flow plastically over the die wall and the junctions so formed are strong, offering resistance to movement of the compact.

Elliot [61] had suggested that, during sintering, the molten tin is held by surface tension forces at the junctions formed by the copper particles. Alloying proceeds with time and this causes an increased mass at the points of contact resulting in an overall growth. Drapeau [62] suggested that the liquid tin overlaps the copper particles completely so that there is an increase in the final diameter of alloy particles giving rise to volume increase. The growth was more at higher tin content when sintered at higher temperature [60]. It was also observed that with copper powders, effect of increasing the compacting pressure is to cause a volume increase upon sintering once a critical compaction stress has been exceeded. As the pressure increases chances that the lubricant or atmosphere being trapped goes high and it is difficult to permeate out because pore spaces are progressively sealed up with increased compaction. This leads to the higher growth at higher compacting pressure.

At low tin content the volume growth could be explained by the model proposed by Elliot [61]. But at higher tin content volume changes occurs in accordance with the postulate of Drapeau [62]. Radial growth as high as 2.15% was observed where the maximum axial growth was reported to be 5.5% [60]. That is, in general terms, the samples grows less in the radial direction. This could possibly be tied up with the direction of applied stress and locked-in elastic stresses.

Whatever the compacting pressure, the effect of sintering time on volume change dependent on the sintering temperature. The sequence of events during sintering of copper-tin mixes is as follows [60]:

(i) A liquid film of tin forms around the copper particles, causing an increase in the effective diameter which manifests itself as an overall volume grow

(ii) As the tin alloys with copper, the liquid phase disappears and the sintering process is analogous to that of a monometallic powder in the solid state, so that shrinkage would be expected.

Sintering at 600°C for 15 min would give rise to twinned α solid solution and an eutectoid α+δ in final microstructure.

Backensto [63] also studied the changes in dimensions during the sintering of bronze mixes made from reduced copper. Among the variables investigated were copper particle size, tin content, tin particle size, lubricant variations, effect of graphite additions, and effect of lead and phosphorus additions. They have also reported that within the sintering time limit the dimensions at first increases and then decreases for further temperature increase. Sintering at around 850°C, they were to get good α-bronze microstructure with good strength, ductility, and machinability.

Berry *et al.* [64] had studied the change in dimensions during heat up to sintering temperature. The common practice of decreasing sintering temperature for dimension control will adversely affects machinability and bearing performance. According to them, for optimum dimension control and structure, the sinter temperature is that which gives peak growth.

Since there is an interest in using bearings containing tin greater than 10%, the effect of tin on properties of pressed and sintered compacts containing tin upto 20% was investigated by Davies and Sarkar [65]. As they increased the tin content, ejection force was found to be greater, suggesting a higher resistance offered at die wall by the tin. This may be because of high contact pressure causes a low melting point metal to solder on to a hard surface and shearing forces to separate these adhered metal junctions can be quite high. They also suggested that shrinkage occurs by solid state sintering of bronze beyond a critical sintering time dependent on the temperature. It can be concluded that effect of increasing tin content in a copper-tin system is to cause a volume growth with increasing sintering time and then a progressive shrinkage. It is probable that the effective diameter of the multi-component system increases while the low melting point phase in the interstices remains fluid. Diffusion, which is temperature and time dependent, during

sintering causes alloying and the system undergoes shrinkage due to solid state sintering. at high compacting pressure and/or at high tin content, the molten phase exudes out giving rise to bloating and porosity.

Mixes containing various combinations of prealloyed and/or elemental tin powders in combination with reduced/unreduced copper powders were published by Peissker [66]. Mukunda *et al.* [67] studied the vacuum sintering of bronze bearings in light of interconnected porosity, sintering parameters and green densities. They selected reduced, electrolytic and atomized copper powders of varying particle sizes. It was suggested that the amount of interconnected porosity is dependent on some ratio of the copper and tin particle sizes. Vacuum sintering was found to offer a slight improvement in the interconnected porosity. The effects of various green densities on the flow of tin into the capillaries and homogenization of the microstructure were summerized by Kim [68]. They selected spherical tin powders of average particle sizes of 30, 65, and 140 μm, while copper powder was irregular shape sieved to a 20 to 60 μm size range. Sintering was carried out at 400°C for 10 min in hydrogen. Their results showed that the flow of the tin-rich melt depends critically on the green density. When the green density was high, the tin-rich melt remained at the initial tin particle size and the resulting compositional and structural inhomogenity persisted even after long sintering at high temperature. On the other hand, when the green density was low, the tin melt spread into the capillaries, thus facilitating a homogeneous microstructure. But since pores are produced at the tin particle sites, it is also desirable to control the tin particle size and its distribution.

Das *et al.* [69] have studied extensively about the control of δ phase in 90/10 bronze bearing. It is already discussed that improper sintering may give rise to brittle tin-rich delta phase in the form of (α + δ) eutectoid. According to them the brittle phase can be controlled by any one or a combination of the following:

(i) Increased sinter temperature.

(ii) Increased sinter time.

(iii) Part or total replacement of elemental copper and tin powder by prealloyed bronze powder.

But none of the above alternatives proved satisfactory because every alternative has its own limitations. At the same time it should be noted that, water atomized prealloyed bronze powder is capable of producing a fully developed microstructure which is free of delta phase when sintered properly. They conducted the experiments with three kinds of powders: elemental mixture of Cu and Sn, mixture of prealloyed bronze , 45% Cu and 5% Sn, and 100% prealloyed bronze. Sintering was carried out at two different temperatures, 750°C and 790°C. Compacts made from elemental mixtures of copper and tin showed mixture of α and δ phases in the microstructure. But all of the three different powder compacts showed only homogeneous α phase after sintering at 790°C for 30 minutes. This implies that by proper selection of sintering temperature and time we can achieve desired α phase in the final microstructure.

Mukunda *et al.* studied the sintering in the copper-tin system elaborately in a series of paper [70-72]. They described about the two school of thoughts. One believes that copper diffuses into tin to from various intermetallics which either decompose or get transformed into less-tin-rich phases as the sintering progresses. The other is that tin melts and spreads, leaving behind secondary pores of approximately the same size and shape. Farmer [73], on the other hand, has formulated an entirely different scenario in which molten tin begins to diffuse into copper to form extremely small grains of α-bronze, which later coalesce to form larger grains. Mukunda *et al.* studied in detail the formation of structure as the compact made from premixed copper and tin is heated from room temperature to 850°C. They also investigated the variables affecting the sintering operation. Differential thermal analysis was also been carried out followed by detailed metallography of those samples. Atmosphere limitations was obvious in their investigations as they selected only argon or nitrogen. As such, their studies are not useful in real sintering practice, but the authors have covered excellently the microstructural features during sintering. They have also described the synthesis of various phases and intermetallics and their identifications [74].

3.3 Dilatometric Study of Cu-Sn System

The application of the dilatometric study for understanding the sintering characteristics of bronze powder mixes is found to be interesting and useful. Evaluation

of the dilation plot provides information regarding phase transformation reactions, completion of phase formations, and powder characteristics. The dilatometric curves are accurately reproducible over and over again. Dilatometric study of copper-tin system has been carried out by several researchers for several years. But copper-tin phase diagram is complicated and makes it difficult to understand the mechanism of alloying in a simple manner. Figure 3.1 shows the dilatometric curve for Cu-10Sn premix at a heating rate of 10°C/min upto 820°C carried out in cracked ammonia [75].

Dimensional change took place in four main stages as illustrated in Figure 3.1 [66]:

230-650°C: Lubricant burns off, tin melts and alloys with copper, producing solid ηphase; at 415°C $\eta \rightarrow \varepsilon + L$ causing further alloying and accompanying growth.

650-799°C: Shrinkage occurs since no liquid phases occur and sintering forces predominate; also ε phase present transforms to γ which is a volume shrinkage transformation. The $\gamma \rightarrow \beta + L$ transformation at 755°C causes further alloying and arrest of shrinkage.

799-820°C: $\beta \rightarrow \alpha + L$ peritectic transformation; remaining tin-rich phases melt, rapid alloying causes growth and produces α bronze, when growth reaches a peak.

> 820°C: Shrinkage by pore coalescence is accompanied by grain growth.

The magnitude of the dimensional changes occurring at each stage, particularly the shrinkage and peritectic growth stages, will depend on factors such as copper morphology, fineness of copper and tin powders, additives like lubricant and graphite, oxide films, atmosphere and heating rates [64].

Peissker [76] further carried out investigations on dilatometry of Cu-5Sn, 90/10, and 85/15 bronze powders. It was found that all three curves showed shrinkage at about 350°C brought about by the transformation of the meta-stable phases induced by the atomization process into the (α+δ) eutectoid. As would be expected, this effect is greatest in the case of the Cu-15Sn, but the effect is also present in the case of the 95/5, showing

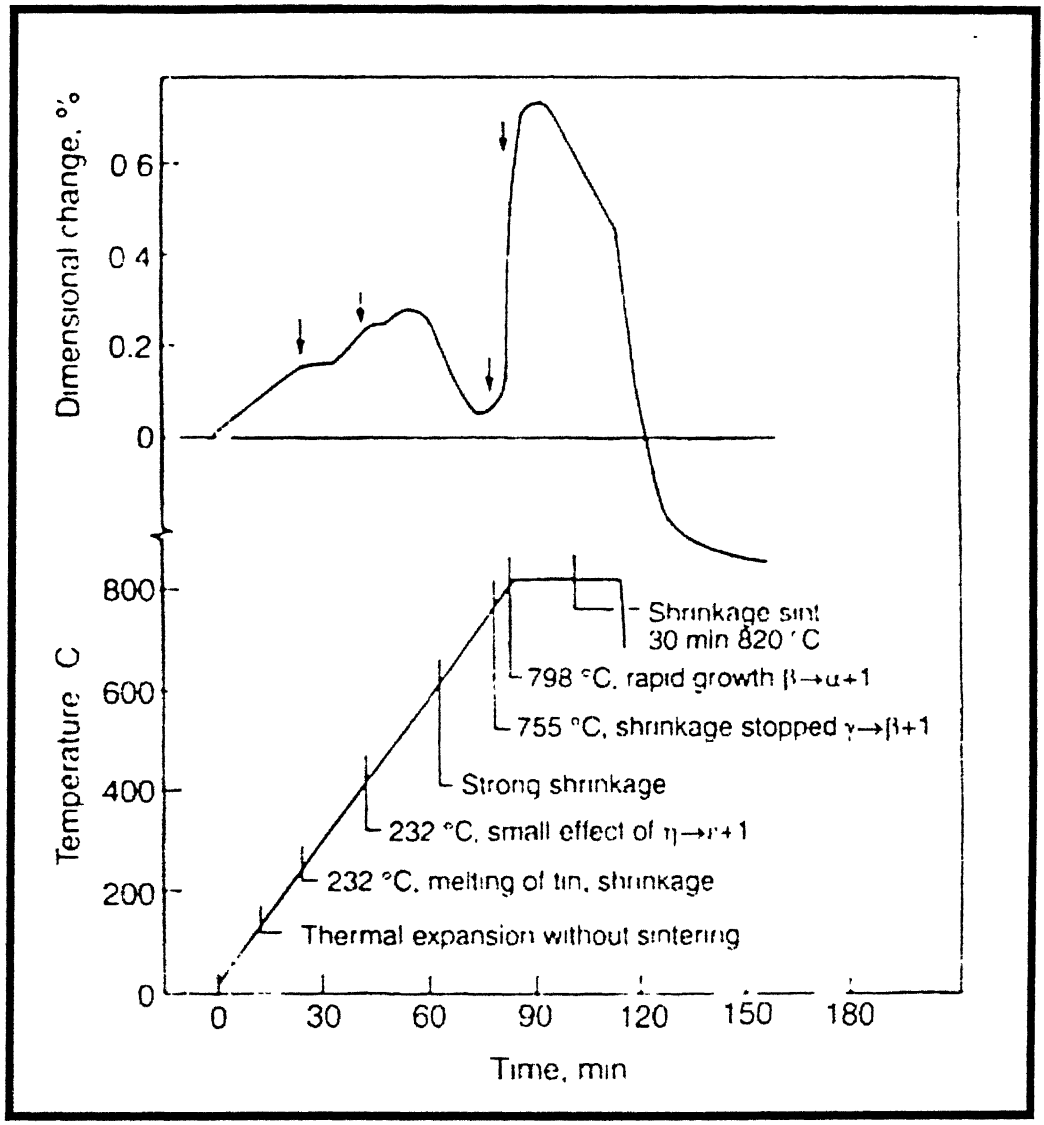

Figure 3.1. Dilatometric curve for Cu-10 Sn Premix during sintering [75].

that even at this composition micro-segregation is present in the case of the atomized material. With the 90/10 an even more marked effect occurs later as the δ phase reaches a temperature of 755°C. He also compared the dimensional changes of mixture of Cu + 85/15, Cu + 70/30, and Cu + 50/50.

The most comprehensive dilatometric study on sintering of 90/10 copper-tin bronze is reported by Patel [77-78]. They varied their test conditions during dilatometric study. That includes: standard grades of premix bronze, comparison of premixes A and B, specimen configurations, effect of green density, effect of heating rate, intermittent hold, atmospheres, additions of graphite and flow rate of atmosphere. From the dilatometric study it is supported that higher green density will lead to higher expansion. They have shown that heating rate affect the dilation curve in a noticeable manner and faster heating rate give rise to higher expansion. However choice of atmosphere also proved to be important and having an useful attribute towards the dilation curve. The dilatometric plots revealed swellings of 1.40%, 1.75%, 2.05%, 2.45% and 2.85% for 5.15, 25.50, 50.40, and 75.30 and 100% vol.% of hydrogen in a hydrogen-nitrogen mixture. The abrupt shrinkage at maximum temperature (i.e. 1.1%, 1.3%, 2.0%, 2.4%, and 3.7%) increased with the reducing potential of the atmosphere. They have concluded that, dilatometer is an effective research tool for the bronze powder manufacturers. The equipment can also be used for quality control checks and to quickly ascertain the consistency of the products at various manufacturing stages. It also a helpful and reliable analytical tool to help characterize the sintering response of premix bronze powders.

For this present study, bronze with the composition of 88Cu-12Sn was selected. From the phase diagram, it was clear that after sintering the system remains in a single phase. No intermetallic phase should be formed for this particular composition. Comparative study of both premixed and prealloyed compacts were made after sintering. Gas atomised spherical prealloyed powder were chosen for the study. Sintering temperatures were selected from the phase diagram. Phase diagram revealed the range of temperature corresponding to different types of sintering of bronze. Temperatures were selected such that they would cover solid-state, transient liquid phase and supersolidus liquid phase sintering conditions. Amount of liquid formation during supersolidus liquid phase sintering could be known form the phase diagram.

Sintering densities and the densification parameters were measured as the post sintering characterizations. Comprehensive studies between the two kinds of compacts were made. Microstructural evolution of both prealloyed and premixed compacts were studied as a function of sintering temperature and compacting pressure. Both optical and scanning electron microscopic micrographs were taken to observe the phase present in the microstructure and the distribution of pores in the matrix. Macrostructural variations were also found by the measurement of dimensions in both axial and radial directions. This observations confirmed the anisotropic change of the compacts after the sintering. In-situ evaluation of the change in sample dimensions were made by the dilatometric study. In-situ phase evaluations as a function of sintering temperatures were done by the differential scanning calorimetric study. XRD studies were also made to confirm the presence of phases in the final microstructures.

Chapter 4

EXPERIMENTAL PROCEDURE

4.1 Raw Materials

4.1.1 Copper Powder

Copper powder for the study was supplied by Royal Powdered Metals, Inc., UK. The chemical composition and powder characteristics are as follows,

Purity %	99.59	Sieve Analysis, Tyler	
Acid Insoluble	0.012	-60 + 100 mesh	trace
Hydrogen Loss	0.242	-100 + 150 mesh	0.20
Apparent Density g/cm^3	2.60	-150 + 200 mesh	9.20
Flow Rate sec/25cc	31	- 200 + 325 mesh	34.30
Compactibility g/cm^3	5.64	-325 mesh	56.30

4.1.2 Tin Powder

The tin powder chosen for this study was a gas atomized powder supplied by Alfa Products, Thiokol, Danvers, USA. This grade is a spherical powder and is sieved to –325 mesh (-45 μm) by the manufacturer. The choice was based on the powder's relatively low sintering temperature and simple chemistry, and the powder's near spherical shape.

4.1.3 Prealloyed Powder

The alloy chosen for this study was gas atomized prealloyed 88Cu-12wt.%Sn bronze. It was produced from the manufacturer called SCM, NY, USA. This grade is also a spherical powder. The chemistry of the sample is simple i.e. without any surface oxide and shape was near spherical.

4.2 Powder Characterization

The as received powders were characterized for their size, size distribution and morphology. Most of the characterization technique require only a small quantity of the sample powder, it is therefore assumed that the powder sample is representative of the bulk.

4.2.1 Particle Size and Size Distribution

Powder size was accomplished using a laser-scattering size analyser (model: Economy, Laser Klasse 1; supplier: Fritsch, Germany). Low angle Fraunhofer light scattering using monochromatic (laser) light and dispersed particles are used in this case. Particles are suspended in a moving fluid. The suspension was made using 1 to 3 g of powder in approximately 60 ml of distilled water with 10% sodium metaphosphate. The particles are passed through a laser beam in a circulating water stream. The light is scattered after the interaction with the particles, and the intensity is measured by strategically placed detectors. Particle size affects both the intensity and angular extent of scattering. With coherent light the angle of scattering varies inversely with the particle diameter. The scattering depends on the refractive index of the particle in the suspending medium, the wave length of light, and the particle size and shape.

From the particle size analysis we got the unimodal size distribution of the tin particles. Figure 4.1. shows the size distribution curve for tin particles. From that graph it is clear that maximum particles are in the range of 10-14 μm size. So we can say that mode size is between 10-14 μm. Figure 4.2. shows the particle distribution of prealloyed powder. That curve shows a bimodal distribution. Maximum particles retained in the range of 35-40 μm.

4.2.2 Particle Shape

A qualitative measure of particle shape was obtained using a JEOL, JSM – 840 A, Scanning Electron Microscopy, in the secondary electron (SE) mode. The SEM permitted far greater viewing magnification than optical equipment. Figures 4.3 to 4.6 show the representative SEM micrographs of the as received powders. The Sn powder was

fabricated by gas atomization and has spherical shape. Figure 4.4 shows the spherical shape of an individual Sn particle. As shown in SEM image of Figure 4.5, the as received Cu-12Sn prealloyed powder has rounded appearance and was fabricated by water atomization. The chemically reduced Cu powders have irregular morphology and are highly agglomerated. This is shown in the Figure 4.6.

4.3 Premix Preparation

Elemental Cu and Sn were weighed to 0.001 g accuracy using an electronic balance (supplier: Mettler, AE 200, USA). The balance was calibrated using a series of standard weights. The alloy composition (88Cu - 12Sn) was then placed in a 1 litre capacity glass jar and mixed in a turbula mixer (type: T2C Nr.921266, supplier: Bachofen AG, Germany) for half an hour. Mixing ensures complete homogeneity in the powder mixture. To prevent segregation, due care was taken to make that the powders were not shaken after mixing.

After the mixing of the powders to make the desire composition, the density of the selected composition was determined by the inverse rule of mixing. Inverse rule of mixing can be written as:

$$\frac{w}{\rho_{th}} = \frac{w_1}{\rho_1} + \frac{w_2}{\rho_2} \qquad (4.1)$$

where, w_1 and w_2 are the weight fraction of the powders to be mixed. Their respective densities are represented by ρ_1 a ρ_2. ρ_{th} is the density of the mixture.

For Cu-12Sn composition,

$$\frac{1}{\rho_{th}} = \frac{0.88}{8.95} + \frac{0.12}{7.27}$$

i.e. $\rho_{th} = 8.71$ g/cc

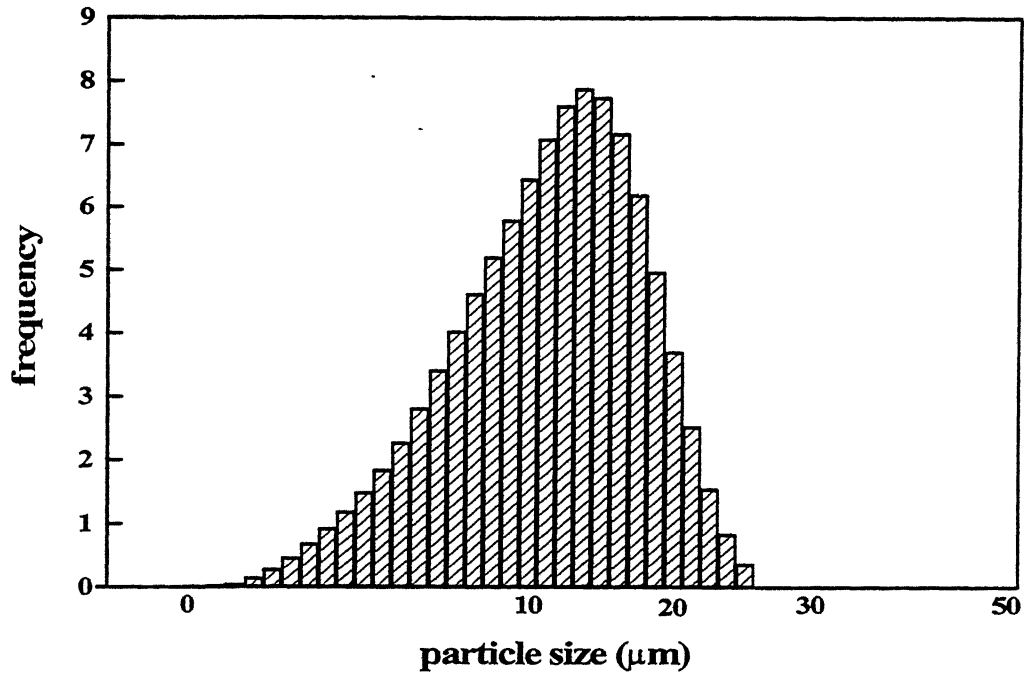

Figure 4.1. A histogram plot of the particle size analysis of Sn powder. Particle size axis is on a logarithmic basis.

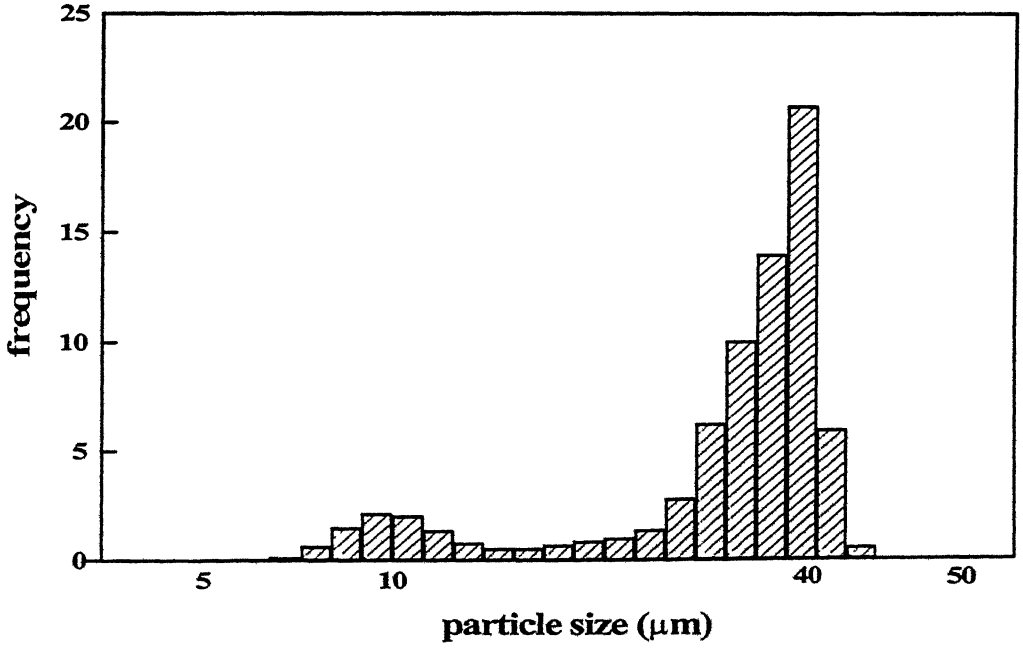

Figure 4.2. A histogram plot of the particle size analysis of prealloyed powder. Particle size axis is on a logarithmic basis.

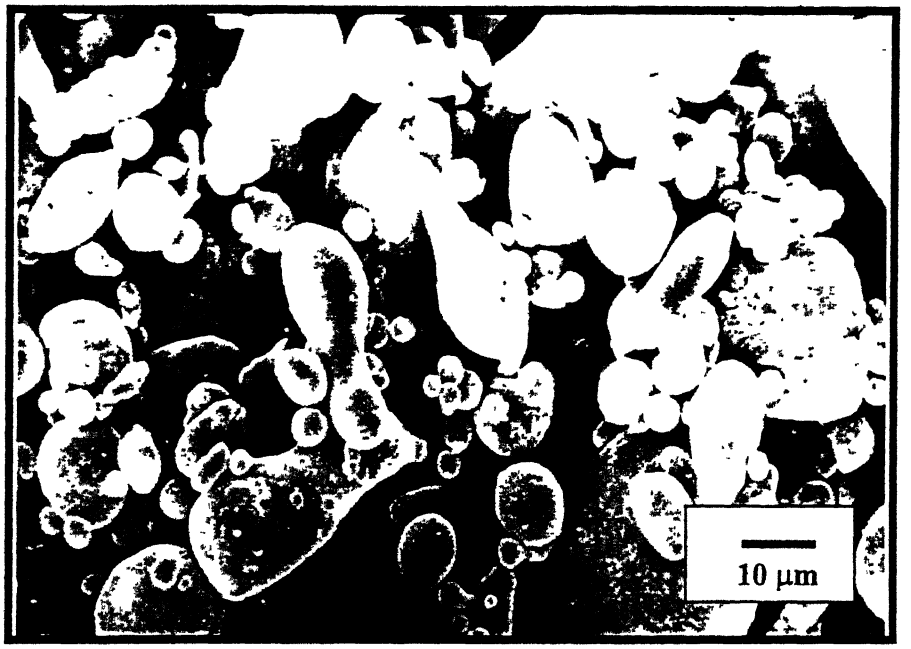

Figure 4.3. SEM micrograph of Sn powder.

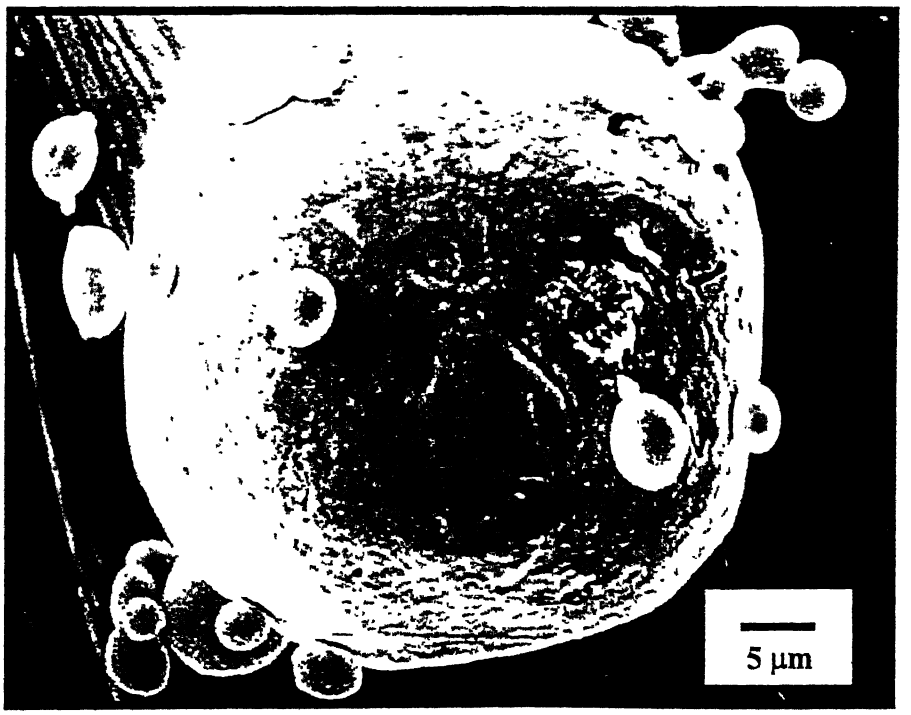

Figure 4.4. SEM micrograph of Sn powder. Showing a single particle.

Figure 4.5. SEM micrograph of prealloyed Cu-12Sn powder.

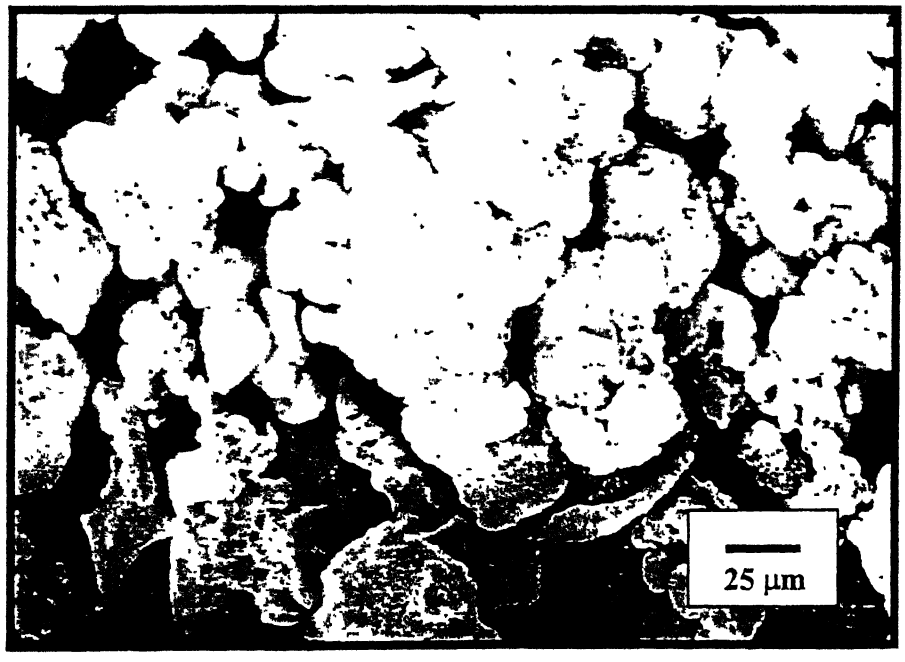

Figure 4.6. SEM micrograph of Cu powder.

4.4 Compaction

Cylindrical green compacts of 12.7 mm diameter and approximately 3 mm to 6 mm height were made from the premixed and prealloyed bronze powder in a single acting hydraulic press. Manually operated hydraulic machine (Apex Construction Ltd, UK) of 20 tons capacity was used for this purpose. We used two extreme pressure conditions for compacting both premixed and prealloyed powder. Minimum compacting pressure was selected as 150 MPa and the maximum was 600 MPa. The die made of high chromium high carbon steel was cleaned with acetone and was lubricated with zinc-stearate prior to each powder fill. Lubrication facilitates compaction and subsequent removal of the compacted samples. For dilatometric study the specimens of both premixed and prealloyed powders were made of another die with inner diameter 6.5 mm. The pressure in these cases were kept less than 150 MPa. Approximate height of these samples were 4 to 6 mm.

4.5 Sintering

Sintering were carried out in our own made laboratory type SiC-heated horizontal tubular furnace (rating 1.5 kVA). The furnace tube was made up of doubly recrystallized alumina. The inner diameter of the tube was 38 mm and length 980 mm. In our present work we use commercially pure hydrogen as sintering atmosphere. The furnace had a heating zone of approximately 105 mm upto a temperature of 1350°C with an accuracy of ± 3°C.

In the present work five different temperatures were selected for sintering. The temperatures were 220°, 275°C, 775°C, 850°, and 880°C. Requisite number of the green cylindrical compacts of premixed and prealloyed bronze were placed over a Inconel boat and transferred in the centre of the tubular furnace. Inconel has got higher melting point than our maximum sintering temperature. So, there should be no sticking problem of the samples with the boat. Both ends of tubular furnace were sealed with SILASTIC (RTV 700) adhesive/sealant to prevent any leakage. Heating rates were same for all the sintering operations (5°C/min). The samples were heated to the final sintering temperature without intermittent holding. Holding time was 40 min at final sintering temperature for each case. Automatic temperature controller was used to control the

temperature within ± 5°C. In all cases cooling was done in prevailing atmosphere at an average rate of 2 –3°C/min.

4.6 Densification Behaviour

4.6.1 Density and Densification Parameter

Densities of green and sintered cylindrical compacts were calculated from the mass and the physical dimension measurements of the sample. Densification parameter was also an way to determine the amount of densification occurred after sintering. Densification parameter (ψ) was expressed as follows

$$\psi = \frac{SD - GD}{TD - GD} \tag{4.2}$$

SD = Sintered Density

GD = Green Density

TD = Theoretical density

Theoretical density of Cu-12Sn premixes was determined from the inverse rule of mixture taking the theoretical density of various elements at room temperature. This is an oversimplification as all the used premixes did not remain as mixture without undergoing any reaction.

4.6.2 Linear and Radial Shrinkage

Linear dimensions of the sintered samples were measured using vernier callipers and screw gauge. Average of four measurements of each dimension is reported. The formula used for calculations are as follows,

$$\delta h = \left(1 - \frac{h_s}{h_g}\right) \times 100\% \tag{4.3}$$

$$\delta r = \left(1 - \frac{r_s}{r_g}\right) \times 100\% \tag{4.4}$$

Where,

$\delta h \rightarrow$ % linear shrinkage in height

$\delta r \rightarrow$ % radial shrinkage

h_g, $r_g \rightarrow$ height and radius of the green compact

h_s, $r_s \rightarrow$ height and radius of the sintered compact.

4.6.3 Total Porosity

The specimens, immersed in xylene, were placed in a vacuum desiccator and the pressure was reduced for a period of 20 min. this treatment removed gas from the open pores and allowed the xylene to enter. The specimens were then removed from the xylene, and after the surface liquid had been wiped off by means of filter paper, they were weighed in air and in water. The xylene being non-miscible with water, prevented the water from entering the pores, so that the difference between the last two weighing gave the total volume of the specimen [79].

Letting A_1 = weight of specimen, B = weight of specimen after impregnation with xylene, and C = weight of impregnated specimen in water:

B – C = volume of specimen

$$\varepsilon_i = \frac{(B - A_1)}{(B - C)\rho_x} \tag{4.5}$$

$$\varepsilon_T = \frac{(B-C) - \dfrac{A_1}{\rho_{Cu-12Sn}}}{(B-C)} \tag{4.6}$$

$$\varepsilon_T = \varepsilon_i + \varepsilon_C \tag{4.7}$$

where ε_i and ε_T are the interconnected and total porosities, respectively, and ρ_x and $\rho_{Cu\text{-}12Sn}$ are the densities of xylene and bronze. The difference between ε and ε_i gives ε_c, the closed porosity.

4.7 Mechanical Properties

4.7.1 Vickers Macrohardness

Vickers Macrohardness of the polished specimens were measured on Leco V-100-C1, Hardness Tester, manufactured by Akashi Corporation, Japan. The machine was automatic and time for indention was pre-programmed. The load of 300 g and indentation time of 15 s was maintained. The diagonal length of the impressions were measured and the hardness was obtained directly in HV scale on the monitor.

4.8 Microstructural Studies

4.8.1 Optical Microscopy

As the height of the cylindrical samples were enough for holding, no mounting was done. The compacts were wet polished on the Lunn Major Unit of Struers, Denmark make 220, 320, 500 and 1000 grit silicon carbide emery papers followed by fine wheel polishing with suspended 0.03 μm size alumina in distilled water. Acidic $FeCl_3$ was used as the etchant. Composition of the etchant was:

$FeCl_3 \rightarrow 5$ g

$HCl \rightarrow 50$ ml

$H_2O \rightarrow 100$ ml

Etching was done on the leather for 15-20 s.

4.8.1 Scanning Electron Microscopy

The microstructures of selected samples were also observed using JEOL, JSM – 840 A, Scanning Electron Microscopy. Operating voltage was 10 – 15 kV and probe current ranged from 1×10^{-10} to 5×10^{-8} A in secondary electron imaging mode. The samples were deeply etched for SEM study to that they can reveal more finer details.

4.9 Dilatometric Study

A dilatometer allows for determination and *in situ* measurement of numerous sintering events, such as shrinkage, shrinkage rate, phase transformation, and melt

formation. Figure 4.7 is a schematic diagram of the vertical pushrod dilatometer (model: Dilamatic II SDP Vertical; supplier: Theta Industries, Washington, NY, USA) used in this study. It consists of a 1600°C alumina sintering furnace capable of operating in numerous atmospheres: air, nitrogen, hydrogen, argon, and low vacuum. The tube, specimen holder, and the pushrod are all made of high density alumina. A photo-optic grating sensor converts the pushrod displacement into an electrical signal, which is processed by a microcomputer. The weight of the pushrod assembly is counterbalanced by weights at the opposite end so that it moves in accordance to the dimensional change in the sample without exerting significant pressure. The sample is placed between two alumina discs to uniformly distribute the load and to eliminate contamination from probe or adhesion. The dilatometer is connected to a personal computer which collects time, temperature, and vertical displacement data. Instrument was calibrated by the method stated in the manual of the machine. By the help of the software it was possible to maintain the sintering cycle according to our requirement. Test conditions were pre-programmed including heating rate and holding time at a specific temperature.

Both premixed and prealloyed samples are subjected to dilatometric study. Sintering atmosphere was argon. For premixed sample heating cycle called Cycle 1 is used. Details of the cycle is given below:

Cycle 1:

Heating rate	**From**	**To**	**Holding time**
3°C/min	Room Temp.	150°C	15 min
7°C/min	150°C	225°C	5 min
7°C/min	225°C	275°C	5 min
7°C/min	275°C	525°C	5 min
7°C/min	525°C	870°C	40 min

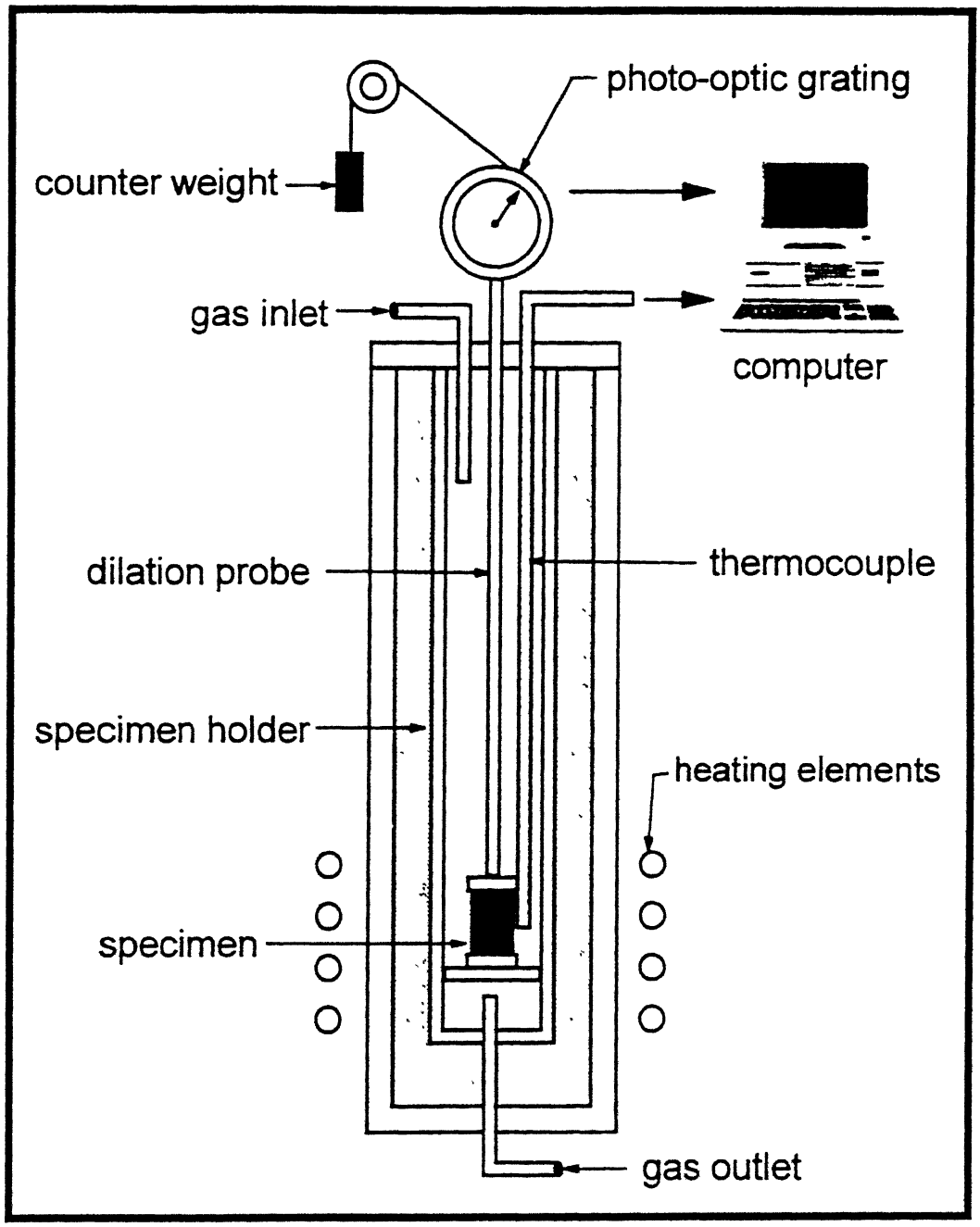

Figure 4.7. Schematic sketch of the dilatometer.

4.10 X-ray Diffraction Analysis

X-ray diffraction studies on the powder (both premixed and prealloyed), green and sintered compacts were carried out on Rich Seifert & Co., Germany make, ISO Debyeflex –2002 diffractometer. Powders were kept in a square holder with very small thickness. Some methyl alcohol was put on the powders so that they would properly adhered during the diffraction study. Compacted samples after grinding upto 1000 grit SiC paper, were put into the holder for analysis. The various parameters during the experiment are as given below,

Target (Radiation) → Cu (K_α)

Wavelength, $\lambda \rightarrow 1.542 \times 10^{-10}$ m

Scanning Speed → 3°C/min, (in 2θ)

Counts/min → 50,000

Time Constant → 3 s

Amperage → 20 mA

Voltage → 30 kV

The X-ray machine is interfaced with computer. While scanning the sample, computer saved all the data (intensity and angle) as a text file. Those files are taken and the intensity vs. angle graphs were replotted by using a software called Origin. Analysis of those peaks were also done by the same software. Indexing of X-ray diffraction patterns were carried out by matching using computer package of Joint Commission for Powder Diffraction Standard (JCPDS), ed. 1996.

4.11 Differential Scanning Calorimetry

The melting characteristics of the bronze alloy chosen were determined by differential scanning calorimetry (DSC) using the TA Instruments NETZSCH STA 409C, Germany make. DSC is a technique which is a part of a group of techniques called Thermal Analysis (TA). Thermal analysis is based upon the detection of changes in the heat content (enthalpy) or the specific heat of the sample with the temperature. As the thermal energy is supplied to the sample its enthalpy increases and its temperature rises

by an amount determined, for a given energy input, by the specific heat of the sample. The specific heat of a material changes slowly with temperature in a particular physical state, but alters discontinuously changes at the change of state. As well as increasing the sample temperature, the supply of thermal energy may induce physical and chemical processes in the sample, e.g. melting or decomposition, accompanied by a change in enthalpy, the latent heat of fusion, heat of reaction etc. DSC, differs fundamentally from DTA in that the sample and reference are both maintained at the temperature predetermined by the program even during a thermal event in the sample. The amount of energy which has to be supplied or to withdrawn from the sample to maintain zero temperature differential between the sample and the reference is the experimental parameter displayed as the ordinate of the thermal analysis curve. In other words, in DSC the measuring principle is to compare the rate of heat flow to the sample and to an inert material which are heated or cooled at the same rate. Changes in the sample that are associated with absorption or evolution of heat cause a change in the differential heat flow which is then recorded as a peak.

In this case, the unit was first calibrated using pure unalloyed metal, such as silver and nickel, to determine the offset temperature. The sample and the reference material were placed in adjacent sample cup holders. Alumina was used as the reference material as it is stable over the temperature range. A temperature difference between the sample and the reference therefore, indicates a change of phase.

The DSC runs were performed on both premixed and prealloyed samples. In both the cases samples were heated upto 900°C at 10°C/min in 100% argon. Premixed and prealloyed both were undergone the test to determine the difference in the homogenization process during sintering.

Chapter 5

EXPERIMENTAL RESULTS

The experimental results of the present investigation are divided into ten sections. The first section presents the result of the sintering parameters and properties of premixed and prealloyed Cu-12Sn composition. In this section density and densification parameters of the samples are discussed. Second section deals with the weight loss comparison for different sintering conditions and also for different powder compacts. In the third section radial and axial shrinkage behaviours are compared. Next section gives the measurement of porosity through xylene impregnation. Hardness testing, SEM and optical microscopy, dilatometric study, x-ray diffraction and differential scanning calorimetry results are given in the subsequent sections.

5.1 Density and Densification Parameter

As described in the earlier chapters, the present work had been carried out with two different approaches of bronze component making. It is already stated that one of them was premix route and second one was prealloyed route. It is interesting to note the variation of green density as a function of compacting pressure for both the cases. Appendix I and Appendix II give the experimental data before and after sintering for all the samples used in the present study. It is evident from Appendix I that in both premix and prealloyed samples, the green density increases with pressure. For premixed bronze, the green density changes from 67% to as high as 87% theoretical as the compaction pressure changes from 150 MPa to 600 MPa. For prealloyed sample, increasing pressure brings the change in density from around 60% to 80%. It is interesting to note that premixed samples have higher density compared to prealloyed powder for a given pressure level. Appendix II presents effect of temperature on the sintering density of both premixed and prealloyed bronze samples. Figure 5.1 shows the variation of sintered density with sintering temperature for both 150 and 600 MPa pressure conditions. In both the pressure conditions, sintered density decreases upto 775°C. Then it increases slightly and finally again decreases as sintering temperature increases. But the situation is quite

different for prealloyed Cu-12Sn compacts. Figure 5.2 shows the variations of sintered density with temperature for the prealloyed samples. It is seen that behaviour is different for both pressure. At low pressure sintered density increases as the sintering temperature increases. But at higher pressure increase in the density occurs upto a certain temperature. Beyond that, increasing sintering temperature cause the reduction in sintered density. In Figure 5.3 sintered density of premixed and prealloyed compacts pressed at 150 MPa are compared. It shows that upto 775°C sintered densities of premixed samples are higher than the prealloyed samples. But the situation is reversed above this temperature because 850°C is above the solidus temperature. Then density of prealloyed samples are higher than the premixed one. In the same way comparison is drawn for 600 MPa pressed bronze compacts in Figure 5.4. Effect of compaction pressure on the sintered densities for both premixed and prealloyed compacts are shown in Figures 5.5 and 5.6, respectively. From Figure 5.5 it can be seen that, for premixed samples initially the sintered densities are higher for 600 MPa. However, density decreases as the temperature increases. Compacts pressed at 150 MPa doesn't show that much change of sintered density. So, it is clear that for premixed sample compaction pressure of 600 MPa has got detrimental effect on the sintered density of the sample. Figure 5.6 indicates the change of densities of prealloyed samples. It is found that higher pressure i.e. 600 MPa doesn't affect the sintered too much. But for 150 MPa the densities increase as the sintering temperature increases.

Densification parameter is also very important to understand the behaviour of sample because it gives a relative measure of densification of compacts with density being normalized with respect to green density. So, densification parameters are plotted for both premixed and prealloyed samples and they are shown in the Figures 5.7 and 5.8. In Figure 5.7 densification parameters variation with temperature of premixed and prealloyed samples compacted at 150 MPa are compared. It is seen that at sintering temperature 775°C, densification parameter is negative for premixed sample, which implies that the sample expands upon sintering. At 850°C premixed sample shrinks. However, on increasing the temperature beyond that (850°C), densification parameter decreases because of the distortion of the sample. Prealloyed sample has undergone

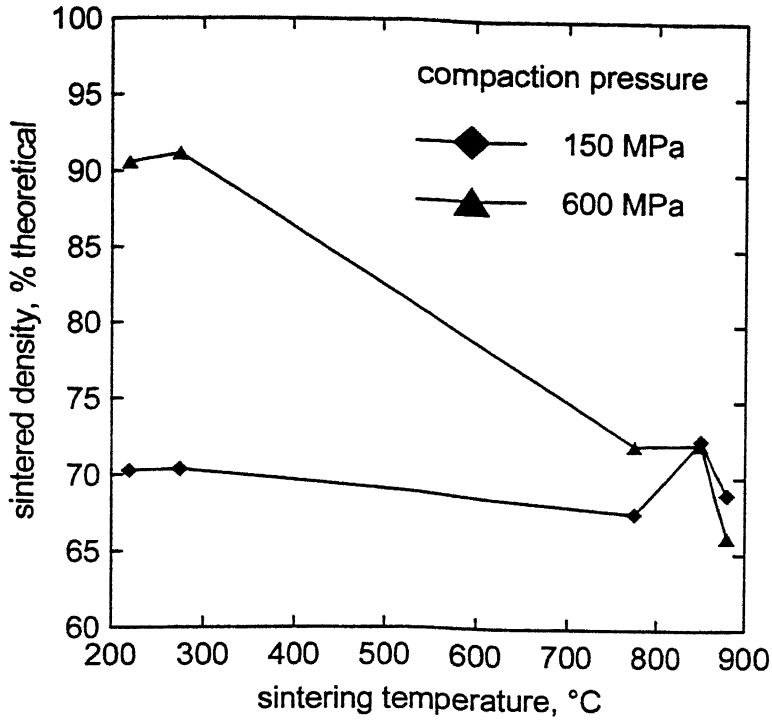

Figure 5.1. Variation of sintered density as a function of temperature for premixed Cu-12Sn

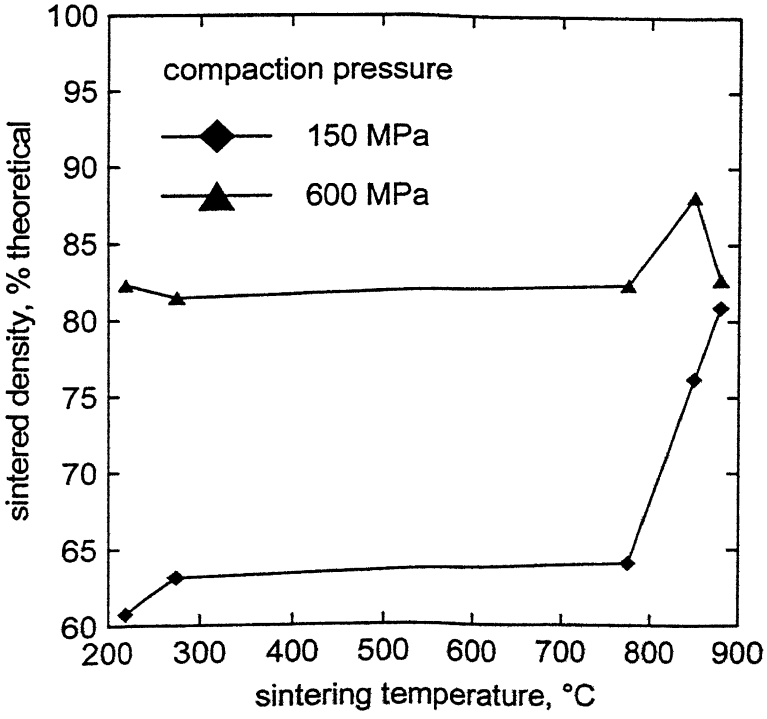

Figure 5.2. Variation of sintered density as a function of temperature for prealloyed Cu-12Sn

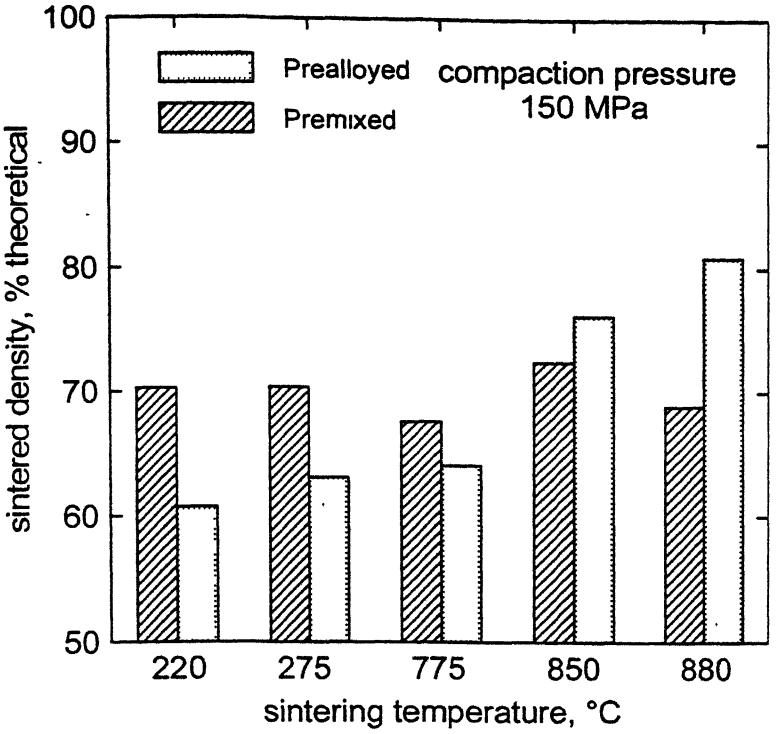

Figure 5.3. Comparison of premixed and prealloyed compact. The samples were pressed at150 MPa.

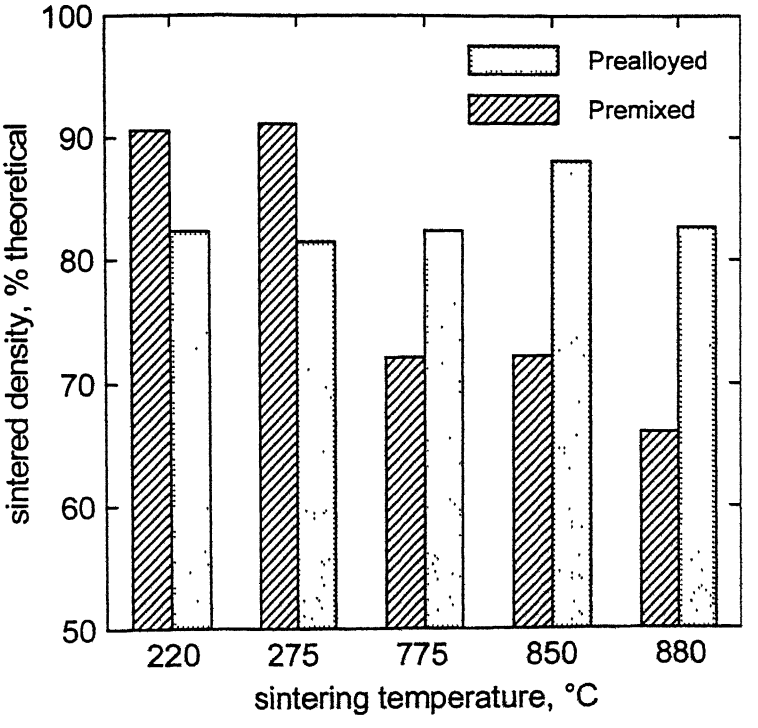

Figure 5.4. Comparison of premixed and prealloyed compact at 600 MPa.

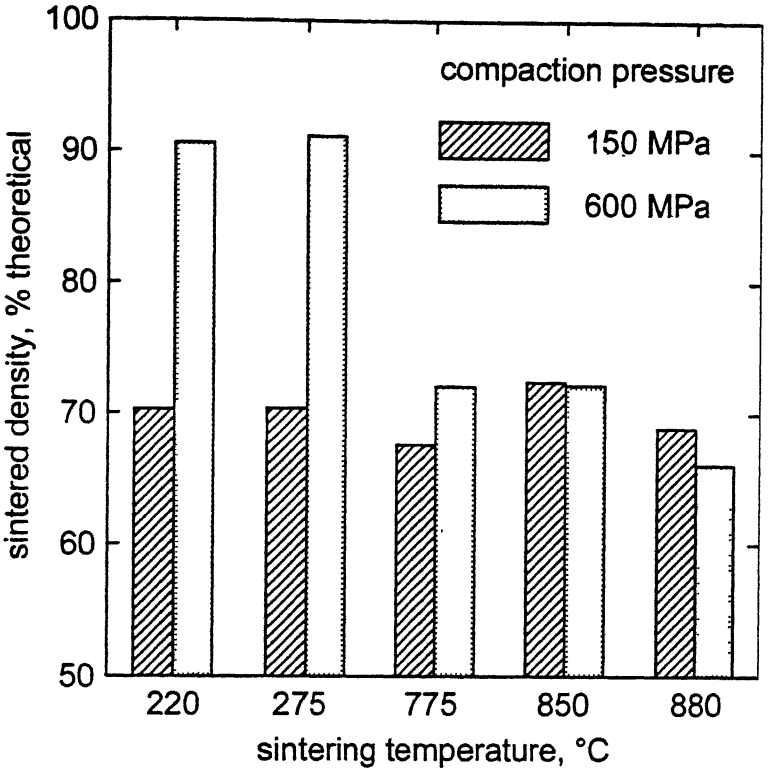

Figure 5.5. Effect of compaction pressure on the sintered density of premixed sample.

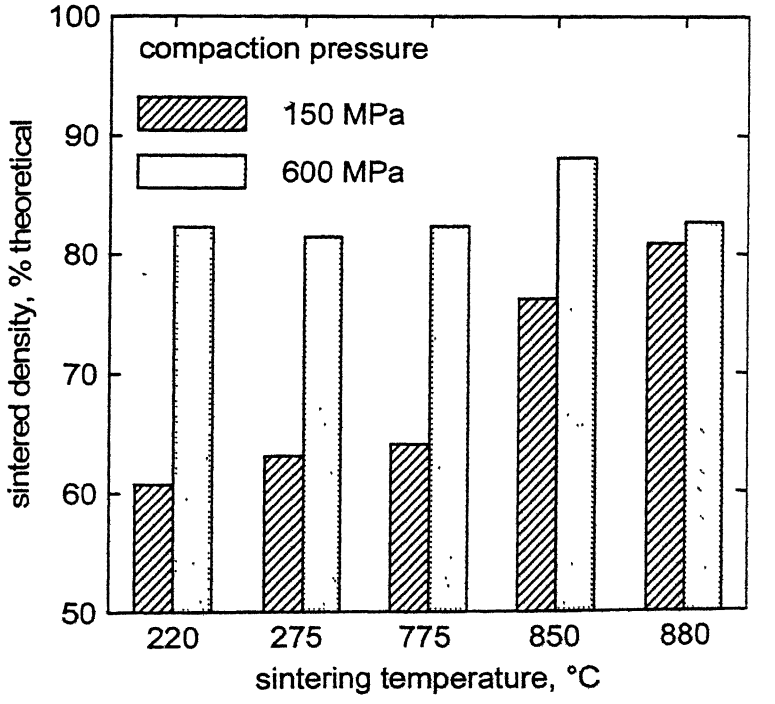

Figure 5.6. Effect of compaction pressure on the sintered density of prealloyed sample.

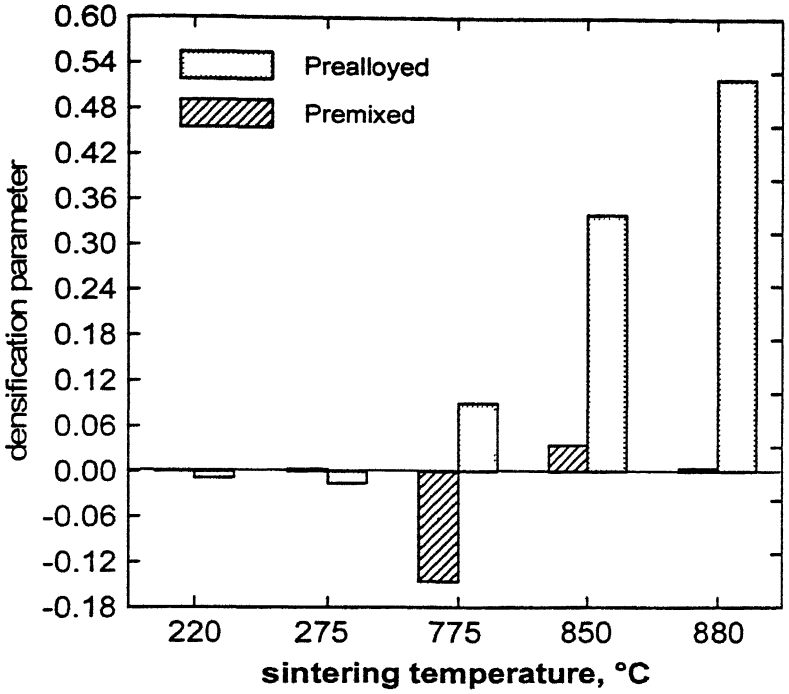

Figure 5.7. Comparison of densification parameter of premixed and prealloyed samples pressed at 150 MPa. Premixed samples sintered at 880°C were distorted.

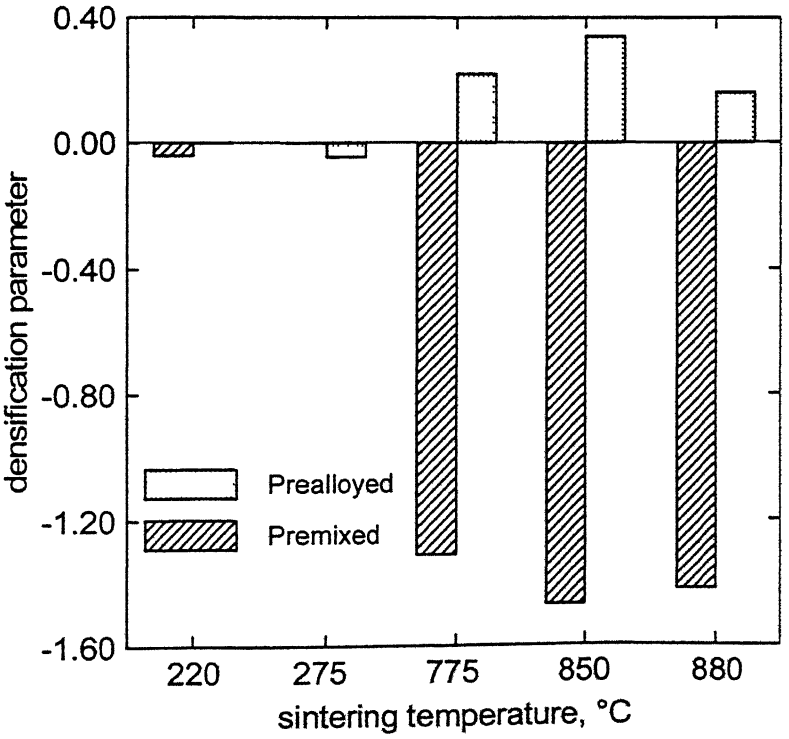

Figure 5.8. Comparison of densification parameter of premixed and prealloyed samples pressed at 600 MPa. Premixed samples sintered at 880°C were distorted.

shrinkage at 775°C. Upto 880°C the amount of densification increases steadily. From Figure 5.8 at 600 MPa the same behaviour of prealloyed sample is observed as 150 MPa. Prealloyed sample densified in this case also. But if we compare with 150 MPa, it is found that the densification parameter is slightly lower in the later case. Premixed sample also behave in the same way as in the case of 150 MPa. Expansion of premixed samples at 600 MPa are larger than 150 MPa.

5.2 Weight Loss

Weight loss is very important for the sintering of the compacts industrially. From Appendix II different weight loss form different samples can be found. Figure 5.9 shows the weight loss comparison for premixed and prealloyed compacts at 150 MPa. For prealloyed samples the weight loss increases upto the sintering temperature of 775°C. But if the samples are sintered at higher temperature than 775°C weight loss becomes constant.

In case of premixed samples, the weight loss increases as the sintering temperature increases. But the loss in weight is much higher for prealloyed samples compared to premixed samples. Figure 5.10 shows the weight loss comparison at compacting pressure of 600 MPa. For both prealloyed and premixed samples the trends are same as in the case of 150 MPa. In summary, by comparing Figure 5.9 and Figure 5.10, it is evident that weight losses are pressure independent. They depends mainly on the sintering temperature.

5.3 Porosity Determination

The porosity of the samples were determined by the xylene impregnation test as described in the Chapter four. The experimental results of that experiment is given in the Appendix III. The total porosities for both premixed and prealloyed samples are plotted in Figure 5.11 and 5.12. Figure 5.11 compares the porosity variation of premixed and prealloyed sample as a function of temperature at compaction pressure 150 MPa. In Figure 5.12 the same kind of comparison have been made but at compaction pressure 600

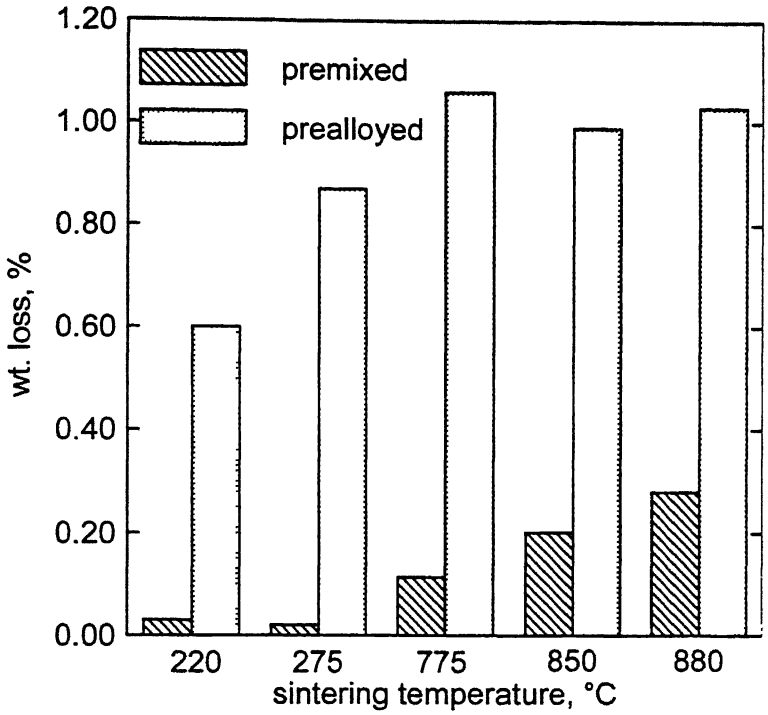

Figure 5.9. Weight loss comparison of premixed and prealloyed samples compacted at 150 MPa.

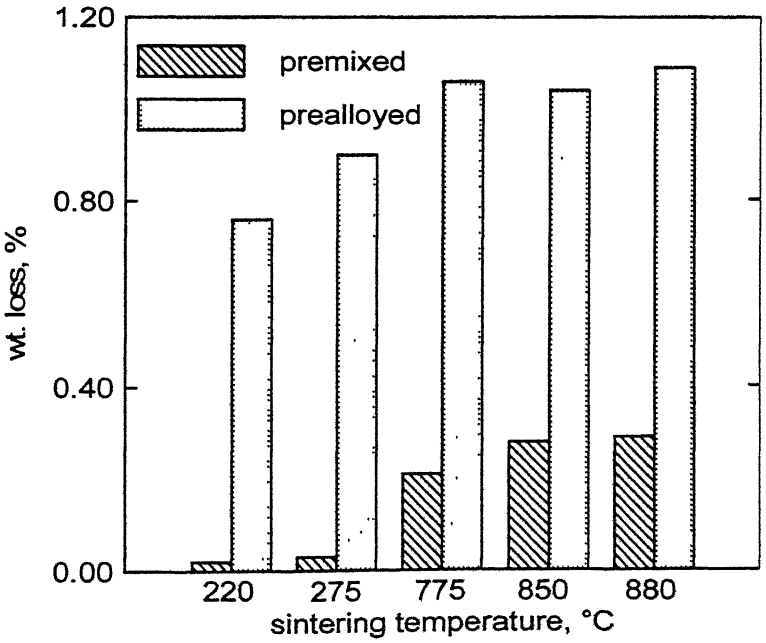

Figure 5.10. Weight loss comparison of premixed and prealloyed samples compacted at 600 MPa.

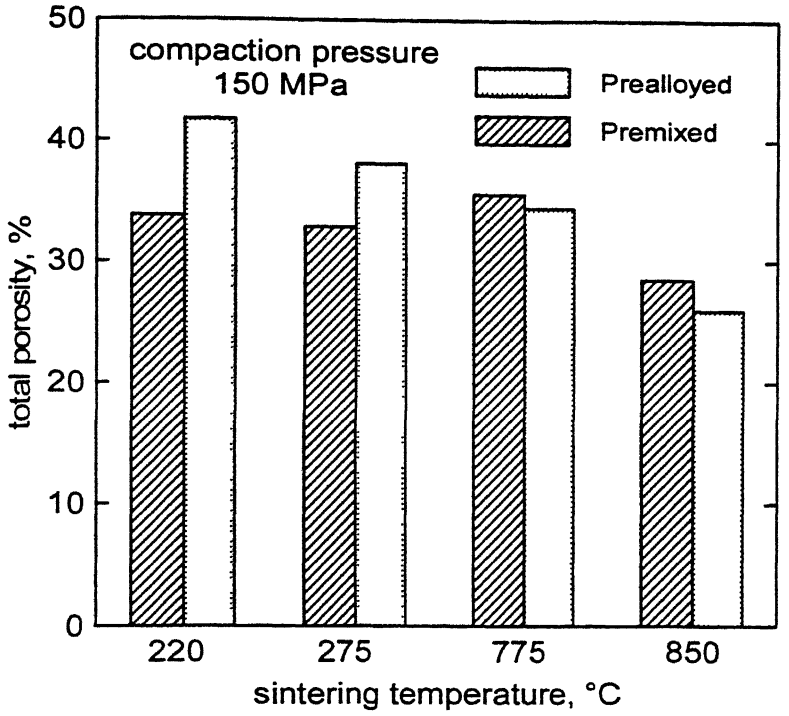

Figure 5.11. Comparison of total porosities measured by xylene impregnation of premixed and prealloyed samples.

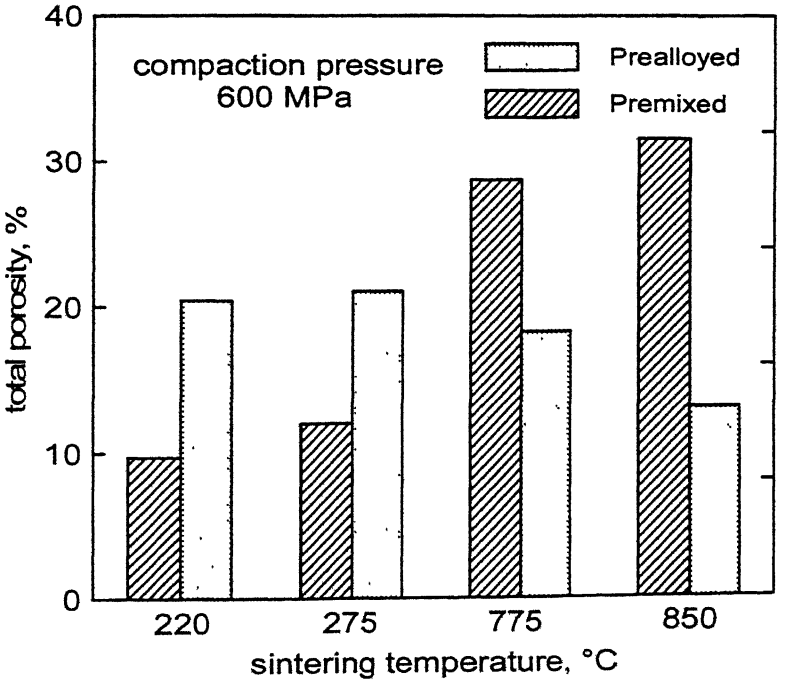

Figure 5.12. Comparison of total porosities measured by xylene impregnation of premixed and prealloyed samples.

MPa. The trend in the porosities determined by xylene impregnation tests are matching with their value predicted from density determinations.

5.4 Axial and Radial Shrinkage

Appendix IV represents the axial and linear shrinkage data for the samples after sintering. Careful observations of the table shows that prealloyed samples have undergone shrinkage on both axial and radial directions. As the sintering temperature increases, the amount of shrinkage also increase for compaction pressure of 150 MPa. But at lower temperatures 220°C and 275°C which corresponds to below and above Sn melting point, no dimensional changes are observed. When the compaction pressure is increased to 600 MPa, the prealloyed samples behave slight differently than 150 MPa samples. At higher compaction pressure, dimensional changes in radial and axial directions are lesser in magnitude compared to 150 MPa.. For premixed samples, at sintering temperature of 775°C expansion occurs. The sample expand in both direction. But at lower temperature (220°C and 275°C) no changes are observed as usual. If the compaction pressure of premixed samples is increased, they are undergone more expansion in both directions.

5.5 Macrohardness

The hardness values obtained from the experimens are given in the Appendix V. Standard deviations are also calculated for all the samples. Variation of hardness with the change in sintering temperature at 150 MPa and 600 MPa can be observed from the Appendix V. For prealloyed samples hardness increase as the sintering temperature is increased. But the hardness variations are almost negligible. But for the prealloyed samples compacted at 600 MPa shows something different. Hardness increase as we increase the sintering temperature from 775°C to 850°C. But at sintering temperature of 880°C hardness decreases. For premixed samples increase in sintering temperature from 775°C to 850°C results in corresponding increase in the hardness for both compaction pressure.

5.6 Optical Microscopy

Optical photomicrographs of the sintered samples are shown from Figure 5.13 to 5.20. The micrographs capture the microstructural evolution trajectory of the samples as a function of sintering temperature. At lower temperatures (220°C and 275°C), the samples couldn't be polished as they are too fragile. Consequently, micrographs aren't shown for those temperatures. Figure 5.13 shows the microstructure of premixed sample sintered at 775°C. The compact was pressued at 150 MPa. The microstructure reveals distinct bimodal distribution of pores. Figure 5.14 shows the microstructure of prealloyed sample pressed at 600 MPa and sintered at 775°C. Pores are distributed all over the microstructure. Very few larger pores observed at the grain boundary. Interestingly most of the pores are appeared rounded.

Figure 5.15 shows the microstructure of premixed sample compacted at 600 MPa and sintered at 850°C. This low magnification micrograph reveals the pore characteristics. Pores are irregular in shape and primarily located at the grain boundaries. Figure 5.16 is the micrograph of the prealloyed sample sintered at 850°C, whereas Figure 5.17 is the micrographs of premixed sample sintered at 850°C. Samples in both cases were pressed at 600 MPa. Microstructure of prealloyed sample for the same condition is shown in Figure 5.18. Figure 5.19 and Figure 5.20 show the micrographs of premixed and prealloyed samples respectively. Sintering temperature for those were 850°C. Interestingly all the optical micrographs shown above reveals the presence of only α- phase in the final product. For all the figures shown, pores are distributed throughout the single phase α matrix. No intermetallic phases such as β, δ, or ε are observed.

5.7 SEM Micrographs

SEM micrographs of the sintered samples are shown from Figure 5.21 to Figure 5.30. These micrographs are taken for some of the selective samples. Main aim was to capture the changes in microstructures brought by the melt formation during sintering. Sintering temperature below 820°C, essentially corresponds to the solid state sintering, whereas 850°C and 880°C fall in the range of supersolidus liquid phase sintering. Figure

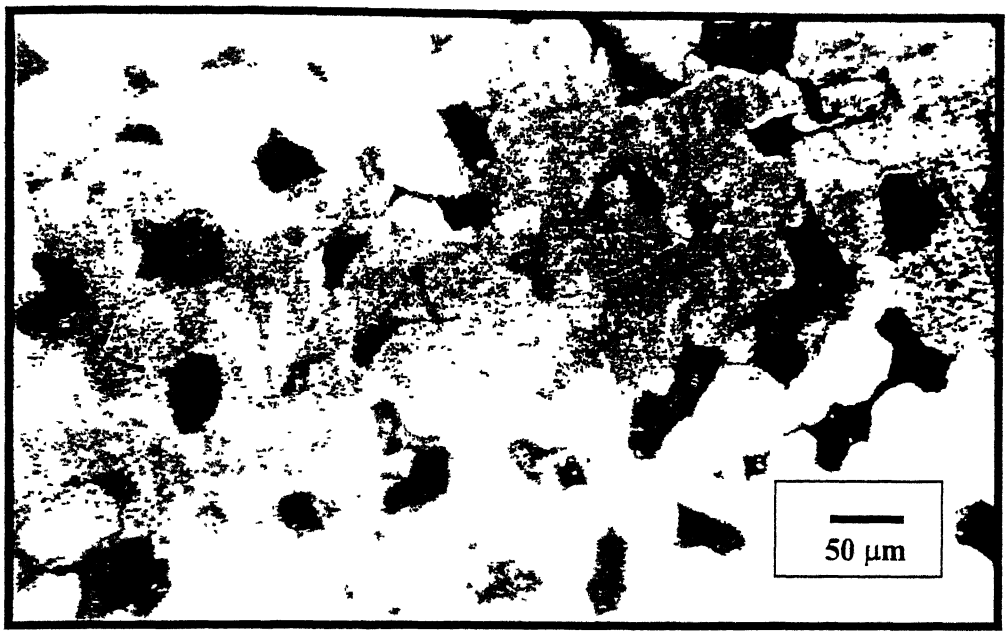

Figure 5.15. Optical micrograph of premixed sample sintered at 850°C. The sample was pressed at 600 MPa.

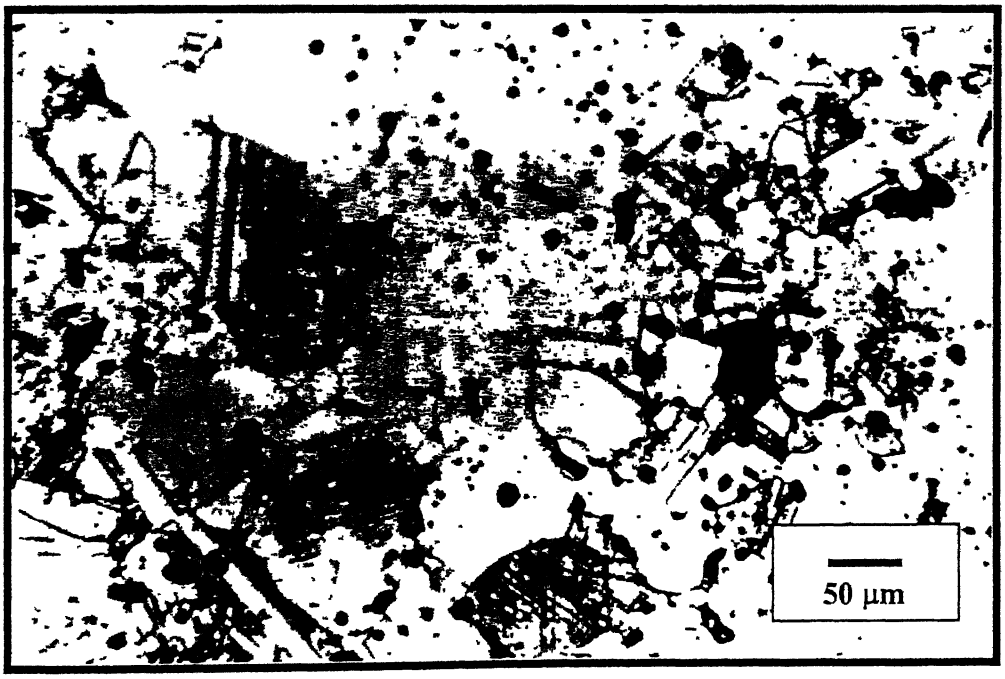

Figure 5.16. Optical micrograph of prealloyed sample sintered at 850°C. The sample was pressed at 600 MPa.

Figure 5.17. Optical micrograph of premixed sample sintered at 850°C. The sample was compacted at 600 MPa.

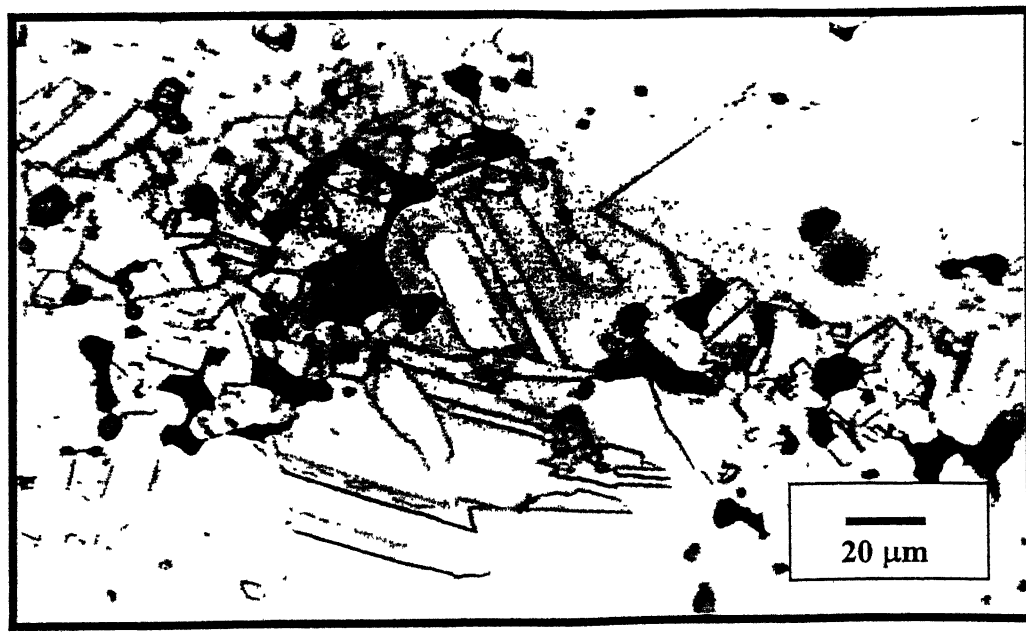

Figure 5.18. Optical micrograph of prealloyed sample compacted at 600 MPa and sintered at 850°C.

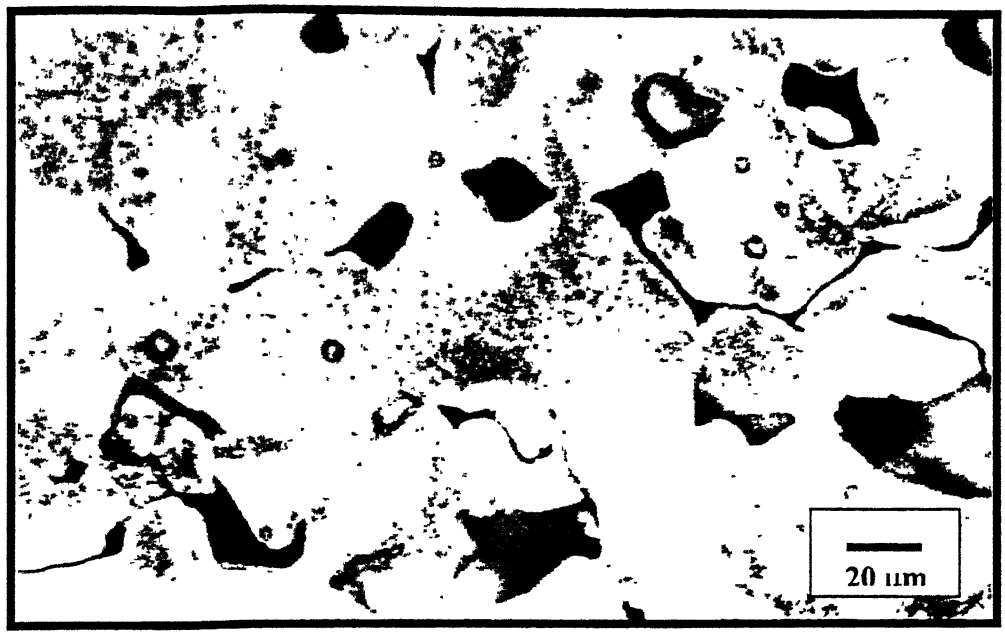

Figure 5.19. Optical micrograph of premixed sample sintered at 850°C. The sample was pressed at 150 MPa.

Figure 5.20. Optical micrograph of prealloyed sample sintered at 850°C. The sample was pressed at 150 MPa.

5.21 shows the microstructure of premixed sample sintered at 850°C. Compaction pressure for this case was 150 MPa. Pores are observed at the grain boundary. Within grains small melt globules are observed. Figure 5.22 shows the microstructure of prealloyed sample. This is also sintered at 850°C. Pores are rounded and uniformly distributed throughout the matrix. They are smaller in size.

Figure 5.23 shows the split image of prealloyed sample sintered at 850°C. The square shaped area in the left hand side is enlarged on the right hand side. Twin bands are observed. Figure 5.24 represents the Back Scattered Electron (BSE) mode micrographs of the same sample as Figure 5.23. Figure 5.25 shows the micrographs of premixed sample sintered at 775°C, compaction pressure being 150 MPa. The BSE image of the premixed sample sintered at 775°C is shown in Figure 5.26. Pores and the matrix have different contrast and they can be easily distinguished.

Figure 5.27 shows the micrographs of prealloyed sample sintered at 775°C. Compaction pressure was 150 MPa. In Figure 5.28 the low magnification micrograph of prealloyed sample sintered at 880°C is shown. The pores are spherical in nature. Well distribution of pores throughout the single α phase matrix is observed. Compaction pressure for this case was 150 MPa. Figure 5.29 also shows the micrograph of prealloyed sample sintered at 880°C. But compaction pressure was 600 MPa. The magnification for this case is double than Figure 5.28. Figure 5.29 shows the location of pores at the grain boundary. Pores are almost spherical. Melts inside the grain as well as along the grain boundary. A classic micrographs of supersolidus liquid phase sintering of prealloyed sample is given by Figure 5.30. Sintering temperature was 880°C. It shows the intragranular and intergranular melt formation. Annealing twins are also observed. As the optical micrographs, SEM micrographs also indicate the presence of only α phase in the microstructure. No other phases are observed.

5.8 Dilatometric Plots

As described in the section 4.9, premixed sample was subjected to dilatometric study. In this case sample was compacted at 150 MPa. The respective data for this study is given by the Table 5.1.

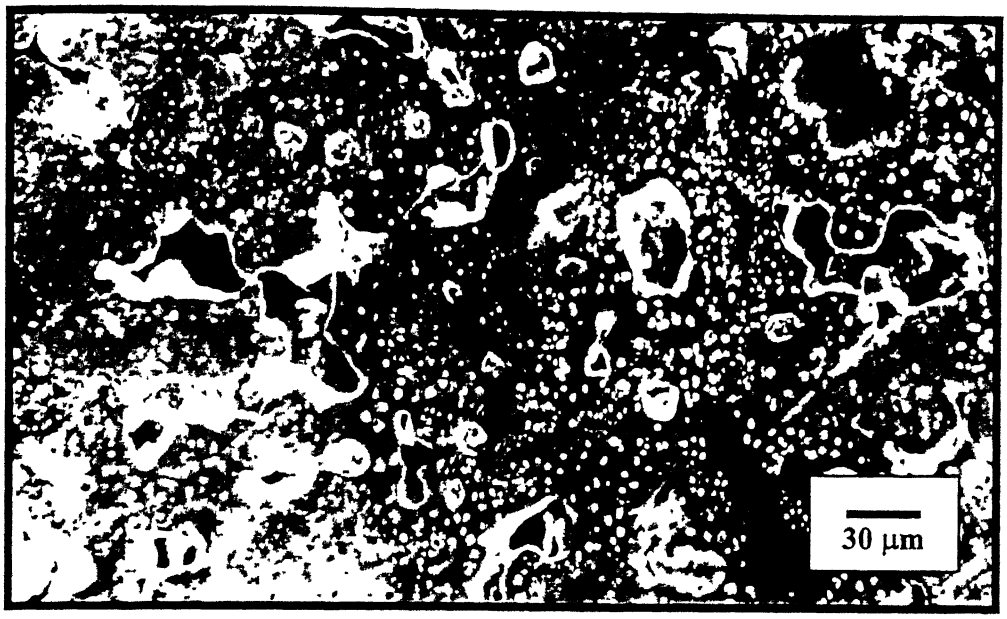

Figure 5.22. SEM micrograph of premixed sample sintered at 850°C. The sample was pressed at 150 MPa.

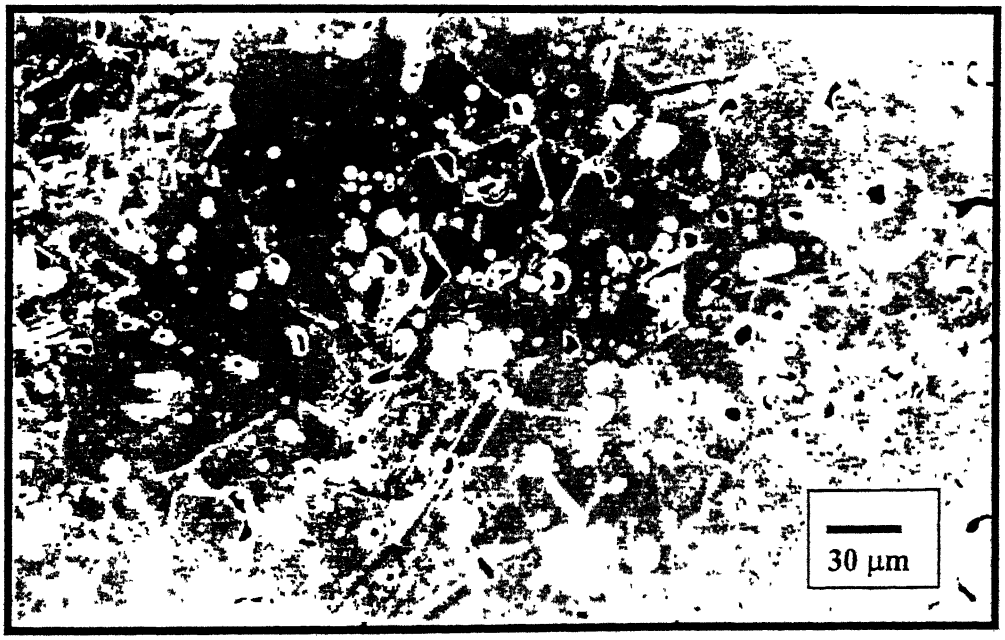

Figure 5.22. SEM micrograph of prealloyed sample sintered at 850°C. The sample was pressed at 600 MPa.

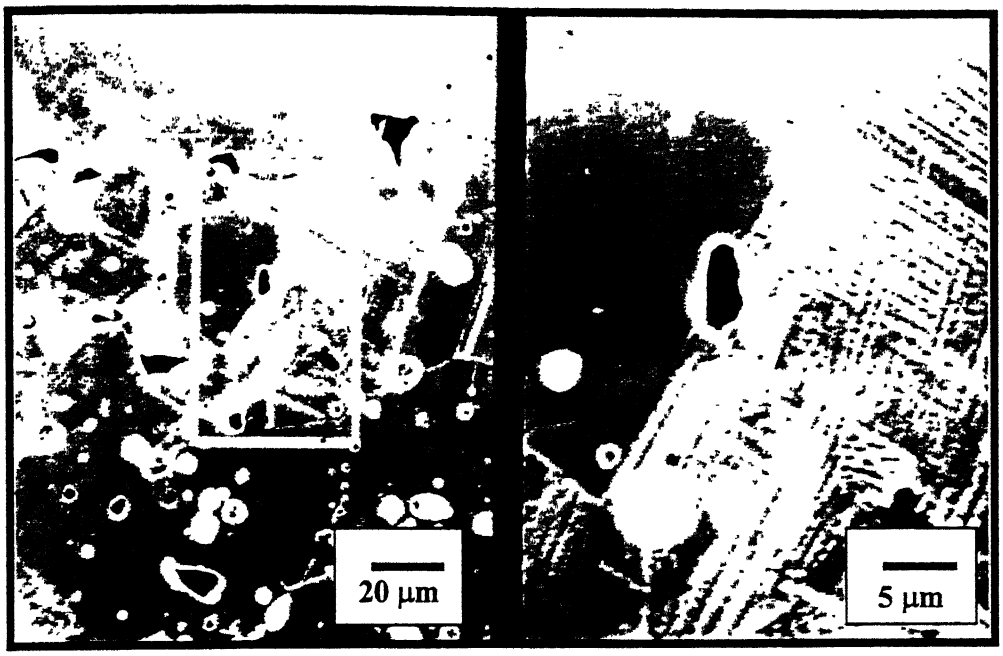

Figure 5.23. Split images of prealloyed sample in SEM. Compacted at 600 MPa. And sintered at 850°C.

Figure 5.24. SEM image in BSE mode of prealloyed sample sintered at 850°C. The sample was pressed at 600 MPa.

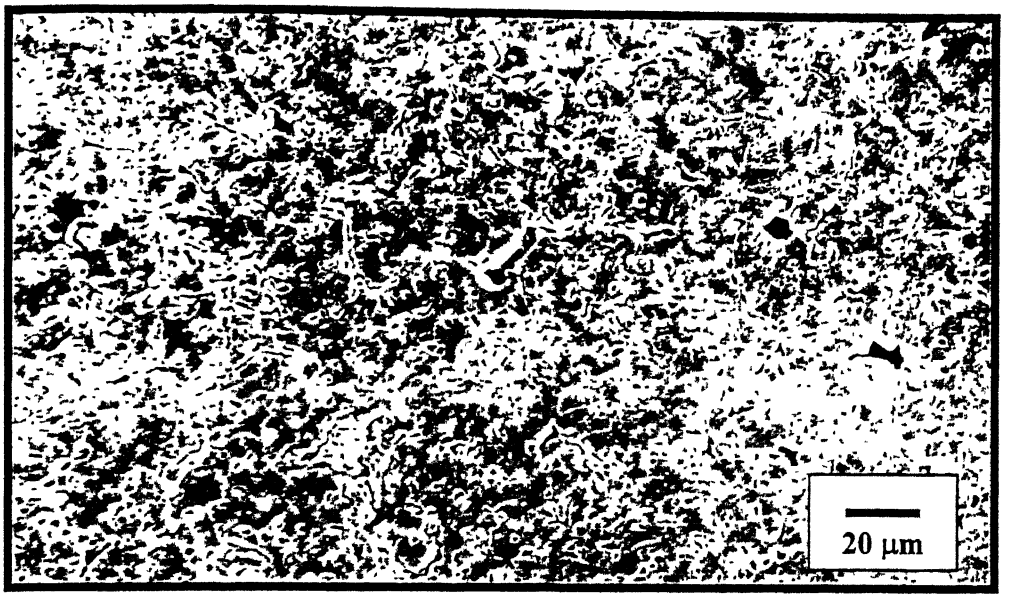

Figure 5.25. Micrograph of premixed sample sintered at 775°C. The sample was compacted at 150 MPa.

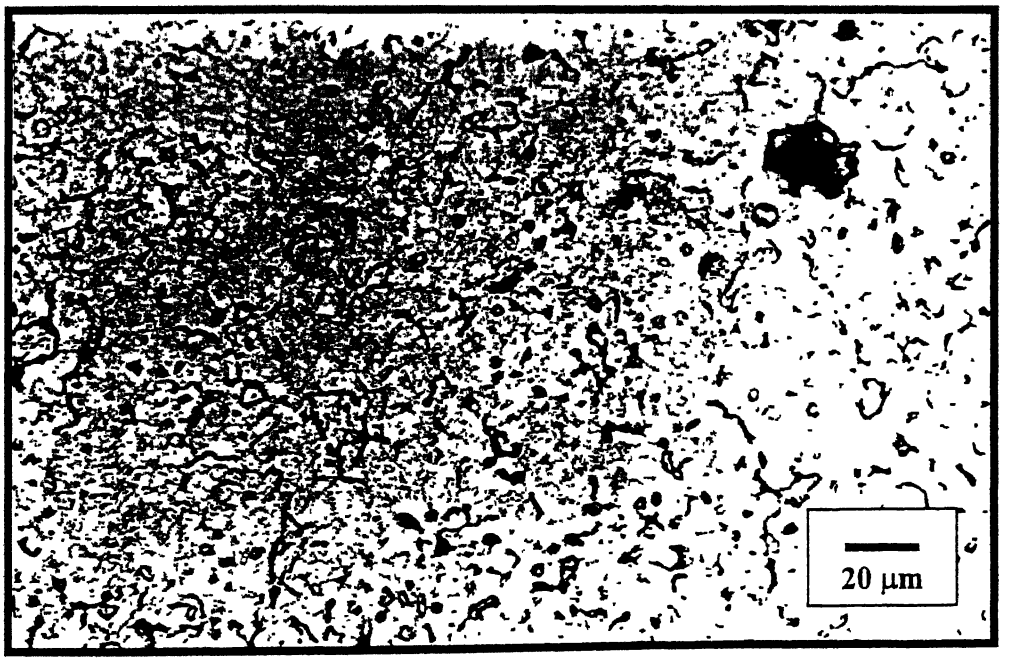

Figure 5.26. SEM image in BSE mode of premixed sample sintered at 775°C. The sample was compacted at 600 MPa.

Figure 5.27. SEM image of prealloyed sample Sintered at 775°C. The sample was compacted at 150 MPa.

Figure 5.28. Low magnification SEM micrograph of prealloyed sample pressed at 150 MPa and sintered at 880°C.

Figure 5.29. SEM micrograph of prealloyed sample sintered at 880°C. The sample was pressed at 600 MPa.

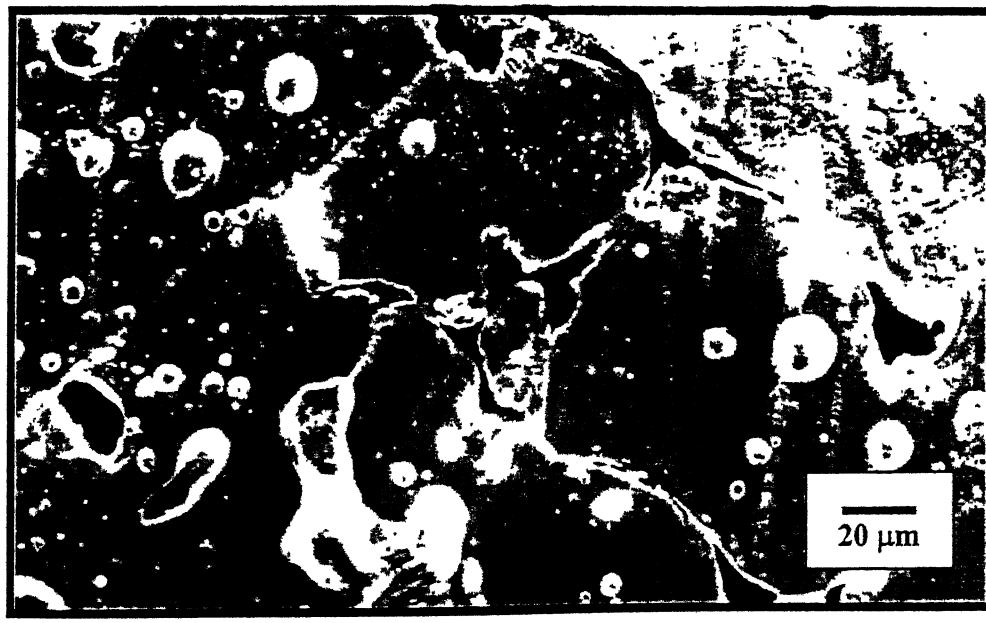

Figure 5.30. SEM micrograph of prealloyed sample sintered at 880°C. The sample was pressed at 600 MPa.

Table 5.1. Experimental data for the dilatometric sample.

Temp Cycle	Before Dilatometric Study				After Dilatometric Study				Wt. loss, %
	Wt. gm	Ht. mm	Dia. mm	Density, % th	Wt. gm	Ht. mm	Dia. mm	Density, % th	
Cycle 1	1.467	6.5	6.5	78.08	1.464	6.48	6.46	79.16	0.18

Dilatometric curve is shown in the Figure 5.31. It shows the expansion of the sample as a function of sintering temperature. Expansion rate of the sample is also plotted in the same curve. The peaks in the curve indicates the phase change during the sintering operation.

5.9 XRD Studies

XRD diffraction measurements were made to determine if any phase change occur in the sintering compacts which could impact the mechanical properties Figure 5.32 shows the evolution of phases of premixed sample as a function of sintering temperature. Compaction pressure for this case was 150 MPa. It can be seen that, in the final structure only single phase α-bronze is present. As the sintering temperature is increased the peaks are shifting towards the left hand side.

Figure 5.33 also shows the XRD study of premixed sample but at compaction pressure 600 MPa. The trends of the phase evolution are same in both the cases. Interestingly XRD study of the Cu-12Sn powder doesn't reveal any tin peak. Figure 5.34 and 5.35 indicates the XRD studies of prealloyed powders compacted at 150 MPa and 600 MPa respectively. Unlike the premixed powder, the prealloyed powder shows α-bronze peak with some intermetallics. The intermetallic phase is identified as β-$Cu_{5.6}Sn$ from the JCPDS standard chart. With the increase in the sintering temperature the intensity of the intermetallic phase is going to decrease. In the final structure only α-bronze is present as in the case of premixed powder.

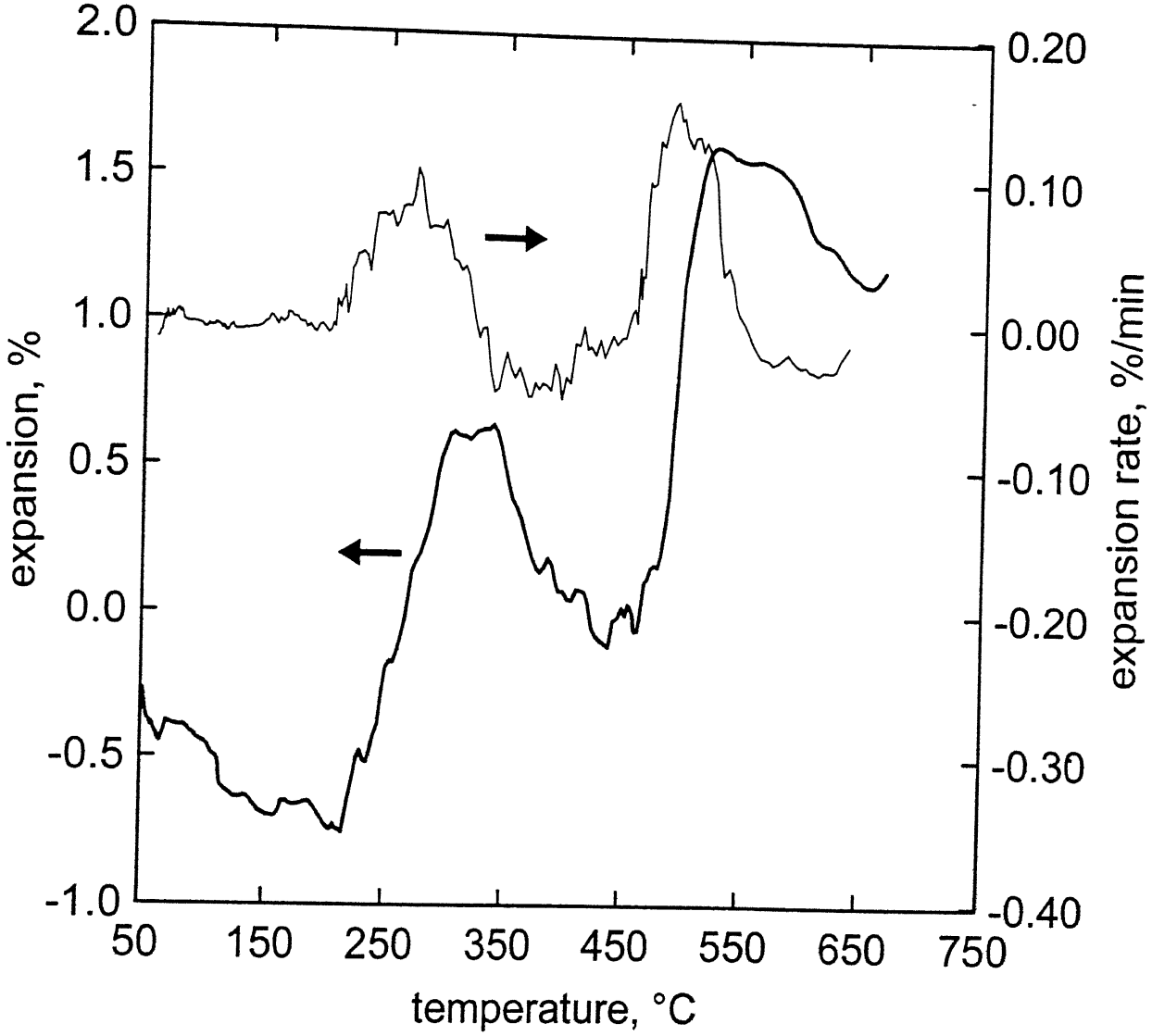

Figure 5.31. Dilatometric plot of premixed sample.

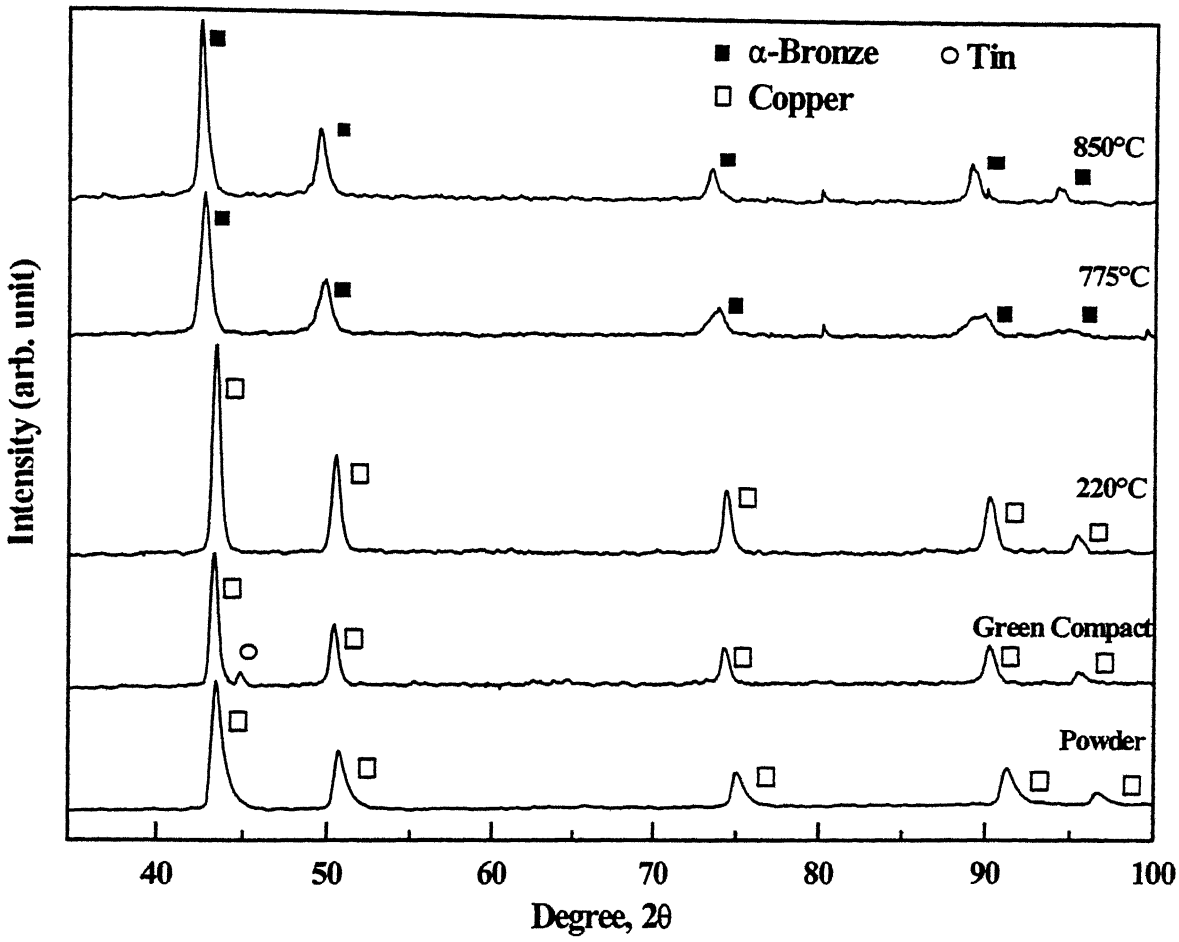

Figure 5.32. Superimposed X-ray diffraction patterns of premixed 88Cu-12Sn. The sample were compacted at 150 MPa.

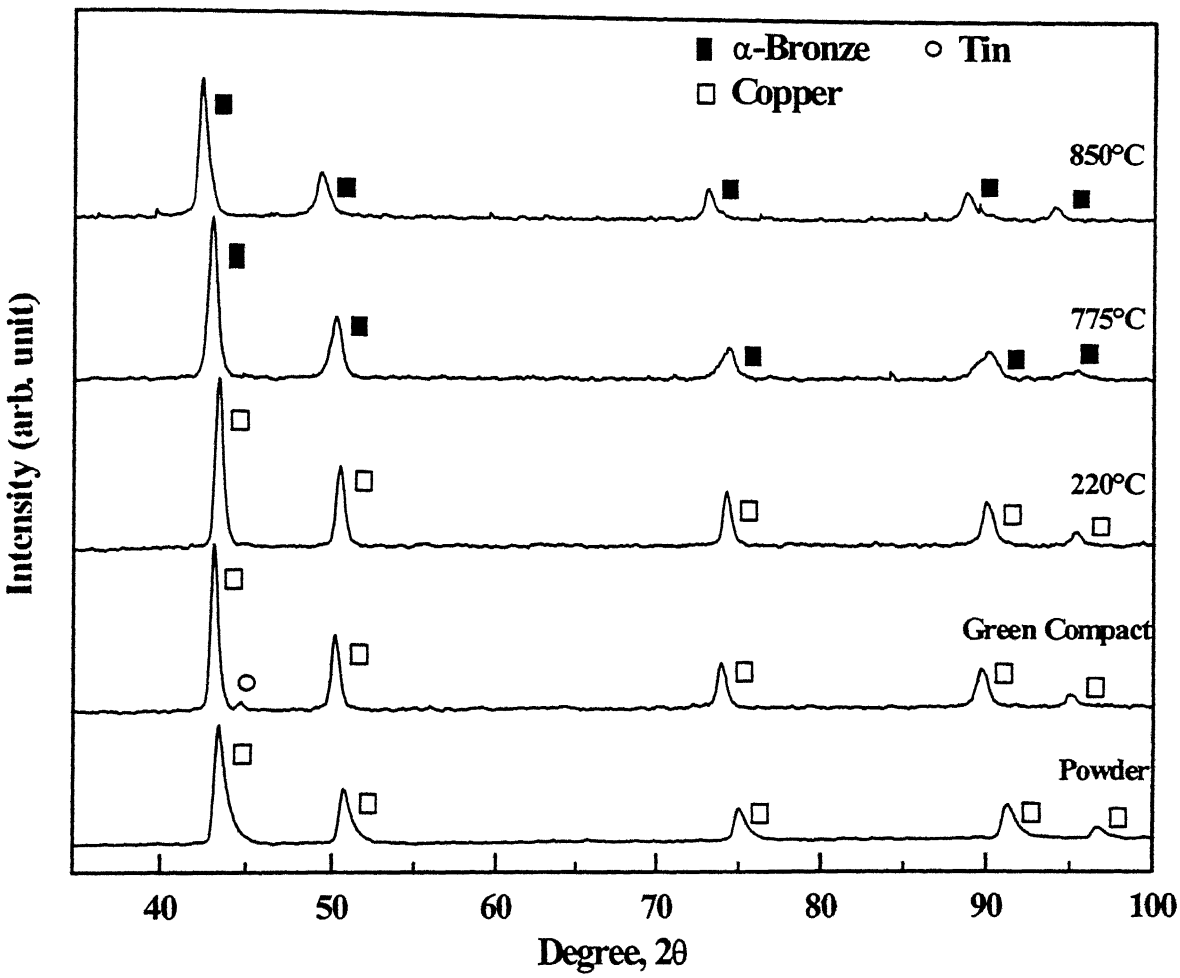

Figure 5.33. Superimposed X-ray diffraction patterns of premixed 88Cu-12Sn. The samples were compacted at 600 MPa.

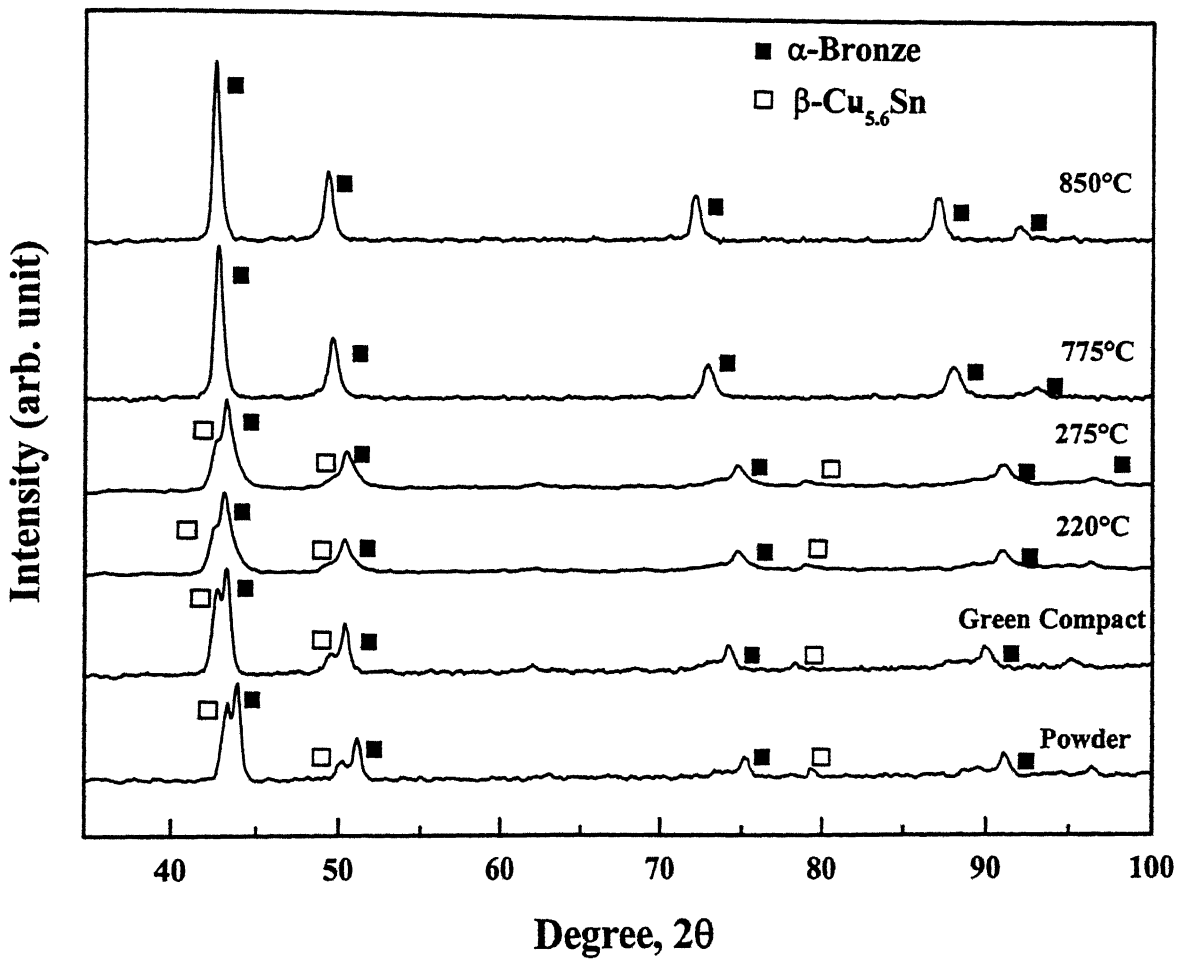

Figure 5.34. Superimposed X-ray diffraction patterns of prealloyed 88Cu-12Sn. The samples were compacted at 150 MPa.

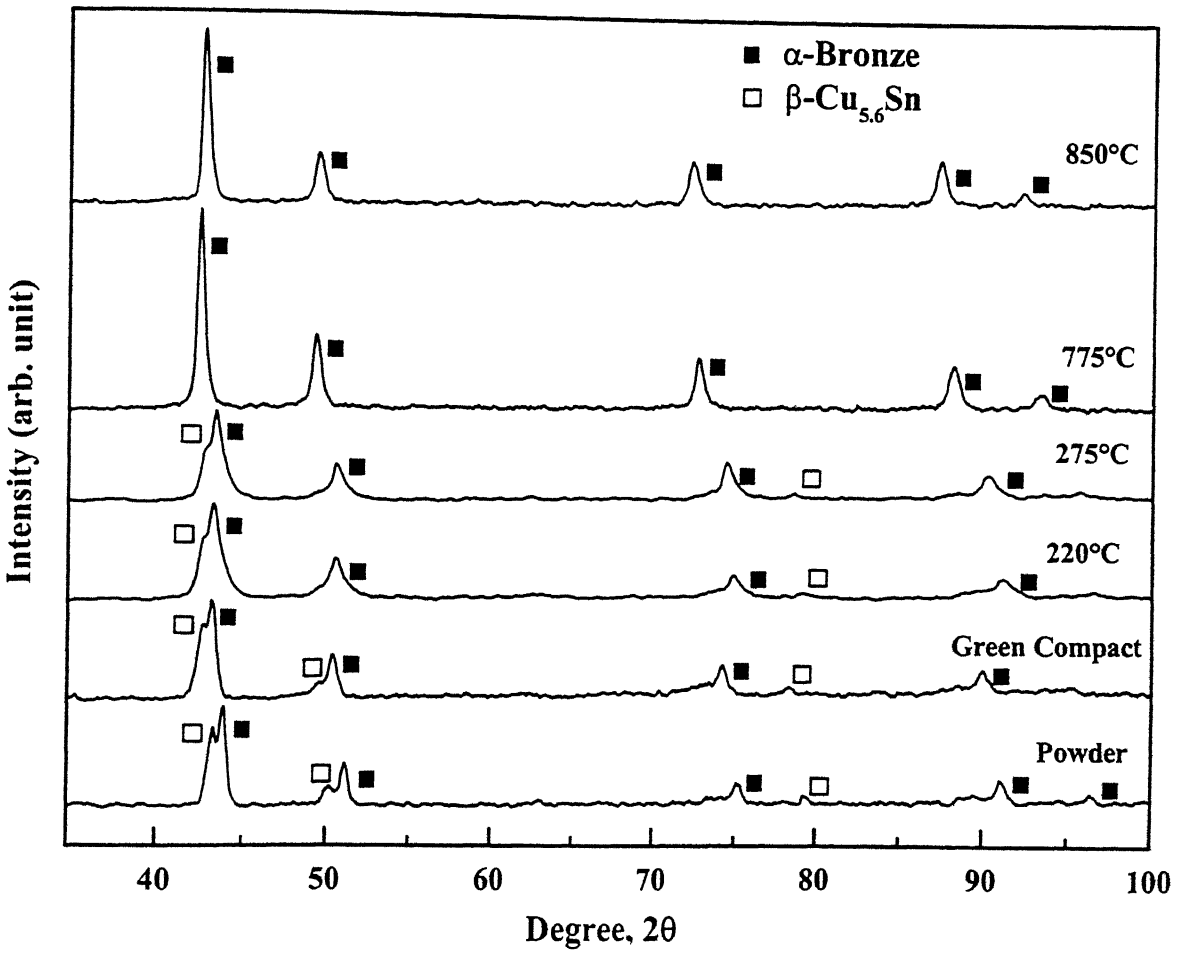

Figure 5.35. Superimposed X-ray diffraction patterns of prealloyed 88Cu-12Sn showing effect of sintering temperature. The samples were compacted at 600 MPa. The compacts were sintered for 40 min.

5.10 Differential Scanning Calorimetry Studies

The temperature corresponding to the formation of the first liquid in an alloy is referred to as the solidus while the temperature where the full transformation to liquid is complete is referred to as the liquidus. Formation of a liquid phase in the compact would have a direct impact on the strength. The phase diagram of Cu-Sn predicts that for Cu-12Sn composition solidus and liquidus temperatures are 820°C and 1000°C respectively. These melting transient points were verified for the prealloyed compact using differential scanning calorimetry (DSC) as described in section 4.10. For the premixed samples, the situations are different. Figure 5.36 shows the DSC plot for premixed sample. Downward peaks correspond to the exothermic reactions. The different phase changes are depicted by the positions of peaks. First derivative of the DSC curve is also shown in the figure. The peaks of this derivative helps to determine the phase change clearly. Figure 5.37 shows the DSC curves for prealloyed sample. First derivative of the DSC curve for this case is also plotted.

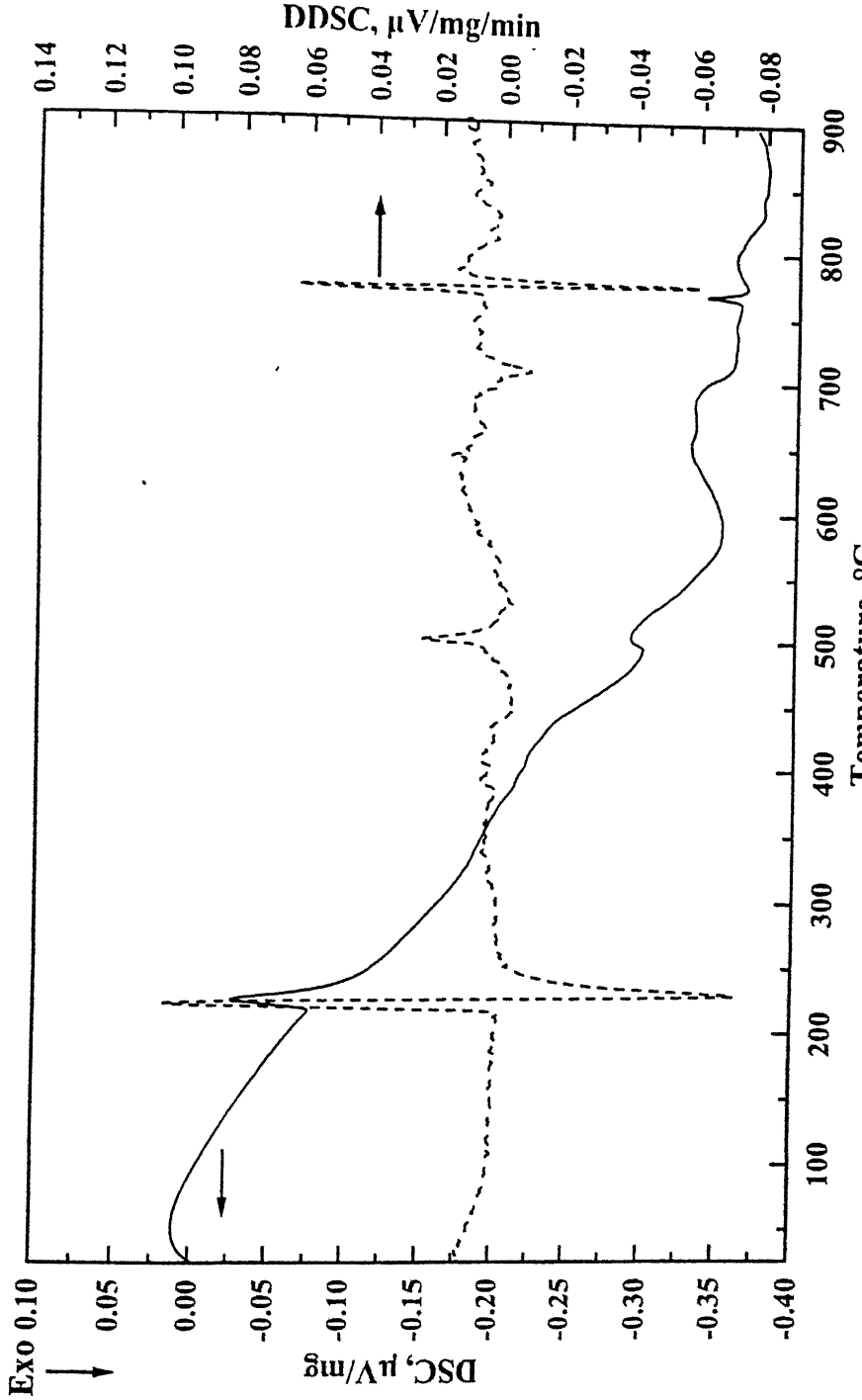

Figure 5.36. Differential Scanning Calorimetry (DSC) plot of premixed Cu-12Sn.

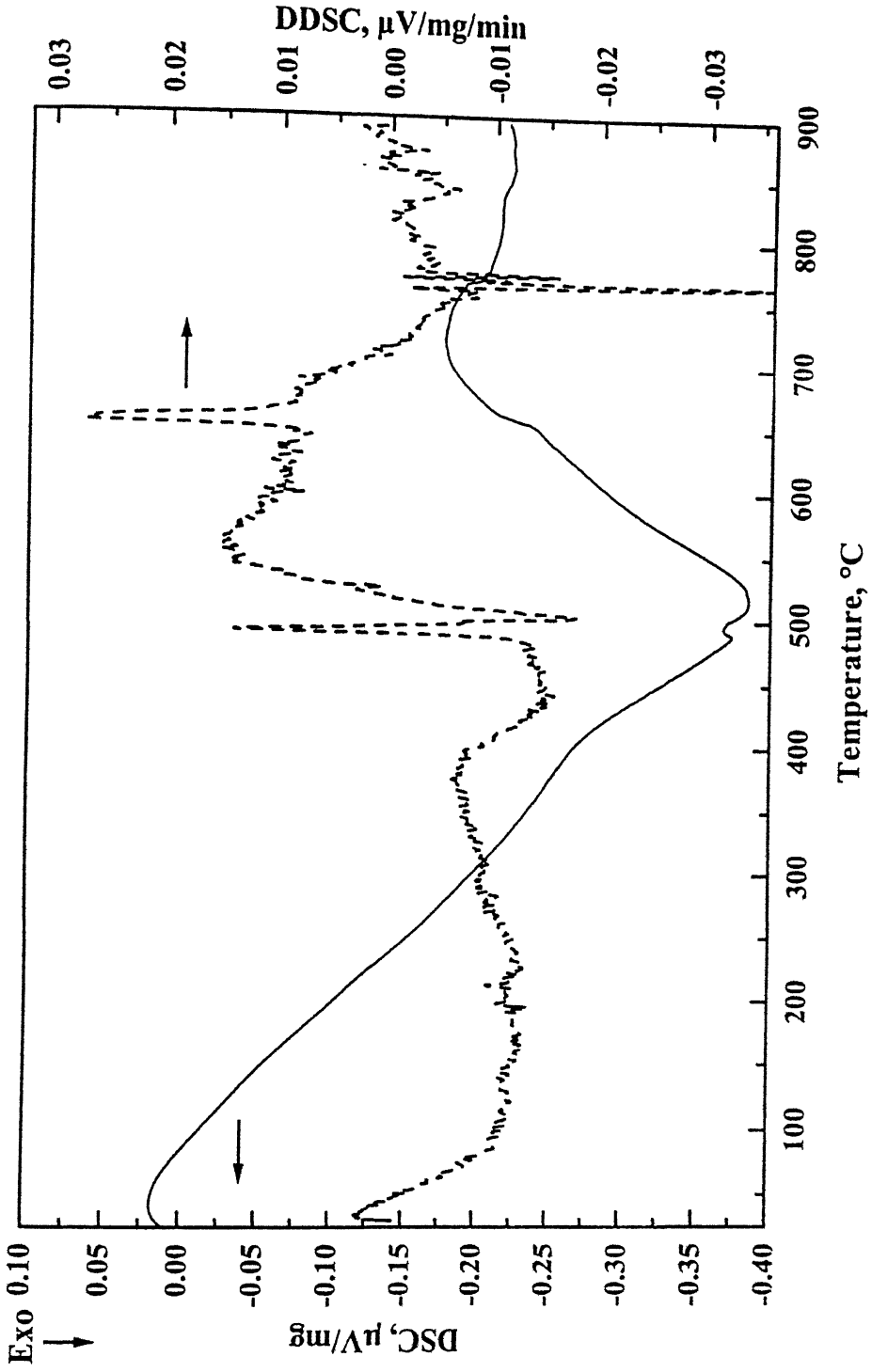

Figure 5.37. Differential Scanning Calorimetry (DSC) plot of prealloyed Cu-12Sn.

Chapter 6

DISCUSSION

The results obtained in the present investigation are discussed in this chapter. The following chapter is presented in eight sections. The first section summarizes the changes in density and densification parameters of premixed and prealloyed compacts as a function of sintering temperature. Second section discusses the weight losses of different samples and reason behind that. Determination of the porosity and its variation after sintering is discussed in section three. Section four discusses about the radial and axial shrinkage aspect of premixed and prealloyed samples. Microstructural features observed in optical and scanning electron microscopy are discussed in subsequent sections. Dilatometric curves, phase evolution on sintering and differential scanning calorimetry results of both premixed and prealloyed samples are discussed in detail in the subsequent sections.

6.1 Effect of Sintering Temperature on Density

As described in the Chapter 4, five different temperatures are selected for the sintering of both premixed and prealloyed powder. The choice of the temperatures depend on the composition of the alloy. For the present investigation Cu-12Sn composition was chosen and rationale for selection of that composition were already mentioned in the section 3.1. From, Figure 1.1 it is evident that the solidus and liquidus temperatures for this particular composition are 820°C and 1000°C respectively.

Two lower temperatures are selected so that, one temperature (220°C) is lower than the melting point of Sn (232°C) and the other temperature (275°C) is above the melting point of Sn. So, the sintering temperature 275°C corresponds to transient liquid phase sintering (TLPS) conditions [24]. Solid state sintering of the compacts was done at the sintering temperature of 775°C.

Accordingly the selected sintering temperature, 850°C and 880°C corresponds to the range between solidus and liquidus temperature. At these two temperatures Cu-12Sn

had undergone supersolidus liquid phase sintering conditions [42]. Liquid fraction can also be estimated from phase diagram using lever rule. Calculation from the phase diagram shows that the liquid fraction at 880°C is 23% whereas about 12% liquid forms at 850°C.

The present work compared the effect of different sintering conditions on both premixed and prealloyed Cu-12Sn compacts. Effects of pressure on the sintered density variations are also considered. In this section, attempt has been made to summarize the result obtained from those sintering experiments.

Both premixed and prealloyed powders are compacted at 150 MPa as well as at 600 MPa. From Appendix I it could be found that for both the cases green densities are on an average about 10% higher for premixed samples compared to prealloyed samples. At 150 MPa the green density of premixed sample is about 71% theoretical, where as for prealloyed sample it is 60% theoretical. Same trend is followed at 600 MPa also. At this pressure, premixed sample got density about 90% theoretical compared to 80% theoretical of prealloyed sample. This can be interpreted in terms of the basic mechanisms of bond formation during compaction. Densification during compaction processes involves particle deformation and is covered with attention to pressure transmission and friction effects [3,12].

As indicated from the Appendix I, as the pressure increased from 150 MPa to 600 MPa for the premixed sample, the initial rate of densification with the application of pressure is high. That is, change in pressure from 150 MPa to 300 MPa caused the density increase from 71% to 79% theoretical. But when pressure increased from 450 MPa to 600 MPa, change in density is 85% to 88% theoretical. It reflects the rate of work hardening. As pressure is applied, the first response is rearrangement of the particles with filling of large pores, giving a higher packing co-ordination. A further increase in pressure provides better packing and leads to decreasing porosity with the formation of new particle contacts. The point contacts undergo elastic and subsequently plastic deformation [12]. Thus, the pressure causes localized deformation at the contacts, giving work (strain) hardening and alloying new contacts to form as the gaps between particles collapse. During deformation, cold welding at the interparticle contacts contributes to the development of strength in the compact.

At higher pressures, plastic deformation is the major form of densification of metal powders. Because of work hardening, pressed densities over 90% of theoretical are difficult to attain for Cu powder. During compaction, the ability of a material to further work-harden gradually decreases as the hardness increases. Subsequently, further densification occurs by fragmentation of hardened particles and their filling interstitial spaces. Those inherent material properties combine with crystallography, chemical bonding, friction, and surface state to determine the ease of compaction for a given powder. The reason of lower density of prealloyed powder attributed to its poor compressibility. Prealloyed powder undergoes higher rate of strain hardening and therefore have poor compressibility. Also the higher hardness of prealloyed particles hinders compaction.

The difference in the sintering behaviour between the premixed and prealloyed compacts originates from the nature of distribution of tin. Tin is a low melting constituent and melts in the early stage of sintering of premixed compacts. The initial melt induces swelling as sketched in Figure 6.1, due to liquid tin penetrating grain boundaries [11]. As we know, the two solubilities of concern in liquid phase sintering are the liquid solubility in the solid (Sn in Cu) and the solid solubility in the liquid (Cu in Sn). A high liquid solubility in the solid leads to a transient liquid phase, and may eventually lead to swelling during sintering [50,80]. In the bronze system Sn has high solubility in Cu and thereby causing swelling of the compacts after it melts (232°C) [48,49]. Pores form at the prior Sn particle sites. In liquid phase sintering the wetting liquid preferentially flows into the smallest pores. If liquid formation is from large particles, then on melting the liquid will flow into neighbouring small pores and leave behind a large pore. Since smaller pores are easier to fill during sintering, it is beneficial to use small tin particles. As the particle size of copper increases, swelling goes through a peak. At large Cu particle sizes, there are fewer interparticle regions for Sn penetration, thus less swelling is observed. For Cu-Sn alloys, the green density effect is very large. A high green density (low initial porosity) contributes to swelling as illustrated in Figure 5.7 and 5.8 for premixed samples. Thus, it is found that swelling occurs only for premixed alloys and at a temperature higher than the melting point of tin. Appendix I indicates that in premixed route, samples pressed at 600 MPa (71 % theoretical) have got higher green density than

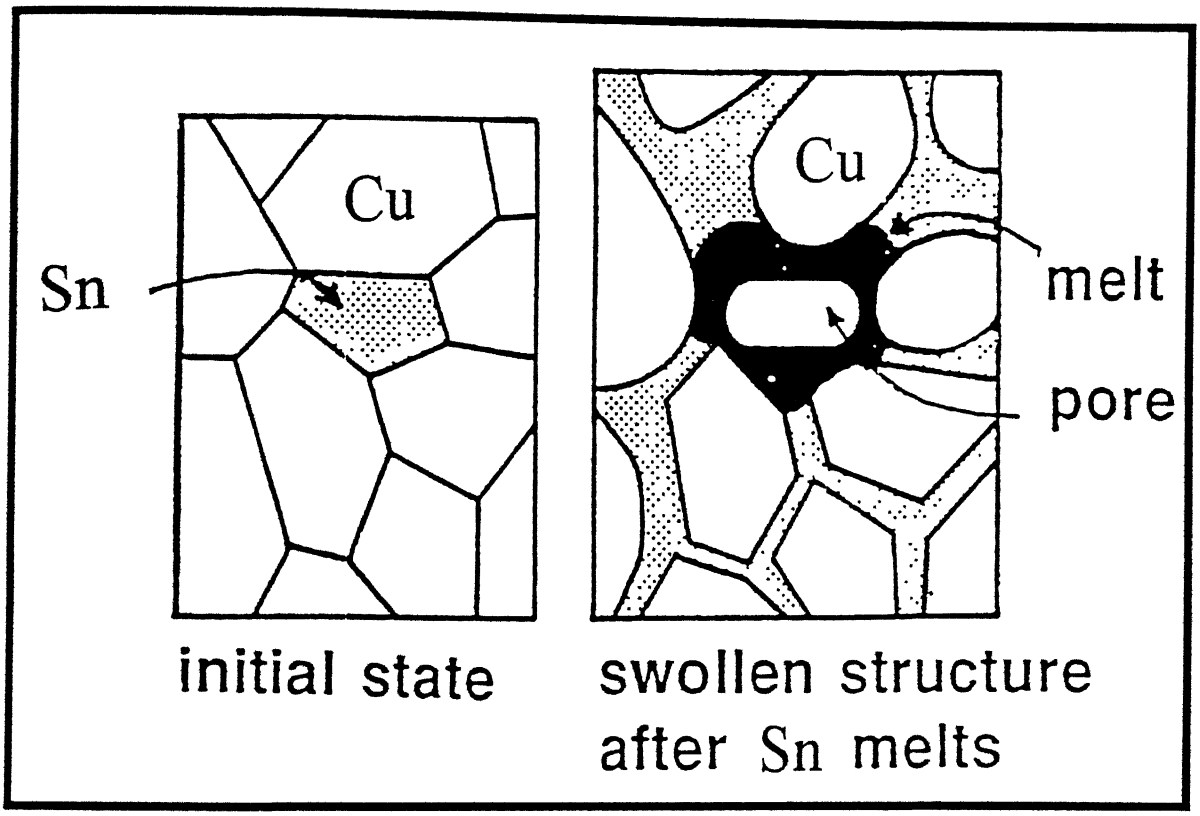

Figure 6.1. Swelling in the Cu-Sn system associated with the melting of tin.

samples pressed at 150 MPa (84 % theoretical). Comparing Figure 5.7 and 5.8, it can be seen that a decrease in the initial green density also reduces swelling. Premixed sample pressed at 150 MPa have undergone expansion by only 0.14% at 775°C, whereas samples pressed at 600 MPa shows expansion of around 1.40% at the same sintering temperature. This variation in the expansion results from the capillary attraction of the melts to the small pores, which inhibits melt penetration between solid grains.

Sintering generally leads to the shrinkage of the compacts. But in this case for bronze system expansion of the samples were observed after sintering. Same trend was observed during the sintering of Fe-Cu compacts. In steels with low copper content (less than 5wt.%), the mechanisms involved with swelling have been extensively studied. There are two schools of thoughts on copper growth. The first is based on the volume increase caused by the diffusion of copper in iron [75]. Simple calculations of the maximum swelling rate which could be produced by this process show that the rapid swelling of the compacts at temperatures just above the melting point of copper cannot be explained by diffusion alone [81]. The second school of thought has proposed that the penetration of liquid copper along the grain boundaries of the solid iron particles may contribute to the swelling. Dautzenberg [82] originally hypothesized this theory.

In order to pinpoint the real contributions at different stages of liquid phase sintering, Kaysser *et al.* [83] made an extensive study on Fe-Cu system. They the swelling mechanism of Fe-Cu compacts with four main contributors: (1) penetration of the melt between iron particles; (2) penetration of the melt along the grain boundaries; (3) diffusion of copper into the iron particles from the particle surface; and (4) diffusion of copper into the iron grains from the grain boundaries. Whereas penetration between the iron particles is the result of pure capillary forces, penetration along the grain boundaries is governed by dihedral angle considerations. Kaysser *et al* [83] found that copper penetration of grains was the faster swelling mechanism and contributed most to the growth phenomenon. It is generally accepted that "copper growth" occurs by the penetration of copper into grain boundaries and diffusion into iron grains. Particle rearrangement during sintering could be separated into stages. Primary particle rearrangements, just after the melting of copper, leads to rapid densification of loose-packed and slightly compacted specimens. Penetration of the melt along the grain

boundaries leads to densification by rearrangement of the individual grains within the iron particles.

Upadhyaya and German [84] recently correlated a link between the measured microstructural parameters and the macroscopic shape change in the liquid phase sintered Fe-50Cu premix alloy. A relatively low dihedral angle (8-25°) and intersolubility between iron and liquid copper doesn't favour binding of solid iron particles. This results in melt penetration.

Carbon is added in Fe-Cu system to control the expansion during sintering. Griffo [85] had made an extensive study to obtain zero dimensional change during sintering of Fe-Cu-C compacts by proper selection of sintering pathways.

So, it can be seen that bronze system behaves almost similarly to the Fe-Cu system. Therefore, the swelling mechanisms described for the Fe-Cu could also be applicable to bronze system with an exception that for bronze system Sn will be acting as a low melting constituent similar to Cu of Fe-Cu system.

Sintering temperatures have also got their influences on the expansion of premixed compacts. For 600 MPa, more the sintering temperature more will be the expansion upto an optimum value in premixed compacts. Sample pressed at 600 MPa shows that, upto 850°C expansion occurs. As the temperature increases further, more liquid will form according to the phase diagram, thereby forming weak regions in sample which cause distortion in premixed compacts sintered at 880°C. For premixed compacts pressed at 150 MPa, the behaviour during sintering is different. Densification starts near 500°C but is offset by another swelling reaction that ends just below 820°C, where a liquid phase forms again [11]. Upto sintering temperature of 775°C, it also shows expansion, but after that at 850°C shrinkage is observed. The low initial green density hinders the expansion as stated before. For this reason, the sintered density curves for premixed compacts in Figure 5.1 decreases upto 775°C and then increases at 850°C. The nature of the premixed samples shown in Figure 5.5 could be explained in the same way as described above. Just like the samples pressed at 600 MPa the premixed compacts pressed at 150 MPa also distort at 880°C

Densification during supersolidus liquid phase sintering (SLPS) is analogous to viscous flow sintering. The prealloyed particles turn mushy and flow once sufficient

liquid forms along the grain boundaries [24,37,39,43,46]. The viscosity of a solid-liquid mixture decreases as the liquid volume fraction increases, so more liquid makes for faster sintering but adversely affects dimensional precision. Compared to solid-state sintering, the densification process shows an extreme temperature sensitivity. This theory could be supported by our results. Premixed samples sintered at 880°C were distorted for both 150 MPa and 600 MPa. The liquid formed at that temperature (23%) couldn't be sustained by the compact. Although the prealloyed compact got the same fraction of liquids at the same temperature, but in their case powder chemistry played an important role. For prealloyed Cu-12Sn samples thermodynamically homogeneous diffusion is expected and as tin was already melted, and the structure is more or less homogenized. So, the liquid which formed is of same composition and is more homogeneously distributed throughout the matrix causing the particles to be rearranged. But for the premixed samples, some tin rich phase could form more liquid than the other portions, which were weak. As a result the samples distorted.

From Figure 5.6, it could be found that the densities for the prealloyed compacts pressed at 600 MPa are almost same for all sintering temperatures. It means that, higher pressure hinders the rate of densification caused by the particle rearrangement through the liquid. But for prealloyed sample compacted at 150 MPa, increase in sintering temperature leads to the increase in sintered densities. These results are characteristic of SLPS, wherein a prealloyed powder exhibits rapid densification when heated slightly above the solidus temperature. Above solidus temperature, melt is nucleated at heterogeneous sites, typically at grain boundaries or interdendritic spaces where last solidification took place in powder fabrication during atomization. The liquid spreads on the grain boundaries, causing particle particle disintegration [12]. Even if nucleation is not uniform, as temperature increases the liquid spreads to form a continuous film. The liquid provides a capillary force on the structure, then solution reprecipitation occurs with its corresponding grain shape accommodation, resulting in further densification. Densification is roughly proportional to the volume fraction of liquid. If the sufficient liquid is spread along the grain boundaries, the densification reaches the optimum densification. Excess liquid will cause the compact slumping. As happened in the case of premixed samples at 880°C. This proves that the premixed compacts doesn't follow the

predicted route from phase diagram, rather it densifies according to its powder chemistry. If the powder is prealloyed, it will distort at higher sintering temperature compared to premixed powder [42].

6.2 Comparison of Weight Losses

Weight losses are different for premixed and prealloyed samples. During the sintering operations hydrogen gas was used. That was a reducing gas and removed the surface oxides during the sintering operations. Generally, commercial powders contain some surface oxides or surface oxide may be formed during powder preparation and/or its subsequent. Oxides and other contaminants hinder diffusion bonding during sintering and the development of adequate properties. Since oxides are present, a reducing atmosphere not only provides protection from further oxidation, but can reduce and existing oxide. Removal of those oxides during sintering by the reducing gas resulted in weight loss of the samples. Metallic powders exhibit upto 1.5% weight loss during sintering cycle [11]. In this case maximum weight loss is about 1.3% for prealloyed sample. It can be found from the Figure 5.10 and 5.9 that, weight loss is more or less independent on the compacting pressure for both premixed and prealloyed samples. But, in case of prealloyed samples, the weight losses on the average are higher compared to premixed samples. Weight losses are dependent on sintering temperature. The water formed from the hydrogen reduction is a vapour; thus it is easily removed by the gas phase provided there is sufficient interconnected porosity present in the green compact. For premixed samples, more the sintering temperature, more is the weight loss. For prealloyed samples, weight loss increases upto 775°C and after that remains constant. Prealloyed powder has poor compressibility than premixed powder. This implies the higher pore level in the prealloyed compact. With the increase in the pore fraction, fraction of interconnected porosity is also increased. This in terms explains the higher weight loss for prealloyed compacts.

Prealloyed samples are gas atomised. During cooling, the chances of oxidation for prealloyed powders are more. These oxides were removed during sintering, causing comparatively higher weight loss. Whereas, pure copper and pure tin powders have got less chance of oxidation. For this reason, weight losses in premixed route are lower.

Higher the sintering temperature, higher will be the amount of reduction for both types of powders. As the weight losses are independent of compacting pressure, it can be stated that weight loss is a surface phenomena. It has a very little connection with the internal structures of the samples. It is imperative to fully reduce surface oxides if maximal properties are to be obtained from the sintered material.

6.3 Porosity After Sintering

Porosities after sintering were measured by the xylene impregnation test as described in section 5.3. Porosities are removed in the final stage for solid-state sintering. In that stage the isolated, spherical pores shrink by a bulk diffusion and grain boundary diffusion mechanism. Pores located at the grain boundaries disappear more rapidly than isolated pores. As shown in the Figure 5.11 and 5.12, the porosity values obtained from xylene impregnation tests are matching with the values determined from the density data. For premixed samples pressed at 600 MPa the porosities are increasing with sintering temperature. That means, the samples are expanding. Higher the compaction pressure, more is the interparticle contact. This gives rise to the area for tin diffusion and hence expansion occurs. Prior tin particle sites will give rise to the pores. But the case is reversed for 150 MPa samples. Here initial pores are more at the grain boundaries after the compaction. They will hinder the flow of tin rich melt. So, the porosity value remains almost same upto 775°C. All the pores upto this temperature are mainly pre-existing (i.e. occurred from compaction). For premixed compacts formation of liquid at 850°C would lead to the particle rearrangement and thereby causing removal of the pores. But for prealloyed samples, pores are decreasing as the sintering temperature is increased at both the compaction pressures. So, it implies that for prealloyed samples, no extra pores are forming during sintering. Only pore removal occurs and thereby causing densification. Total porosity is the summation of closed and interconnected porosity. The general trend of sintering is that, if open pores increase, close pores are going to be decreased [11]. Pore shapes are depended on the powder chemistry and sintering temperature. The pore shapes observed by SEM and optical microscopy are presented from Figure 5.13 to Figure 5.20. It is clear from those micrographs that at SLPS conditions basically two types of pores are observed. Larger (irregular pores) at the grain boundary and smaller

(rounded) intragranular pores. Comparing Figure 5.13 and 5.14, it can be found that for premixed sample the pores are bigger compared to prealloyed sample. Pores are also irregular in shape. This indicates that those pores are not green as pressed porosities rather they formed in the later stage by pore coarsening. Tin-rich phase formed porosities during sintering operations. The absence of irregular pores in the prealloyed samples indicates the homogeneity of the samples.

6.4 Variation in Axial and Radial Shrinkage

Figure 6.2 compares the axial vs radial shrinkage of premixed and prealloyed samples compacted at 150 MPa. Figure 6.3 gives the comparison of the same but at the compaction pressure of 600 MPa. The difference between the ideal and real behaviour of the prealloyed samples compacted at 150 MPa are shown in Figure 6.4.

This figure compares the axial Vs radial shrinkage of premixed and prealloyed sample.

From Figure 6.2 it is clear that the radial and axial shrinkage for premixed and prealloyed samples are different. Let us first consider the case of prealloyed samples. It can be found from the curve that the prealloyed samples at all temperature show shrinkage in both radial and axial direction. In the plot the points are marked for different temperatures. A line is drawn diagonally which indicates the ideal case, which means that, any point on this line indicates uniform shrinkage in both the directions i.e. the compact aspect ratio is maintained during sintering. In other words the compact undergone isotropic dimensional change. In practice however it is often difficult to achieve isotropic shrinkage during sintering. Because we know that the shrinkage or expansion will occur under the influence of two factors, namely, chemically induced shrinkage and stress induced factor. Stress induced factor will play an important role in case of cylindrical compacted sample. As the samples are compacted in a single acting press there will be a density gradient from the top to bottom. In general terms, the sample grows or shrinks less in the radial direction compared to the axial direction. This could possibly be tied up with the direction of applied stress and locked-in elastic stresses [60]. The data points for the prealloyed samples are very close to the ideal line. This indicates that the prealloyed samples follow a regular trend. More the temperature more the

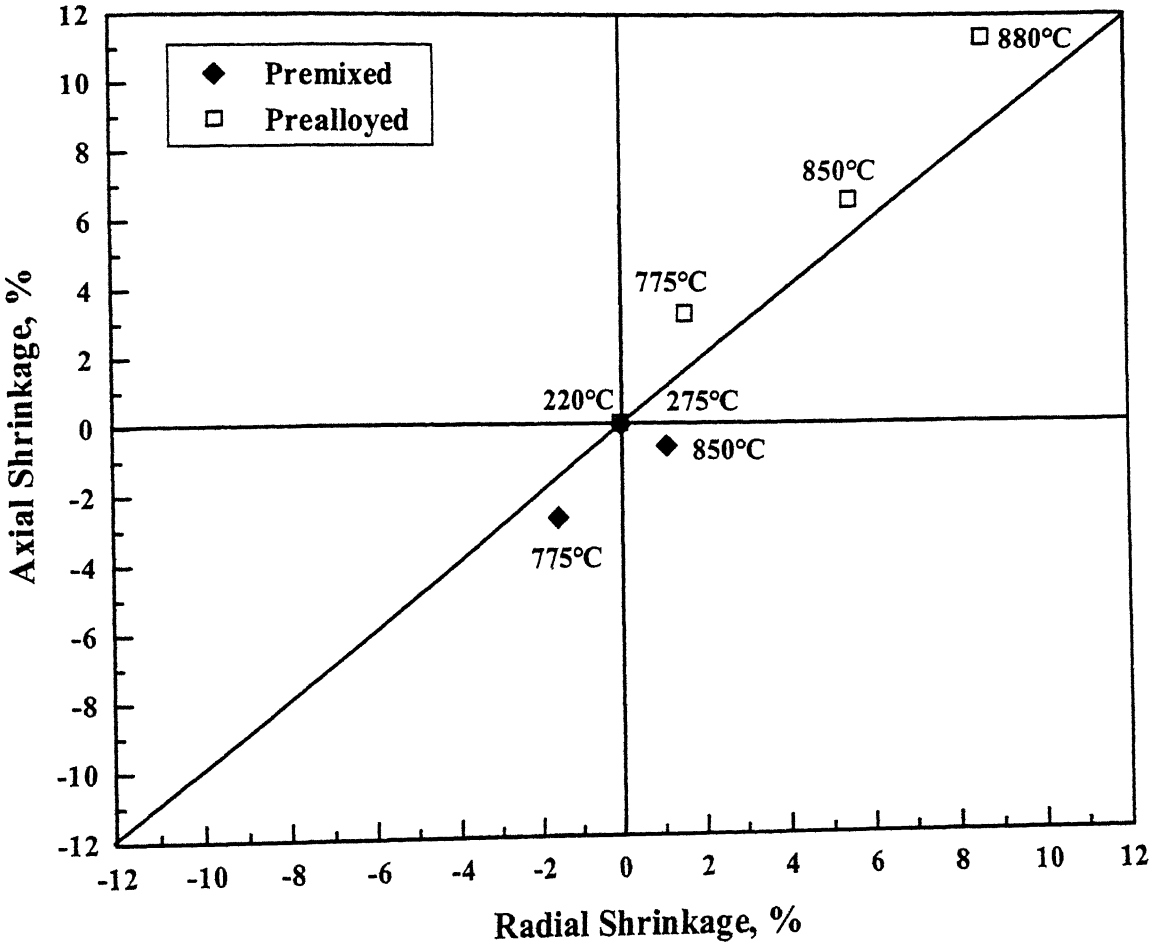

Figure 6.2. Comparison of the axial vs radial shrinkage of premixed and prealloyed samples compacted at 150 MPa.

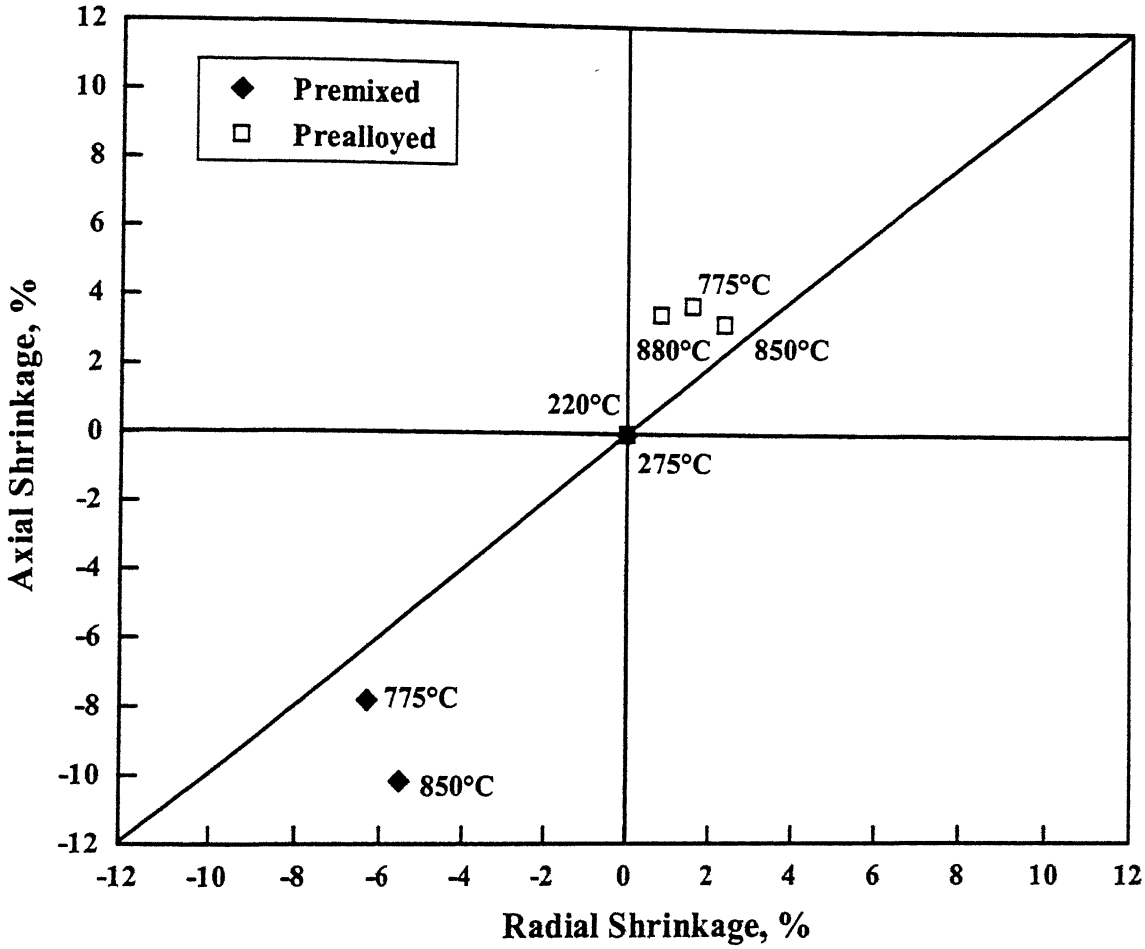

Figure 6.3. Comparison of the axial vs radial shrinkage of premixed and prealloyed samples compacted at 600 MPa.

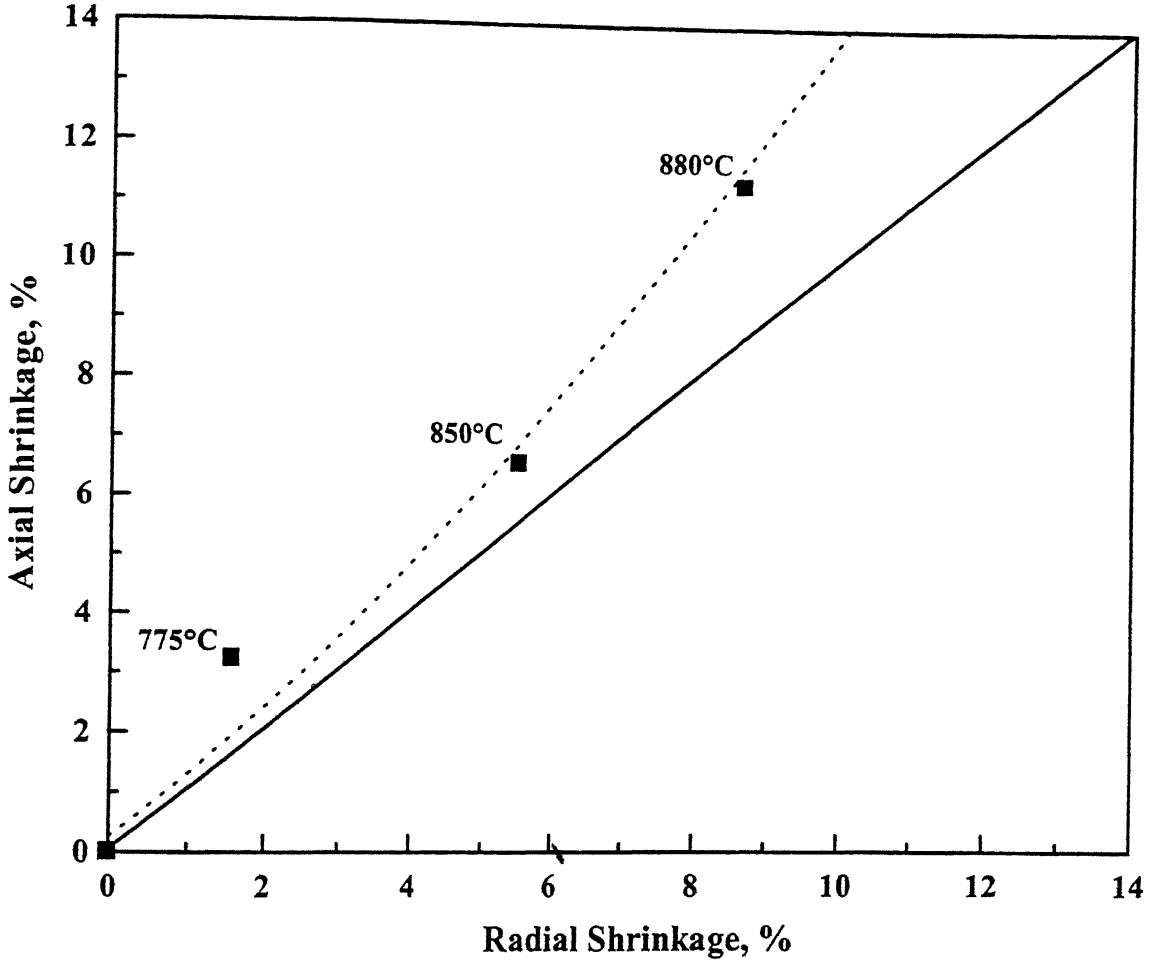

Figure 6.4. Deviation of prealloyed samples from the ideal behaviour. The samples were compacted at 150 MPa.

shrinkage. At 775°C, prealloyed compact was undergone solid-state sintering. Here also likewise shrinkage was observed after sintering.

The case is different for the premixed (PM) sample at the same temperature. PM sample showed expansion rather than shrinkage. This phenomena can be explained from the different powder characteristics for both cases. PM sample might not be homogenous after extensive mixing also.

Some difference in the composition might occur because of the segregation problem owned to the density difference of the copper and tin powders. Tin melts at about 232°C and diffuses in the copper matrix thereby expanding the copper lattice. These tin-rich areas would lead to the formation of pore. Above solidus temperature (i.e. at 850°C and 880°C) the premixed sample had undergone liquid phase sintering condition. Liquid formed above solidus temperature and thereby helping the rearrangement of the particles. So, shrinkage is expected. In the radial direction shrinkage was observed, but in axial direction expansion remained. It is to be noted that, at 850°C the amount of expansion in the axial direction decreased compared to 775°C. So, it can be concluded that at 775°C the amount of liquid that was formed was insufficient for the complete rearrangement of the particles. Increase in the temperature above solidus line will increase the amount of liquid, therefore at higher temperature shrinkage is expected to be observed. But, it is to be remembered that too much liquid could distort the sample as shown by the behaviour at 880°C. Photographs of the premixed and prealloyed samples sintered at 880°C are shown from Figure 6.5 to 6.7. Figure 6.5 shows the distorted premixed compacts sintered at 880°C. It is found that compact pressed at 600 MPa distorted more compared to sample pressed at 150 MPa. The reasons for that were described in the earlier sections. Figures 6.6 and 6.7 compare premixed and prealloyed compact shape pressed at 150 MPa and 600 MPa respectively. The compacts were sintered at 880°C. As stated earlier, the premixed samples show distortion whereas prealloyed compacts were undergone shrinkage.

For prealloyed case uniform shrinkage indicates the homogeneity of the sample. The powders were already gone under alloying during their melting-atomization fabrication procedure. So, localized inhogeneities were not expected. At 775°C, prealloyed compact went for solid state sintering. Amount of pores were decreased and as

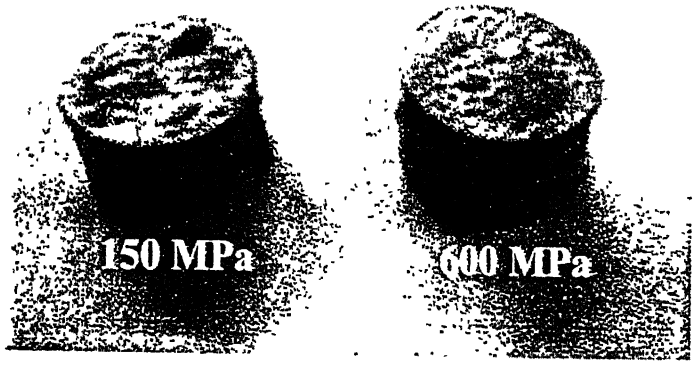

Figure 6.5. Distortion of Premixed samples sintered at 880°C.

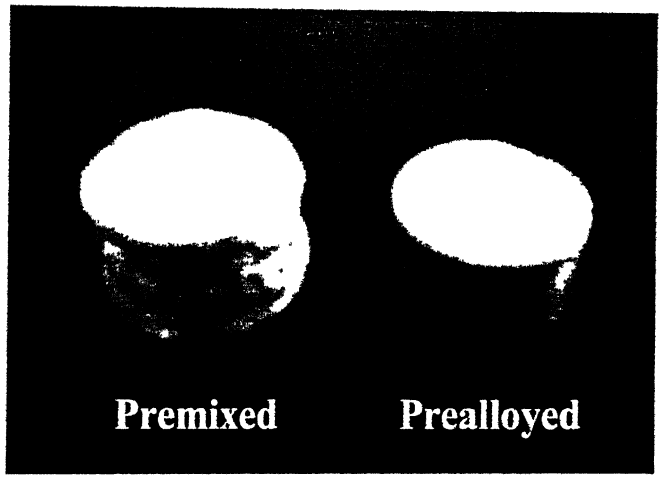

Figure 6.6. Comparison of sample shape sintered at 880°C. Compacting pressure 150 MPa.

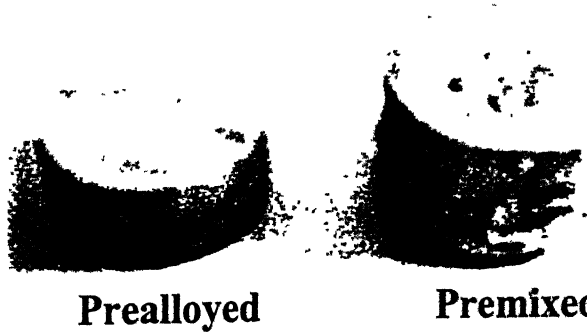

Figure 6.7. Comparison of sample shape sintered at 880°C. Compacting pressure 600 MPa.

a result shrinkage occurred. This could be referred as a classic case of solid state sintering. At 850°C, PA compact was super solidus liquid phase sintered. The temperature was above the solidus temperature. Melt formation took place all over the matrix at the same rate. Particles are rearranged themselves accordingly. Homogeneity would cause the rearrangement properly with the amount of liquid formed. This led to shrinkage of the compact.

As shown in the Figure 6.3 the situation is quite different in this case compared to 150 MPa. For the premixed sample, expansions are higher than 150 MPa sample at both 775°C and 850°C. Induced stress during compaction may be the reason for that. The residual stress should be more for the samples pressed at 600 MPa. Liquid phase sintering of premixed compact also leads to expansion. Localized higher quantity of liquid was the reason for that.

For prealloyed samples we could see that the increasing temperature didn't bring any significant change. All the data points are clustered together, indicating almost same dimensional change as a function of temperature. At could be explained by the fact that, at this high pressure green densities were already higher. Because the powder is ductile, a higher compaction pressure will result in a more uniform density distribution. So, though the liquid forms at 850°C, it could not bring the rearrangement of the particles in an effective way. Same theory should be followed for 880°C also.

It is to be noted that, at 880°C for both 150 MPa and 600 MPa premixed samples got distorted. Porosity level became higher by the expansion and made those compacts weak.

6.5 Microstructural Evolution

Microstructural evolutions of the premixed and prealloyed samples are observed by the optical microscopy and SEM as a function of sintering temperature. Effects of pressures on the microstructure are also described in the early sections. At lower sintering temperatures (232°C and 275°C) there are not much change in microstructures. The samples are also very fragile due to the lack of proper sinter bonding. So, the samples at lower temperatures and at lower compacting pressure couldn't be polished and etched.

For the study of microstructural evolution, the samples sintered before and after melt formations are taken into account.

The optical micrographs mainly reveal the phase present in the microstructure with the distribution of pores. All the micrographs show the presence of only α-bronze in the matrix. No second phases are observed. The presence of only single phase throughout the matrix ensure the homogeneity in the properties of the samples. The reasons are quite obvious Dowson [58] discussed the evolution of phases during sintering in a concise fashion and are discussed in Chapter 3. It was mentioned that at lower temperature solubility of tin decreases and below 340°C second phase should begin to appear. Decomposition of α phase requires extremely slow cooling rate. But, in this present study cooling rate was not that much slow and far from the equilibrium. So, in the final microstructure we can get phases which may not support by the phase diagram. When we are heating elemental Cu and Sn powder under the fairly rapid heating and short sintering cycle, it is possible to get, at various stages in the heating process, significant amounts of δ, γ, and β phases. Theoretically, at room temperature α and little ε should be present but it is clear from the micrographs that no second phase was present. So, it is found that proper sintering in this case leads to homogeneous α phase in the microstructure.

Comparing Figure 5.13 and 5.14, not much difference can be observed for these samples except the pore shape and distribution. For the premixed sample the pores are more bigger compared to prealloyed sample. Pores are also irregular in shape. This indicates that those pores are not green as pressed porosities rather they formed in the later stage by pore coarsening. Tin-rich phase formed porosities during the sintering operation. Small rounded pores are pre-existing and formed after compaction. For prealloyed sample absence of irregular pore indicates the homogeneity of the sample. Pores became more rounded as a function of time.

Figure 5.15 and 5.16 mainly compares the pore shapes at the lower magnification. Pores are irregular in the case of premixed samples compared to prealloyed one. Typical supersolidus liquid phase sintering condition. But at these lower magnification no melt formation could be observed. Twin bands are found only in the case of PA sample. No twin bands in PM sample. Small rounded pores are seen inside the grains. The reasons for that is described in the following paragraphs.

The observation from the SEM clearly reveals the formation of melts and the twins in the microstructures. The following paragraphs summarizes the analysis of the of the micrographs and the basic mechanisms for that.

Comparison between premixed and prealloyed samples sintered at 850 ℃

Prealloyed samples have more tendency to form twin as compared to premixed one. It is because more tin copper induces more twin formation tendency. Tin decreases the stacking fault energy of copper after alloying and thereby increases the twin band formation. Slip line should not be present in case of sintered product because sintering is after all an annealing phenomena. As the micrographs reveal that the structure is single phase (no second phase or intermetallic) one.

From the density comparison for prealloyed products we can see that the pressure has got a little effect on it. Varying pressure doesn't bring any significant change on the microstructure. Pore morphology may slightly alter. So, we can easily compare the premixed samples with prealloyed irrespective of pressure conditions.

Sintering temperature 850°C corresponds to the supersolidus sintering for prealloyed compact. As this particular temperature exceeds the solidus line, melt formation will take place according to the phase diagram. But for the premixed condition, this temperature corresponds to persistent liquid phase sintering. Here also melt formation will take place, but the nature of the melt should be different from that of the prealloyed one. Exactly the same thing is revealed by those micrographs.

Melt globules are of much bigger size for premixed case. It can be explained from its basic nature of mixing inhomogenity. Though the powder composition is made very carefully, but it is impossible to be sure about the uniform composition throughout the mixture. There will be always a composition gradient. Some areas are richer in tin amount and the other portions are depleted of the same. Now these play an important role during melt formation. During heating tin melts and diffuses to copper. Thus those portions richer with tin amount lead to tin rich copper phase. At higher temperature more tin areas will form more liquid compared to others thereby resulting bigger globules. As compared to nominal composition.

Tin powders are also of different sizes. Here the kinetics takes over its importance over the thermodynamics. Smaller the particle size, more is the chemical reactivity. So, small tin particles melts at a faster rate and alloyed very fast in the grain boundaries. Thus the melt forms at the grain boundaries (intergranular melts) are bigger in size. But the tin inside the grain can't diffuse that faster. Intragranular melt globules are smaller in size because of this reason.

In case of prealloyed one, the sample is almost homogeneous. During heating the melt formation took place at the same rate all over the structure. So, no tin rich phase should occur. Pores are naturally well distributed and finer compared to premixed samples.

Comparison between premixed and prealloyed samples sintered at 775 ℃

Solid state sintering for both the cases. No melt formation observed. For both prealloyed and premixed compacts at lower magnification the pores can be seen. In the BSE mode for premixed one pores are seen along the grain boundary. Microstructures are not much different for premixed and prealloyed compacts at this temperature. Grain sizes are also similar. Pressure has got very little effect on the microstructures. For both the cases sintered densities (ρ_s) are same. Pores are of uniform size because of the absence of melt formation. But for premixed compacts, as the compaction pressure is increased pore morphologies are changed.

Effect of pressure (150 MPa & 600 MPa) on the prealloyed samples sintered at 880 ℃

Significant grain shape accommodation. Total rounding of the grains. Intragranular melt formation and also twin formation. Sintered densities are not much different. But grain morphology is very much different for both the cases. Clearly higher stress has got its effect on modifying the grain shape.

6.6 Analysis of the Dilatometric Plots

As describes in the earlier sections, the theory proposed for the expansion of premixed compact during sintering could be supported by the dilatometric studies.

L = height of the sintered sample

From Table 5.1 sintered density obtained from axial dimension measurement is

$$\rho_s(\%th) = \frac{78.08}{(1-\frac{6.5-6.3}{6.5})^3} = 78.81$$

By volumetric calculation ρ_s = 79.12% theoretical. So, it is found that found that the density values obtained from the linear expansion rule is matching with the calculated value of volumetric study. That means, in this case dilatometric study could properly explain the sintering behaviour of premixed sample.

6.7 Phase Identification by XRD

Change of phase can have significant impact on many alloy properties. This is particularly true when transition to the new phase includes a change to a different crystal structure. An example is the α (BCC) to γ (FCC) transition of Fe at 910°C. The transition to a close packed crystal structure would likely cause an influence on strength. Such transitions are temperature dependent and are predictable for a given alloy composition by the appropriate phase diagram.

Phase diagram (Figure 1.1) for Cu-12%Sn predicts transition from two phased α + δ to single phase α at 370°C. Dowson [58], however, observes that the two phased structures is rarely the case due to the extraordinary cooling rate required to decompose the α-Cu phase. But from Figure 5.34 it is clear that, prealloyed powders got some second phase with it. The prealloyed powders are gas atomized and during that non-equilibrium cooling those intermetallic may be formed. This is an expected result due to the slight segregation of the alloy during powder production cooling. The small amount of two-phased material would form with slight variations in composition as the melt cooled to progressively lower temperatures. From the JCPDS file the second phase is identified as β- $Cu_{5.6}Sn$. Such composition variation would cause shift in the lattice constant and therefore the diffraction pattern. As the temperature is increased, the contribution of the intermetallic is decreasing. Above 275°C the intermetallic phase is

absent. So, it can be said that, more homogenization is taking place as the temperature is increased and as a result the intermetallic phase is annealed out. As the prealloyed powders are made by the melting of the constituent, the tin peaks are absent. All the results indicated an overwhelming dominance of α-bronze.

An interestingly result was found while taking the diffraction pattern of premixed Cu-12Sn powder. It can be seen from the Figure 5.32 that, for premixed powder no peak of tin are coming. This is quite unusual and was investigated further. The weight percent of tin is increased to 30% and tin peaks are observed but with very low intensity compared to copper peaks. Further increase in the tin content to 60 wt.% showed the tin peaks. But, the intensity of the copper peaks were bought down. The results of those analysis were shown in Figure 6.8. So, it is clear that the copper powder is producing a massing effect on the premixed powders. For that reason the XRD pattern of premixed powder doesn't reveal the tin peaks.

Another interesting incident was found in the XRD pattern of premixed green compact. Here the tin peak is observed though with a small intensity. The reason can possibly be explained in terms of the work by Davis and Sarkar [65]. They demonstrate that greater ejection force was experienced with increasing tin content, suggesting a higher resistance offered at the die wall by the tin. High contact pressure causes a low melting point metal to solder on to a hard surface. So, after the compaction may be the tin comes to the surface. And the x-ray analysis reveals the presence of the tin peak.

For the premixed samples as the sintering time is increased tin melts and goes into the copper, thereby causing alloying. At 775°C and 850°C for the premixed samples at both 150 MPa and 600 MPa conditions only α-bronze is observed. The reason for that is described in the earlier sections. After the melting of tin, the peaks are shifted to the left hand side. This indicates the increase in the lattice parameters of the sample. So, it can be concluded that alloying of tin into the copper increase the lattice parameter.

For prealloyed samples a continuous shift of the peaks on the left-hand side was observed. It reveals that, more the temperature of sintering, more will be the alloying. And more alloying leads to the increase in the lattice parameter. The prealloyed samples also showed single-phase α phase at higher temperature.

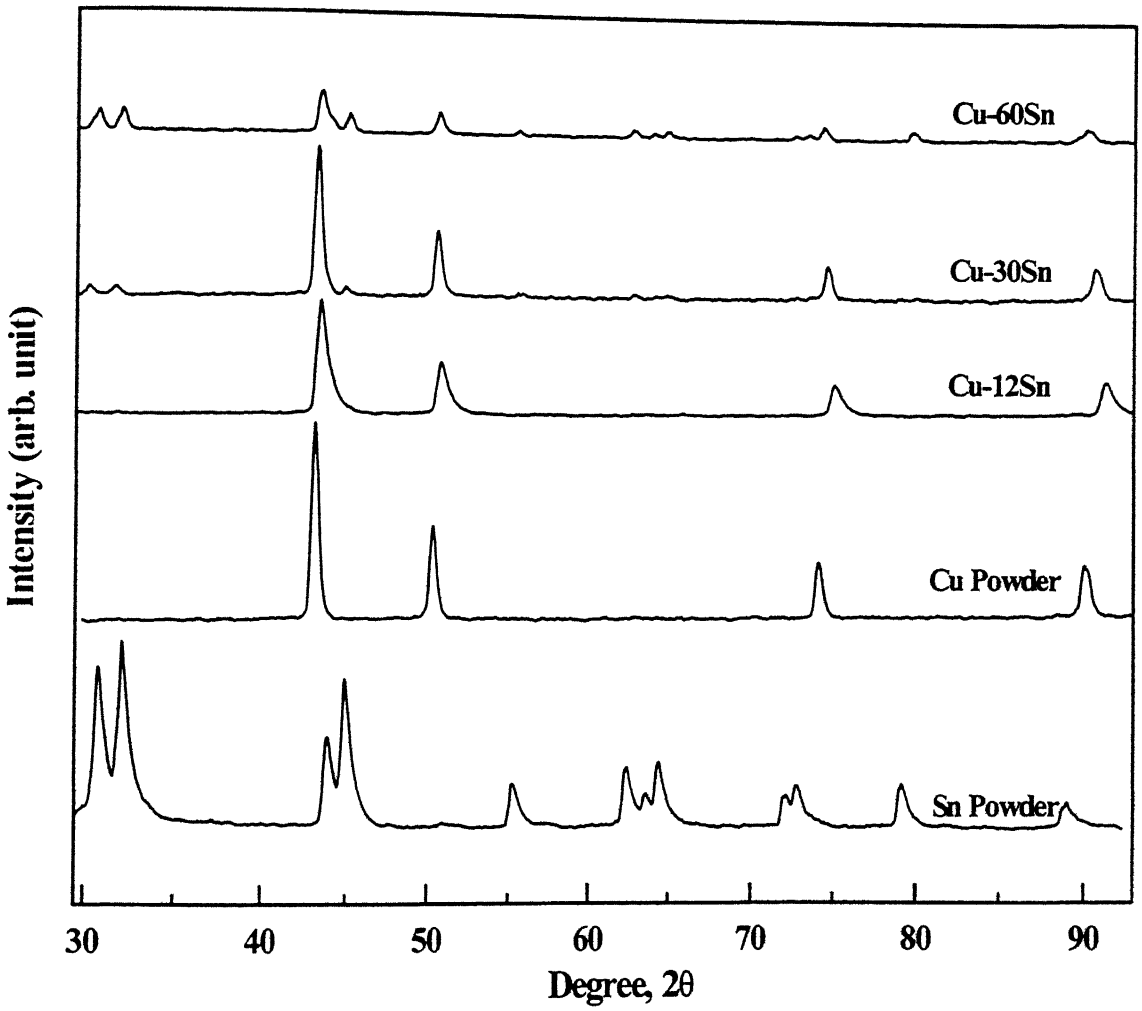

Figure 6.8. Comparison of premixed powder with different tin content.

6.8 Thermal Analysis by Differential Scanning Calorimetry

The formation of a liquid phase in a sintering compact has been shown to have significant influence on its ability to hold shape. German [37] concluded that yield strength of a sintering powder compact with a liquid phase varies with the liquid fraction. The loss of yield strength due to liquid fraction is the major factor leading compact slumping under the influence of gravity. Controlled experiments to visually measure slumping relative to sintering conditions were performed by Lal, Shoale and German [86].

A detailed investigations on the thermal analysis of bronze were done by Mukunda *et al.* [70-71]. Figure 5.36 shows the dilatometric plots for premixed compact. The sharp peak at 232°C indicates the melting of tin. This peak corresponds to the eutectic reaction ($\eta + Sn \rightarrow L$) or liquefaction of the copper-enriched tin. After the endothermic reaction, the DSC curve dips down (exothermic) and starts to form ε phase during continuous heating. The formation of γ by the diffusion of copper into δ between 500°C and 550°C can be seen in Figure 5.36 obtained during sintering of premixed Cu-12Sn compact. As the temperature is increased at around 700°C, the diffusion of tin in copper is almost complete. The diffusion of tin in the copper will increase the tin content of α. A stage will occur when the α reaches its tin saturation, and further diffusion, favours the formation of β. This β does not form by the invariant reaction, but does so over a range, and therefore, its formation does not produce a very sharp peak in the DSC.

Figure 5.37 shows the DSC plot of prealloyed Cu-12wt.%Sn. It reveals only two reactions: the eutectoid formation of γ at 500°C, and the peritectic decomposition of $\beta = \alpha + L$ at about 780°C. This peak is very small. This also means that although the composition is in the homogeneous α zone, non-equilibrium cooling of this alloy from temperatures greater than 850°C invariably gives some small amount of β, which ultimately transforms to $\alpha + \delta$.

The DSC curve for premixed sample is showing a continuous decreasing trend. But the prealloyed curve decreases upto 500°C and then increase. It implies that for prealloyed compact at 500°C all becomes as a homogeneous solid solution. After that they behave like a single phase and as a result not much variations in the DSC curve. But

the curve for premixed sample is different. All the peaks after 500°c indicate the phase change. And it implies the structure is not homogeneous throughout. Though from the phase diagram premixed sample should behave like prealloyed sample after the tin melts and homogenization is complete, but actually it doesn't happen in real system. Activity and chemical affinity are different for copper and tin powders. For that reason, kinetics is different than predicted by phase diagram. The same difference in the behaviour of premixed and prealloyed samples during densification, macro and microstructure, compact distortions were observed earlier. These DSC results may be treated as the confirmations of our previous studies and their explanations.

Chapter 7

CONCLUSIONS

The current work investigates the processing of premixed and prealloyed bronze through transient and supersolidus liquid phase sintering. Considering the results and discussion of the present investigation, the following conclusions can be drawn:

- Premixed and prealloyed Cu-12Sn powders behave differently.
- Premixed samples show expansion upto sintering temperature of 775°C for compacting pressure of 150 MPa. Increase in temperature beyond that leads to shrinkage. But if the sintering temperature increase beyond certain limit compact distortion occurs. In this case the critical temperature is 850°C. For premixed compacts at a fixed sintering temperature, expansion increases with the increase in compaction pressure. Prealloyed samples show shrinkage as the sintering temperature is increased. Thereby showing the opposite trend compared to premixed samples.
- Supersolidus sintering for the prealloyed compacts lead to the higher densification compared to the solid state sintering of the same.
- Prealloyed samples compacted at 150 MPa show isotropic shrinkage as a function of sintering temperature.
- For premixed samples, higher the compaction pressure, higher is the anisotropy.
- Tendency of twin formation is more in prealloyed samples compared to premixed sample. Absence of twins in the premixed samples indicate that the samples are less homogeneous compared to prealloyed samples.
- In prealloyed samples more or less rounded pores are observed. All these pores are the as pressed green porosities. Elimination of the pores occurs as the function of sintering time. No extra pores are formed during the sintering operation.
- For the premixed samples, the amount of pores are increased during sintering. The irregular pores are formed from the tin-rich phase. Intragranular and intergranular melts are formed during the sintering of premixed compacts.

- In both premixed and prealloyed samples, final phase in the microstructure only consists of α-bronze. No intermetallics are observed.
- X-ray diffraction study of the prealloyed powder reveals the presence of an intermetallic phase with α-bronze. Increase in the sintering temperature shifts the peaks to the lower angle side for both kind of powders. This proves the gradual homogenization of the samples, and the increase in the lattice parameter.
- Dilatometric plot of premixed sample shows the melting of tin and change of different phases. The expansion observed earlier in the premixed sample can be supported by the changes observed here.
- Differential scanning calorimetry explains the difference in the behaviour of premixed and prealloyed samples. Though from the phase diagram premixed sample should behave like prealloyed sample after the tin melts and homogenization is complete, but actually it doesn't happen in real system. Activity and chemical affinity are different for copper and tin powders. For that reason, kinetics is more important than the thermodynamics in this case. The same difference in the behaviour of premixed and prealloyed samples during densification, macro and microstructure, compact distortions were observed earlier.
- If the bronze is to be used for bearing applications, premixed powders are more suitable than the prealloyed one. Expansion of premixed compact gives rise to interconnected pores, which will be able to contain the oil. On the other hand, for structural applications, prealloyed seems to be the best route. Because, prealloyed compacts undergo densification during sintering.

REFERENCES

1. V. Singh, Physical Metallurgy, Standard Publishers, New Delhi, India, 1999, pp. 664-668.
2. B.T.K. Barry and C.J. Thwaites, Tin and Its Alloys and Compounds, Ellis Horwood Ltd., West Sussex, England, 1983.
3. G.S. Upadhyaya, Powder Metallurgy Technology, Cambridge International Science Publishing, Cambridge, UK, 1999.
4. S.A. Tsukerman, Powder Metallurgy, Pergamon Press, NY, USA, 1965.
5. E. Klar, Powder Metallurgy: Applications, Advantages and Limitations, American Society for Metals, Metals Park, OH, USA, 1983.
6. ASM Handbook, v.7, Materials Park, OH, USA, 1998, pp. 864-866.
7. From web: http://www.epma.com
8. ASM Handbook, v.2, Metals Park, OH, USA, 1990.
9. W.D. Jones, Fundamental Principles of Powder Metallurgy, Edward Arnold Ltd, London, England, 1960.
10. J.S. Hirschhorn, Introduction to Powder Metallurgy, American Powder Metallurgy Institute, Princeton, NJ, USA.
11. R.M. German, Sintering Theory and Practice, John Wiley & Sons, New York, NY, USA, 1998.
12. R.M. German, Powder Metallurgy Science, MPIF, Princeton, NJ, USA, 1994.
13. F.V. Lenel, Powder Metallurgy Principles and Applications, Metal Powder Industries Federation, Princeton, NJ, USA, 1980.
14. G.C. Kuczynski, "Self-Diffusion in Sintering of Metallic Particles," *Transactions AIME*, 1949, v. 185, pp. 169-178.
15. W.D. Kingery and M. Berg, " Study of the Initial Stages of Sintering Solids by Viscous Flow, Evaporation-Condensation, and Self-Diffusion," *Journal of Applied Physics*, 1955, v. 26, pp.1205-1212.
16. W. Schatt, W. Hermel, E. Friedrich, and P. Lanyi, "On the Status of Sintering Theory of One Component Systems," *Science of Sintering*, 1983, v. 15, pp. 5-26.

17. R.L. Coble, "Initial Sintering of Alumina and Hematite," *Journal of the American Ceramic Society*, 1958, v. 41, pp. 55-62.

18. F.B. Swinkels and M.F. Ashby, "Role of Surface Redistribution In Sintering by Grain Boundary Transport," *Powder Metallurgy*, 1980, v.23, pp. 1-7.

19. R.M. German, "Some Sources of Activation Energy Errors in Sintering Experiments," *Powder Metallurgy*, 1979, v. 22, pp.29-30.

20. H.E. Hall, "Sintering of Copper and Tin Powders," *Metals and Alloys*, 1939, v. 10, pp. 297-299.

21. S.L. Hoyt, "Hard Metal Carbides and Cemented Tungsten Carbides," *Transactions AIME*, 1936, v. 89, pp. 9-58.

22. L.L. Wyman and F.C. Kelley, "Cemented Tungsten Carbides: A Study of the Action of the Cementing Material," *Transactions AIME*, 1931, v. 93, pp. 208-229.

23. F.V. Lenel, "Sintering in the Presence of Liquid Phase," *Transactions AIME*, 1948, v. 175, pp. 878-896.

24. R.M. German, Liquid Phase Sintering, Plenum Press, New York, NY, 1985, pp. 1-155.

25. A. Upadhyaya, "A Microstructure-Based Model For Shape Distortion During Liquid Phase Sintering," Ph.D. Thesis, The Pennsylvania State University, University Park, PA, USA, 1998.

26. G.H.S. Price, C.J. Smithells, and S.V. Williams, "Sintered Alloys, Part I – Copper-Nickel-Tungsten Alloys Sintered With a Liquid Phase Present," *Journal of Institute of Metals*, 1938, v. 62, pp.239-264.

27. W.D. Kingery, "Densification During Sintering in the Presence of a Liquid Phase. 1. Theory," *Journal of Applied Physics*, 1959, v. 30, pp. 301-306.

28. W.D. Kingery and M.D. Narashimhan, "Densification During Sintering in the Presence of a Liquid Phase. 2. Experimental," *Journal of Applied Physics*, 1959, v. 30, pp. 307-310.

29. H.S. Canon and F.V. Lenel, "Some Observations on the Mechanism of Liquid Phase Sintering," Plansee Peoceedings, F. Benesovsky (ed.) Plansee Metalwerk, Reutte, Austria, 1953, pp. 106-122.

30. W.J. Huppmann and H. Riegger, "Modelling of Rearrangement Process in Liquid Phase Sintering," *Acta Metallurgica*, 1975, v. 23, pp. 965-971.

31. L. Liu, "Synthesis, Activated Sintering and Microstructural Evolution of Tungsten-Based Composites," Ph.D. Thesis, The Pennsylvania State University, University Park, PA, USA, 1998.

32. A. Belhadjharndia, "Theoretical Concepts for the Liquid Phase Sintering of a New Low Temperature Tungsten Heavy Alloy," Ph.D. Thesis, The Pennsylvania State University, University Park, PA, USA, 1993.

33. V. Smolej, S. Pejounik, and W.A. Kaysser, "Rearrangement During Liquid Phase Sintering of Large Particles," *Powder Metallurgy International*, 1981, v. 14, pp. 126-128.

34. W.F. Huppmann, "The Elementary Mechanisms of Liquid Phase Sintering: II. Solution-Reprecipitation," *Zeitschrift fur Metallkunde*, 1979, v. 70, pp. 792-797.

35. W.A. Kaysser, M.Zivcovic, and G. Petzow, "Shape Accommodation During Grain Growth in the Presence of a Liquid Phase," *Journal of Material Science*, 1985, v.20, pp. 578-584.

36. S. Farooq and R.M. German, "An Update on the Theory of Liquid Phase Sintering," Sintering 87, v. 1, S. Somiya, M. Shimada, M. Yoshimura, R. Watanabe (eds.), Elisevier Applied Science, London, UK, pp. 459-464.

37. R.M. German, "Supersolidus Liquid Phase Sintering. Part I. Process Review," *International Journal of Powder Metallurgy*, 1990, v. 26, n. 1, pp. 23-34.

38. L. Cambal and J. Lund, "Supersolidus Sintering of Loose Steel Powders," *International Journal of Powder Metallurgy*, 1972, v. 8, pp. 131-140.

39. J.A. Lund and S.R. Bala, "Supersolidus Sintering," Modern Developments in Powder Metallurgy, v. 6, H.H. Hausner and W.E. Smith (eds.), Metal Powder Industries Federation, Princeton, NJ, USA, 1974, pp. 409-421.

40. M. Jeandin, S. Rupp, J. Massol, and V. Bienvenu, "Structural Study and Image Analysis of Rapidly Cooled Supersolidus-Sintered Astroloy," *Material Science and Engineering*, 1986, v. 77, pp. 139-147.

41. P. Murley and R.M. German, "Supersolidus Sintering of Coarse Powders and its Application to Powder Injection Moulding," Advances in Powder Metallurgy, v. 3, Metal Powder Industries Federation, Princeton, NJ, USA, 1989, pp. 103-120.

42. A. Lal, "Mechanisms and Mechanics of Shape Loss During Supersolidus Liquid Phase Sintering," Ph.D. Thesis, The Pennsylvania State University, University Park, PA, USA, 1999.

43. R.M. German, "Supersolidus Liquid Phase Sintering. Part II. Densification Theory," *International Journal of Powder Metallurgy*, 1990, v. 26, n. 1, pp. 35-43.

44. Y. Liu, R. Tandon, and R.M. German, "Modeling of Supersolidus Liquid Phase Sintering: I. Capillary Force," *Metallurgical and Materials Transactions A*, 1995, v. 26A, pp. 2415-2422.

45. Y. Liu, R. Tandon, and R.M. German, "Modeling of Supersolidus Liquid Phase Sintering: II. Densification," *Metallurgical and Materials Transactions A*, 1995, v. 26A, pp. 2423-2430.

46. R. Tandon and R.M. German, "Particle Fragmentation During Supersolidus Sintering," *International Journal of Powder Metallurgy*, 1997, v. 33, n. 1, pp. 54-60.

47. R. Tandon, "Densification Mechanisms and Microstructural Evolution Leading to High Density Processing of Prealloyed Powders in Supersolidus Liquid Phase Sintering," Ph.D. Thesis, The Pennsylvania State University, University Park, PA, USA, 1995.

48. D.F. Berry, "Factors Affecting the Growth of 90/10 Copper/Tin Mixes Based on Atomized Powders," *Powder Metallurgy*, 1972, v. 15, pp. 247-266.

49. W. Kehl and H.F. Fischmeister, "Liquid Phase Sintering of Al-Cu Compacts," *Powder Metallurgy*, 1980, v. 23, pp. 113-119.

50. D.J. Lee and R.M. German, "Sintering Behaviour of Iron Aluminium Powder Mixes," *International Journal of Powder Metallurgy*, 1985, v. 21, pp. 9-21.

51. R.M. German, "Phase Diagrams in Liquid Phase Sintering Treatments," *Journal of Metals*, 1986, v. 38, n. 8, pp. 26-29.

52. Y. Zhou, W.F. Gale, and T.H. North, "Modelling of Transient Liquid Phase Bonding," *International Materials Reviews*, 1995, v. 40, n. 5, pp. 181-195.

53. From web: www.tlptechnologies.com

54. S.F. Corbin and P. Lucier, "Thermal Analysis of Isothermal Solidification Kinetics During Transient Liquid-Phase Sintering," *Metallurgical and Materials Transactions A*, 2001, v. 32A, n. 4, pp. 971-978.

55. R.M. German, "Dimensional Changes in Mixed Powder Sintering," Advances in Powder Metallurgy and Particulate Materials-1995, Metal Powder Industries Federation, Princeton, NJ, 1995, pp. 4.113-4.126.

56. B. Krishnakant and M. Patel, "Superior Quality Bronze Bearings," Modern Developments in Powder Metallurgy, v.19, P.U. Gummeson and D.A. Gustafson (eds.), MPIF, Princeton, NJ, USA, 1988, pp. 621-640.

57. H.E. Hall, "Sintering of Copper and Tin Powders," *Metals and Alloys*, 1939, pp. 297-299.

58. G. Dowson, " The Sintering of Bronze," *Metal Powder report*, 1984, v. , n.2, pp. 71-73.

59. D.F. Berry, "Factors Affecting the Growth of 90/10 Copper/Tin Mixes Based on Atomized Powders," *Powder Metallurgy*, 1972, v. 15, pp. 247-266.

60. E. Deegan and A.D. Sarkar, "Effect of Sintering Variables on the Dimensional Changes of Copper-Tin Compacts upto 10% Tin," *Metallurgia and Metal Forming*, 1973, v.40, n.8, pp. 148-151.

61. J.E. Elliot, *Metallurgia*, v. 59, pp. 17.

62. J.E. Drapeau, Powder Metallurgy, J. Wulf (ed.), ASM, Metals Park, OH, USA, 1942.

63. A.B. backensto, "Changes in Dimensional Change for Bronze Premixes as Premix Components Changes," Modern Developments in Powder Metallurgy, v.19, P.U. Gummeson and D.A. Gustafson (eds.), MPIF, Princeton, NJ, USA, 1988, pp. 641-652.

64. D.F. Berry, E. Klar and N. Veloff, "Aspects of Dimensional Control During Manufacture of Bronze Self Lubricating Bearings," Advances in Powder Metallurgy and Particulate Materials, v. 6 , 1992 , Metal Powder Industries Federation, Princeton, NJ, USA, pp. 51-61.

65. R. Davis and A.D. Sarkar, "Volume Growth of Copper-Tin Compacts Due to Sintering With Tin Content Between 12–20%," *Metallurgia and Metal Forming*, 1973, v.40, n.8, pp. 260-261.

66. E. Peissker, "Pressing and Sintering Characteristics of Powder Mixtures for Sintered Bronze 90/10 Containing Different Amounts of Free Tin," Modern Developments in Powder Metallurgy, v. 7, H.H. Hausner and W.E. Smith (eds.), 1974, pp. 597-614.

67. N.N. Acharya, P.G. Mukunda, and A. Bose, "Properties of Vacuum Sintered Bronze Bearings – Influence of Copper Powder," *Powder Metallurgy International*, 1984, v. 16, n. 5, pp. 212-216.

68. J.W. Kim, S.J. Kang, D.N. Yoon, "The Flow Behaviour of Sn Melt During Sintering of 90Cu-10Sn Powder Compacts, *Powder Metallurgy International*, 1987, v. 19, n. 3, pp. 41-42.

69. K. Das and J.A. Bas, "Control of Delta Phase in 90/10 Bronze Bearings," Advances in Powder Metallurgy and Particulate Materials, v. 6 , 1992 , Metal Powder Industries Federation, Princeton, NJ, USA, pp. 23-34.

70. N.N. Acharya and P.G. Mukunda, "Sintering in the Copper-Tin System, Part I: Identification of Phases and Reactions," *The International Journal of Powder Metallurgy*, 1995, v.31, v.1, pp. 63-71.

71. N.N. Acharya and P.G. Mukunda, "Sintering in the Copper-Tin System, Part II: Alloy Behaviour," *The International Journal of Powder Metallurgy*, 1995, v.31, v.1, pp. 73-79.

72. N.N. Acharya and P.G. Mukunda, "Sintering in the Copper-Tin System, Part III: Influences of Variables," *The International Journal of Powder Metallurgy*, 1995, v.31, v.1, pp. 81-88.

73. J.I. Farmer, "Microstructure of Non-Ferrous PM Materials," *Metal Powder Report*, 1983, v.38, n. 5, pp. 256-260.

74. N.N. Acharya and P.G. Mukunda, "Metallography of Copper-Tin alloys," *Metallography*, 1988, v.21, pp. 137-150.

75. G.S. Upadhyaya, Sintered Metallic and Ceramic Materials Preparation, Properties and Applications, John Wiley and Sons Ltd., West Sussex, England, 2000, pp. 219.

76. E. Peissker, "Sintered 90/10 Bronze from Powders with Different Tin Contents," *Metal Powder Report*, 1983, v.38, n. 5, pp. 260-262.

77. K.L.Patel, "Use of Dilatometer to Study the Sintering Response of Bronze Powder Mixes: Part 1," *Metal Powder report*, 1985, v. , n.6, pp. 358-360.

78. K.L.Patel, "Use of Dilatometer to Study the Sintering Response of Bronze Powder Mixes: Part 2," *Metal Powder report*, 1985, v. , n.7, pp. 424-431.

79. G. Arthur, "Porosity and Permeability Changes During the Sintering of Copper Powder," *Journal of the Institute of Metals*, 1954-55, v. 83, pp. 329-336.

80. A.P. Savitskii, "Current Views on the Processes of Sintering in the Presence of Liquid Phase," *Soviet Powder Metallurgy and Metal Ceramics*, 1987, v. 26, pp. 631-636.

81. D. Berner, H.E. Exner and G. Petzow, Modern Developments in Powder Metallurgy, H.H. Hasuner and W.E. Smith (eds.), v. 6, Metal Powder Industries Federation, Princeton, NJ, 1974, pp. 237.

82. N. Dautzenberg and H.J. Dorweiler, "Dimensional Behaviour of Copper-Carbon Sintered Steels," *Powder Metallurgy International*, 1985, v. 17, n. 6, pp. 279.

83. W.A. Kaysser, W.J. Huppmann and G. Petzow, *Powder Metallurgy*, 1980, n. 2, pp. 86.

84. A. Upadhyaya and R.M. German, Proceedings 14th International Plansee Seminar, Reutte, Austria, v. 2, G. Kneringer, P. Rodhammer and P. Wilhartitz (eds.), 1997, pp. 68.

85. A. Griffo, "Powder and Sintering Pathway Selection to Achieve Zero Dimensional Change in Fe-2 wt.% Cu-0.8 wt.% C," M.S. Thesis, The Pennsylvania State University, University Park, PA, USA, 1993.

86. A. Lal, G.A. Shoales and R.M. German, "Thermal Characterization to Study the Sintering of Bronze Powders," *Twenty-Fourth International Thermal Conductivity Conference / Twelfth International Thermal Expansion Symposium*, Pittsburgh, PA, 1997.

Appendix I

Experimental data for the green samples

Sample	Compaction Pressure (C.P.) (MPa)	Weight (g)	Height (cm)	Diameter (cm)	Volume (cm^3)	Density (g/cm^3)	Density (% theo)
PM	150	4.6678	0.59	1.27	0.747	6.25	72
PM	300	5.1158	0.59	1.27	0.747	6.85	79
PM	450	5.2327	0.56	1.27	0.709	7.38	85
PM	600	6.2143	0.64	1.27	0.810	7.67	88
PA	150	4.158	0.62	1.27	0.785	5.30	61
PA	600	4.539	0.53	1.27	0.671	6.76	78
PM	150	4.3263	0.57	1.27	0.722	5.99	69
PM	600	5.634	0.594	1.27	0.752	7.49	86
PA	150	3.5365	0.53	1.27	0.671	5.27	61
PA	600	4.9968	0.57	1.27	0.722	6.92	79
PM	150	4.9492	0.628	1.27	0.795	6.22	71
PM	600	5.7858	0.59	1.27	0.747	7.75	89
PA	150	4.324	0.61	1.27	0.772	5.60	64
PA	600	5.621	0.62	1.27	0.785	7.16	82
PM	150	4.8915	0.63	1.27	0.798	6.13	70
PM	600	6.0375	0.6	1.27	0.760	7.95	91
PA	150	4.2165	0.6	1.27	0.760	5.55	64
PA	600	4.9907	0.55	1.27	0.696	7.17	82
PM	150	4.7316	0.61	1.27	0.772	6.13	70
PM	600	5.8984	0.59	1.27	0.747	7.90	91
PA	150	3.776	0.56	1.27	0.709	5.33	61
PA	600	5.9522	0.65	1.27	0.823	7.23	83

Appendix II

Experimental data after sintering

Sample	C.P. (MPa)	Temp (°C)	Time (min)	Weight (g)	Height (cm)	Dia. (cm)	Volume (cm^3)	Density (g/cm^3)	Density (% theo.)	Wt. Loss (%)	Densification Parameter
PM	150	775	40	4.6625	0.606	1.29	0.792	5.89	68	0.11	-0.15
PM	300	775	40	5.1040	0.620	1.31	0.835	6.11	70	0.23	-0.40
PM	450	775	40	5.2207	0.608	1.34	0.857	6.09	70	0.23	-0.97
PM	600	775	40	6.2010	0.690	1.35	0.987	6.28	72	0.21	-1.33
PA	150	775	40	4.1137	0.600	1.25	0.736	5.59	64	1.06	0.09
PA	600	775	40	4.4910	0.510	1.25	0.626	7.18	82	1.06	0.21
PM	150	880	40	4.3140	Distorted			6.00	69	0.28	0.00
PM	600	880	40	5.6177				5.76	66	0.29	-1.42
PA	150	880	40	3.5000	0.470	1.16	0.496	7.05	81	1.03	0.52
PA	600	880	40	4.9420	0.550	1.26	0.685	7.21	83	1.09	0.16
PM	150	850	40	4.9392	0.632	1.26	0.783	6.31	72	0.20	0.31
PM	600	850	40	5.7693	0.650	1.34	0.916	6.30	72	0.29	-1.50
PA	150	850	40	4.2810	0.570	1.2	0.644	6.64	76	0.99	0.34
PA	600	850	40	5.5624	0.600	1.24	0.724	7.68	88	1.04	0.34
PM	150	275	40	4.8905	0.630	1.27	0.798	6.13	70	0.02	0.00
PM	600	275	40	6.0358	0.600	1.27	0.760	7.95	91	0.03	0.00
PA	150	275	40	4.1800	0.600	1.27	0.760	5.50	63	0.86	-0.02
PA	600	275	40	4.9460	0.550	1.27	0.696	7.10	81	0.89	-0.04
PM	150	220	40	4.7300	0.610	1.27	0.772	6.12	70	0.03	0.00
PM	600	220	40	5.8970	0.590	1.27	0.747	7.89	91	0.02	0.00
PA	150	220	40	3.7533	0.560	1.27	0.709	5.29	61	0.60	-0.01
PA	600	220	40	5.9070	0.650	1.27	0.823	7.18	82	0.76	-0.04

Appendix III

Experimental data for the xylene impregnation tests.

Sample	Compaction Pressure MPa	Sintering Temperature °C	Wt. before Impregnation A1 (g)	Wt. after Impregnation		Total Porosity %
				In Air B (g)	In Water C (g)	
PM	150	775	3.5965	3.7454	3.1048	36
PM	600	775	6.2270	6.4225	5.4200	29
PA	150	775	4.1376	4.3244	3.600	34
PA	600	775	4.5132	4.6674	4.0338	18
PA	150	880	3.5222	3.6964	3.1765	22
PA	600	880	4.9648	5.1024	4.4029	19
PM	150	850	4.8528	5.0100	4.2300	29
PM	600	850	5.7943	5.9936	5.0212	32
PA	150	850	4.3041	4.4663	3.7986	26
PA	600	850	5.5846	5.7314	4.9941	13
PM	150	275	4.9108	5.1422	4.3025	33
PM	600	275	6.0576	6.1687	5.3780	12
PA	150	275	4.2041	4.5014	3.7218	38
PA	600	275	4.9700	5.1127	4.3900	21
PM	150	220	4.7514	4.9154	4.0916	34
PM	600	220	5.9182	6.0066	5.2540	10
PA	150	220	3.7757	4.0117	3.2674	42
PA	600	220	5.9315	6.0442	5.1883	20

Appendix IV

Axial and radial dimensions of the samples.

Sample	Condition	Before Sintering		After Sintering		Axial Shrinkage %	Radial Shrinkage %
		Ht. (mm)	Dia. (mm)	Ht. (mm)	Dia. (mm)		
PM	150 MPa, 775°C	4.8	12.7	4.9	12.7	-2.08	0.00
PM	300 MPa, 775°C	5.9	12.7	6.2	13.1	-5.08	-3.15
PM	450 MPa, 775°C	5.6	12.7	6.08	13.4	-8.57	-5.51
PM	600 MPa, 775°C	6.4	12.7	6.9	13.5	-7.81	-6.30
PA	150 MPa, 775°C	6.2	12.7	6	12.5	3.23	1.57
PA	600 MPa, 775°C	5.3	12.7	5.1	12.5	3.77	1.57
PA	150 MPa, 880°C	5.3	12.7	4.7	11.6	11.32	8.66
PA	600 MPa, 880°C	5.7	12.7	5.5	12.6	3.51	0.79
PM	150 MPa, 850°C	6.3	12.7	6.3	12.5	0.00	1.57
PM	600 MPa, 850°C	5.9	12.7	6.5	13.4	-10.17	-5.51
PA	150 MPa, 850°C	6.1	12.7	5.7	12	6.56	5.51
PA	600 MPa, 850°C	6.2	12.7	6	12.4	3.23	2.36
PM	150 MPa, 275°C	6.3	12.7	6.3	12.7	0.00	0.00
PM	600 MPa, 275°C	6.0	12.7	6	12.7	0.00	0.00
PA	150 MPa, 275°C	6.0	12.7	6	12.7	0.00	0.00
PA	600 MPa, 275°C	5.5	12.7	5.5	12.7	0.00	0.00
PM	150 MPa, 220°C	6.1	12.7	6.1	12.7	0.00	0.00
PM	600 MPa, 220°C	5.9	12.7	5.9	12.7	0.00	0.00
PA	150 MPa, 220°C	5.6	12.7	5.6	12.7	0.00	0.00
PA	600 MPa, 220°C	6.5	12.7	6.5	12.7	0.00	0.00

+ : shrinkage

- : expansion

Appendix V

Hardness values of the samples

Condition	No. of Observ.	D1	D2	Mean	Hardness HV	Average Hardness	Standard Deviation	
							σ_n	σ_{n-1}
Prealloyed 150 MPa 880°C	1	99.1	101	100.1	56	55	5.94	6.50
	2	107.7	106.9	107.3	48			
	3	116.2	104.8	110.5	46			
	4	98.7	97.2	97.9	58			
	5	95.3	96.3	95.8	60			
	6	95.4	95.1	95.3	61			
Prealloyed 600 MPa 880°C	1	90.5	94.4	92.5	65	67	7.24	8.09
	2	101.2	102.4	101.8	54			
	3	87.1	87.7	87.4	73			
	4	88.4	89.1	88.8	71			
	5	85.6	88.9	87.3	73			
Premixed 300 MPa 775°C	1	118.3	121.8	120.1	39	42	2.02	2.26
	2	113.7	115.8	114.8	42			
	3	116.2	116.6	116.4	41			
	4	112.5	113	112.8	44			
	5	109.1	115.2	112.2	44			
Premixed 450 MPa 775°C	1	111.1	112.5	111.8	45	44	2.27	2.54
	2	108.5	112.1	110.3	46			
	3	109.6	110.6	110.1	46			
	4	117.8	116.5	117.2	41			
	5	115.3	117.1	116.2	41			
Prealloyed 150 MPa 775°C	1	103.3	107.6	105.5	50	48	1.43	1.6
	2	104.1	110	107.1	49			
	3	108.1	109.2	108.7	47			
	4	107.6	108.3	107.9	48			
	5	109.2	111.5	110.4	46			
Prealloyed 600 MPa 775°C	1	82.7	83.4	83.1	81	76	3.66	4.01
	2	83.8	84.5	84.2	79			
	3	84.1	85	84.6	78			
	4	89.2	90	89.6	70			
	5	87.5	86.1	86.8	74			
	6	85	85.4	85.2	76			

Prealloyed 150 MPa 850°C	1	108.4	107.2	107.8	48	53	8.70	9.53
	2	109.5	107.5	108.5	47			
	3	98.4	97.1	97.8	58			
	4	104.9	104.4	104.7	51			
	5	89.5	88.7	89.1	69			
	6	113.8	112.8	113.3	43			
Prealloyed 600 MPa 850°C	1	85	85.2	85.1	77	85	5.33	5.84
	2	79.4	78.9	79.2	89			
	3	77.7	77.5	77.6	92			
	4	80.4	79.8	80.1	87			
	5	78.5	79.9	79.2	89			
	6	82.3	83.9	83.1	81			
Premixed 150 MPa 775°C	1	112.2	112.4	112.3	44	47	5.73	6.28
	2	116.2	117.1	116.7	41			
	3	104	110.1	107.1	49			
	4	110.5	113.3	111.9	44			
	5	97.5	96.8	97.6	59			
	6	107.5	109.4	108.5	47	58	1.41	1.55
Premixed 600 MPa 775°C	1	98.2	96.8	97.5	58			
	2	100.5	98.3	99.4	56			
	3	98.7	96.8	97.8	59			
	4	96.6	94.8	95.7	61			
	5	100.2	96.4	98.3	58			
	6	97.3	98.3	97.8	58			
Premixed 150 MPa 850°C	1	97.4	99.6	98.5	57	54	5.57	6.10
	2	99.8	97.1	98.5	57			
	3	102.6	103.9	103.3	52			
	4	92.8	94.8	93.8	63			
	5	106.9	107.6	107.3	48			
	6	108.3	109.3	108.8	47			
Premixed 600 MPa 850°C	1	94.9	97.2	96.1	63	70	5.70	6.24
	2	85.3	82.2	83.8	79			
	3	87.2	89.4	88.3	71			
	4	91.8	95.3	93.6	63			
	5	87	87.5	87.3	73			
	6	89.8	85.1	87.5	73			
Prealloyed 600 MPa 275°C	1	97.6	98.2	97.9	58	67	7.69	8.42
	2	98.7	99.6	99.2	56			
	3	89.4	87.5	88.5	71			
	4	86.1	86.8	86.5	74			
	5	90.8	91.8	91.3	67			
	6	83.6	86.7	85.2	77			

Prealloyed 600 MPa 220°C	1	83.1	85.5	84.3	78	80	3.43	3.76
	2	84	82.9	83.5	80			
	3	79.8	80.7	80.3	86			
	4	84.3	83.7	84	79			
	5	83.3	84	83.7	79			
	6	86.9	85.5	86.2	75